HIGH RESOLUTION PALEOCLIMATIC REGISTERS FROM RED DUNE SANDS (TERI SANDS) OF TAMIL NADU COAST: A MULTI-PROXY STUDY

THESIS

Submitted by

VIDYA SAKAR A

in partial fulfillment of the requirements for the degree of

DOCTOR OF PHILOSOPHY

OCTOBER 2016

CENTRE FOR RESEARCH

ANNA UNIVERSITY, CHENNAI-600 025

U.PORTO

Proceedings of the Ph.D. Viva-Voce Examination of Mr. VIDYA SAKAR. A held at 12.30 PM on 13.10.2016 in Koodal Hall, Institute for Ocean Management, Anna University, Chennai.

The Ph.D. Viva-Voce Examination of **Mr.VIDYA SAKAR. A** ((Reg. No.1214719809 India)/ (Reg.No.201306794 Portugal)) on his Ph.D. Thesis Entitled **"HIGH RESOLUTION PALEOCLIMATIC REGISTERS FROM RED DUNE SANDS(TERI SANDS) OF TAMIL NADU COAST:A MULTI-PROXY STUDY"** was conducted on **13.10.2016** at **12.30 pm** in **Koodal hall, Institute for Ocean Management, Anna University, Chennai.**

The following Members of the Oral Examination Board were Present:

1.	**Prof.S.Srinivasalu** (Ph.D.), Institute for Ocean Management, Anna University, Chennai- 600025.	Thesis Director
2.	**Dr.HelenaSant'Ovaia** (Post-Doc), Faculty of Science, University of Porto, Portugal-4169-007.	Thesis Director
3.	**Dr.P.Saravannan** (Ph.D.),Dept of Geology, University of Madras, Chennai-600 025.	Panel member
4.	**Dr.LakshmiNarashiman**(Ph.D.), Dept of Applied Geology, Anna University, Chennai-600 025.	Panel member
5.	**Dr.B.Gowtham** (Ph.D.), Dept of Geology, Presidency College, Chennai-600 005.	Panel member

External Examiner

6.	**Dr. P.Raja** (Ph.D.) Senior Scientist, ICAR- Indian Institute of Soil and Water Conservation, Nilgiris-643 004.	Subject Expert

The research Scholar, **Mr.VIDYA SAKAR**. A presented the salient features of his Ph.D. work. This was followed by questions from the board members. The questions raised by the Foreign and Indian examiners were also put to the scholar. The scholar answered the question to the full satisfaction of the board members.

Based on the scholars research work, his presentation and also the clarification and answers by the scholar to the board recommends that **Mr. VIDYA SAKAR. A** be awarded Ph.D. degree in the Faculty of Science and Humanities in Anna University and Ph.D. degree in Faculty of Sciences in University of Porto.

1. S. Srinivasalu
2. Helena Sant'Ovaia
3. P. Saravannan
4. 13/10/2016
5. 13/10/16
6. 13/10/2016

ABSTRACT

Sand dunes are unstable ecosystems and are organized at the juncture between sea and land. They are formed from sand, which is eroded and ground rock, derived from terrestrial and oceanic sources. This system is influenced by several factors, such as ocean swell, coastline, shape of beach, prevailing wind, frequency of storm events, and particle size of the sands forming the dune. Though not directly controlled by climate, the landward movement of coastal dunes is facilitated by arid and semi-arid conditions.

Red sand dunes (locally known as 'teri sand') occur in the coastal plains of South India between Muttom on the south west coast (~16km south west of Nagercoil) and Rameswaram in Tamil Nadu (8°00' to 9°30' N; 77°18' to 79° 00' E). The teri sands exhibit shades of red with yellow and brown, colour varying from 2.5YR 3/4 to 10R 3/6 in Munsell colour chart and in thickness from 1m to greater than 10m.

From the spatial distribution of teri sands, the dunes are identified as inland teri deposits (ITD) and coastal teri deposits (CTD). The ITD occur as sand sheets of medium to coarse-grained sand with thin gravel layers at variable depth, located near to the foothills of Western Ghats and are limited in number. Whereas the CTD occur as vast discontinuous accumulations of medium to fine grained sand in the form of dunes and sheets, roughly parallel to coast and are ~6-8 km away from modern shoreline

The Teri sands from the southeast coast of Tamil Nadu were examined by magnetic methods, including magnetic susceptibility measurements, acquisition of isothermal remanent magnetization,

geochemical, X-ray diffraction and optically stimulated luminescence (OSL) dating. Five sections were excavated up to 5-7m with three inland deposits (KCV, SKM, TPV, THOP and MUT) and one near coastal (THOP). Magnetic parameters show the important contribution of hematite structures to the studied sands, namely in SKM and KCV samples.

In TPV, MUT and THOP samples, magnetic parameters indicate the presence of multidomain magnetite or mixed mineral contents of magnetite and antiferromagnetic minerals. The SKM samples present the highest quantity of hematite and smallest quantity of magnetite, as is shown by the highest values of HIRM% and smallest of S_{-300} and SIRM. The positive correlation between χ with clay in TPV, THOP and KCV sections indicates that the clay matrix carries magnetic susceptibility.

In SKM, magnetic susceptibility is due to the silt fraction. The presence of magnetite in THOP and TPV sections is probably of oceanic origin carried by strong offshore winds. In SKM the wet environments due to cultivation (associated with a arid climate) may contribute to the prevalence of the necessary conditions for the dominant presence of hematite.

Marine sediments are extremely sensitive indicators of chronological variations in concentration and grain size of deposited terrigenous/lithogenous material. In correspondence with geochemistry data, the variation of χ depends upon the deposition because they would have been deposited in both dry and wet periods, and it also depends upon the mode of haulage.

These outcomes corresponded well with the previous work on Teri sand available on the southeast coast of India by several authors and this effort can be used for future comparative studies on Teri deposits. In XRD data, correlation analysis indicated TPV and MUT sections have a similar

type of deposition and THOP did not show any positive correlation with TPV and MUT and even with its own deposition. In a comparsion with geochemistry data, χ variation and OSL dates, it was shown that the sample [MUT 21 (200cm) with an OSL age of 14±2 ka indicated deposition during humid interval and at [~17±2 ka to ~19±2 ka MUT 61 (600cm) depicts the dry period of deposition.

RESUMO

As dunas são ecossistemas instáveis que se organizam na junção entre o mar e a terra. São formadas a partir de areia, que é erodida e derivada de fontes terrestres e oceânicas. Os sistemas de dunas são influenciados por vários factores, tais como as ondas oceânicas, a dinâmica litoral, a forma da praia, o vento dominante, a frequência de tempestades e tamanho das partícula de areia que formam a duna. Apesar de não ser controlado diretamente pelo clima, o movimento das dunas costeiras é facilitado por condições áridas e semiáridas.

As dunas de areia vermelha (localmente conhecidas como "terisand") ocorrem nas planícies costeiras do sul da Índia, entre Muttom na costa sudoeste (~ 16 km a sudoeste de Nagercoil) e Rameswaram em TamilNadu (8 ° 00' a 9 ° 30 'N; 77 ° 18' e 79 ° 00 'E). As "terisands" exibem tonalidades de vermelho a amarelo e castanho, cores que no Sistema de cores de Munsell variam de 2.5YR 3/4 a 10R 3/6 e a sua espessura varia de 1m a mais que 10 m.

A partir da distribuição espacial das "teri, sands" as dunas são identificadas como depósitos interiores ou depósitos costeiros. Os depósitos interiores ocorrem em lençóis de areia de granulometria média a grosseira com finas camadas de cascalho a profundidades variáveis, e localizam-se próximo do sopé das Western Ghats e são limitados em número. Por outro lado, os depósitos costeiros ocorrem como vastas acumulações descontínuas de areia com granulometria média a fina sob a forma de dunas e lençóis de areia, mais ou menos paralelos à costa e estão localizados a cerca de 6 a 8 km de distância da linha atual de costa.

As "terisands" da costa sudeste de TamilNadu foram estudadas através de métodos de caracterização magnética, incluindo medições de

susceptibilidade magnética (χ) e aquisição de magnetização remanescente isotérmica (MRI), geoquímica, difração de raios-X e datação por luminescência oticamente estimulada. Várias seções foram escavadas até 5 a 7 m, cinco secções em depósitos interiores (KCV, SKM, TPV, THOP e MUT) e uma secção num depósito costeiro (THOP).

Os parâmetros magnéticos mostraram a importante contribuição de estruturas como a hematite nas areias estudadas, nomeadamente nas amostras de SKM e KCV. Em amostras de TPV, MUT e THOP, os parâmetros magnéticas indicaram a presença de magnetite multidomínio e minerais antiferromagnéticos. As amostras de SKM apresentaram a maior quantidade de hematie e menor pequenas percentagens de magnetite, como foi demonstrado pelos maiores valores de HIRM% e os baixos de S_{-300}e SIRM. A correlação positiva entre χ e argila nas secções TPV, THOP e KCV indicou que é na matriz de argila que estão os minerais responsáveis pela susceptibilidade magnética.Nas amostras de SKM, susceptibilidade magnética é devida a minerais da fracção silte. A presença de magnetite nas amostras de THOP e TPV é provavelmente de origem oceânica, transportada por ventos marítimos fortes. Em SKM os ambientes permanentemente húmidos devido ao cultivo (associado a um clima árido) podem contribuir para a prevalência das condições necessárias para a presença dominante de hematite.

Os sedimentos marinhos são indicadores extremamente sensíveis das variações cronológicas na concentração e tamanho de grãos de material terrígeno/ litológicos depositado. Em correspondência com os dados geoquímicos, a variação da suscetibilidade magnética dependeu da deposição, porque teriam sido depositados em períodos quer secosquer húmidos, e isso também depende do modo de transporte.

Os resultados obtidos estão de acordo com trabalhos anteriores sobre “terisands” da costa sudeste da Índia. As análise de correlação tendo em

conta os dados da difração de raios X, indicaram que as seções TPV e MUT tiveram um tipo semelhante de deposição e a secção THOP não mostrou nenhuma correlação com TPV e MUT.

Os dados de datação por luminescência oticamente estimulada juntamente com a caracterização magnética e geoquímica, permitiram identificar na secção MUT, o período húmido de deposição à profundidade de 200 cm e o período seco à profundidadede 600 cm.

ACKNOWLEDGMENT

Here I try to greet everyone who has offered their help and encouragement during the past four years of my study. As the list is too lengthy I hope you would exonerate me for my briefness. First I would like to thank the Erasmus Mundus (India4EU II) Project for their financial support and laboratory facilities during the 32 months course of my study during my stay in Portugal.

I wish to record my deep sense of gratitude and profound thanks to my research supervisors **Dr. S. Srinivasalu** Professor and Director, Institute for Ocean Management, Anna University, Chennai and my Co-supervisor **Dr. Helena Santo'ovaia** Associate Professor, Earth Sciences Institute, Pole of the Faculty of Sciences, Rua do Campo Alegre 4169-007 Porto, Portugal for their keen interest inspiring guidance, constant encouragement with my work during all stages, to bring this thesis into fulfillment. I wish to thank my Doctoral Committee members **Prof. N. Rajendran**, Department of Chemistry, Anna University, Chennai, **Dr. V. Ram Mohan (Retd)**, Department of Geology, University of Madras, Chennai, **Prof. Deolinda Flores** and **Prof.Fernando Noronha** Faculty of sciences, University of Porto, Portugal for their suggestions and encouragement throughout this research. I express my sincere gratitude to **Dr. L. Elango** Professor and Head, Department of Geology, Anna University Chennai for giving me permission and lab facilities to carry out my work successfully. My special thanks go to **Dr. HemaAchyuthan**, Professor, **Dr. S. Sanjeevi**, Professor, **Dr. R. Nagendra** Professor, **Dr.Lakshmi Narashiman** Assistant Professor, **Dr. K. Sivaraj** Assistant Professor, Department of Geology, Anna University, Chennai for giving inspiration during this research work. A very special thanks to **Dr. Linto Alappat** Assistant professor, Dept of Geology Christ college, Kerala, **Dr. P. Morthekai**, Scientist B, BirbalSahni Institute of Palaeobotany, Lucknow, **Dr. Jorge Ferreira** Senior Scientist, Laboratory national of Energy in Geology (LNEG), Porto, Portugal, **Prof. (Late)Celeste Santos Gomes, Geophysical Institute, University of Coimbra, Portugal** for giving great solutions and ideas during my research. I also thank **Dr. K.Anandasabari, Dr. P. Saravanan** (Asst. Prof)**, Mr. K.Neelavannan, Mr.ArulBritto, Dr. Neha Shreya** and other research scholars for rendering me support and help throughout my research work. Finally, I acknowledge my family who have constantly encouraged and supported me in all my accomplishments, who have always stood there to care my learning, never questioning my selections. My various friend network stretches far and wide and as always they have been there to help me out.

VIDYASAKAR ANBURAJ

TABLE OF CONTENTS

CHAPTER NO. **TITLE** **PAGE NO.**

CHAPTER NO. **TITLE** **PAGE NO.**

CHAPTER NO. **TITLE** **PAGE NO.**

LIST OF TABLES

LIST OF FIGURES

FIGURE NO. **TITLE** **PAGE NO.**

FIGURE NO. **TITLE** **PAGE NO.**

LIST OF SYMBOLS AND ABBREVIATIONS

ASTM	-	American Society for Testing and Materials
A.D	-	Anno Domini
B.C	-	Before Christ
BP	-	Before Present
BSL	-	Blue Light
Br	-	Bromine
$CaCO_3$	-	Calcium Carbonate
C	-	Carbon
CCl_4	-	Carbon tetrachloride
cm	-	Centimeter
°C	-	Degree Celsius
D	-	Depth
E	-	East
D_e	-	Equivalent natural dose
gm	-	Gram
gm/cc	-	Gram per cubic centimeter
g	-	Gravity
GSL	-	Green Light
HIRM	-	Hard isothermal remanent magnetization
HM	-	Heavy mineral
HTL	-	High Tide Line
HCl	-	Hydrogen Chloride
IOC	-	Indian Oil Corporation
IRSL	-	Infrared
Fe	-	Iron
IRM	-	Isothermal remanent magnetization
Ka	-	Killoannum

km	-	Kilometers
km^2	-	Kilometers
K	-	Kurtosis
LF	-	Laminated Facies
χ	-	Mass specific susceptibility
m	-	Metre
m/sec	-	Metre per second
m/s^2	-	Metre per second squared
mts	-	Metres
mL/L	-	Milliliters into liters
mm	-	Millimeter
'	-	Minutes
NOAA	-	National Oceanic and Atmospheric Administration
N	-	North
OSL	-	Optically Stimulated Luminescence
OM	-	Organic matter
%	-	Percentage
ϕ	-	Phi
PTTL	-	Photo-Transferred
K	-	Potassium
RSL	-	Red Light
Bocr	-	Remanent coercive force
Rb	-	Rubidium
ROF	-	Runoutfacies
SIRM	-	Saturation isothermal remanent magnetization
”	-	Seconds
SAR	-	Single Aliquot Regenerative
Sk	-	Skewness
Na	-	Sodium
S	-	South

TL	-	Thermal
Th	-	Thorium
~	-	Tilde
USA	-	United States of America
UFR	-	Upper Flow Regime
U	-	Uranium
c	-	Velocity
W	-	West
XRD	-	X-ray Diffraction
yr	-	Year

CHAPTER 1

INTRODUCTION

1.1 GENERAL

Ruling beyond than 70% of the Earth's surface, the oceans are a very important cause of Paleoclimatic evidence. Amid 6 and 11 billion metric tons of sediment collect in the ocean basins yearly, and this keeps an archive of climatic conditions near the ocean surface or on the neighboring continents. Sediments are composed of both biogenic and terrigenous materials. The biogenic component comprises the remains of planktic (near surface-dwelling) and benthic (bottom-dwelling) bodies, which provide a record of past climate and oceanic circulation (regarding surface water temperature and salinity, dissolved oxygen in deep water, nutrient or trace element concentrations, etc.). By contrast, the nature and abundance of terrigenous material mainly provides a record of humidity- aridity variations on the continents, or the intensity and direction of winds blowing from land areas to the oceans, and other modes of sediment transport to, and within, the oceans (fluvial erosion, ice-rafting, turbidity currents, etc.).

Sand dunes are unstable ecosystem and organize at the tie-up between sea and land (http://www.doc.govt.nz/). They are formed from sand, which is eroded and ground rock, derived terrestrial and oceanic source. This system is influenced by several factors as swell of ocean, coastline, shape of the beach, prevailing wind, frequency of storm events, and particle size of the sands to form a dune (http://www.doc.govt.nz/). Though not directly

controlled by climate, the landward movement of coastal dunes is facilitated by arid and semi-arid conditions. Strong onshore winds are as important as reduced rainfall (Sarnthein 1978). Red dunes on the east coast (referred as 'teri sands/ teris' in literature) are categorized as inland coastal and near-coastal (teri) dunes (Joseph et al. 1997, 1999). According to the standard Tamil dictionary, teri means 'a heap of sand'. Jeyangondaperumal et al. (2012) used 'wasteland' because the local people called so as it was useless for agriculture (personal communication). Joseph et al. (1997), observing its texture, inferred that teri deposits were derived from exposed continental shelf during a period of low relative sea level and that these sediments were transported by high landward winds. So the shelf is rich in heavy minerals like ilmenite, rutile, zircon, garnet, monazite and sillimanite. Chandrasekharan & Murugan (2001) suggest that these rich, heavy minerals belong to Precambrian. The current research applies on teri sands with new dimensions of environmental magnetism using several methodologies such as Magnetic Susceptibility and Isothermal Remanent Magnetization (IRM) measurements, optical luminescence Dating (OSL), X-ray Diffraction (XRD) and geochemistry data.

1.2 OBJECTIVES OF THE PRESENT STUDY

- To determine the robust line between dry and wet climate.
- To determine the hematite and magnetite presence in the deposits.
- To determine the grain size of the deposition with magnetic parameters.
- To understand the climatic changes based on magnetic measurements and geochemistry of marine sediments.

1.3 BACKGROUND OF THE STUDY

Red sand dunes (locally known as 'teri sand') occur in the coastal plains of South India between Muttom on the south-west coast (~16km south-west of Nagercoil) and Rameswaram in Tamil Nadu (8°00' to 9°30' N; 77°18' to 79° 00' E). The teri sands exhibit shades of red with yellow and brown, colour varying from 2.5YR 3/4 to 10R 3/6 in Munsell colour chart and thickness from 1m to greater than 10m (Figure 1.1). From the spatial distribution of teri sands, the dunes are identified as inland teri deposits (ITD) and coastal teri deposits (CTD). The ITD occur as sand sheets of medium to coarse-grained sand with thin gravel layers at variable depth, located near to the foothills of Western Ghats and are limited in number. Whereas the CTD occur as vast discontinuous accumulations of medium to fine grained sand in the form of dunes and sheets, roughly parallel to the coast and are ~6-8 km away from the modern shoreline (Sabu et al. 1999).

Figure 1.1 Picture is showing the red dunes area. Gullies were formed up to ~10m depth in the unconsolidated sediment surface due to heavy rain. Microliths were found on the surface of the dunes

From morphological interpretation Zeuner & Allchin (1956) suggest that a sequential development of lagoons and offshore bars lead to the formation of dunes, weathering of dunes in the lagoon owing to low sea level in turnresult in formation of red dunes. Based on further studies on morphology, Gardner (1986) identified the presence of marine sediments along the entire coast at heights of 15-18m (Ovari series) and 6-9m (Idindakarai series) above the present day sea level. Gardner and Martingell (1990) suggested an age of ≥38 ka for Ovari and Idindakarai series based on radiocarbon dating of aragonite pelecypod from ~8m raised marine sediments. This series was exposed leading to the formation of calcrete capping on their surface. The aragonite land snails from this unit have given radiocarbon ages between 25ka BP and 21 ka BP (Gardner 1981). The unconsolidated red dune sand was deposited on top of aeolianites. The sands are devoid of internal microscopic structure and are reddened throughout the profile by intense insitu weathering and chemical leaching of Fe- bearing silicates, releasing iron oxides and forming authigenic kaolinites and illites (Gardner1981, Sabu et al. 1999). It was proposed that the red dunes were deflated from the exposed continental shelf probably under the influence of strengthened NE wind regime and arid conditions during the peak of last glacial period (Gardner & Martingell 1990).

The teri sands found along the Southeast coast of India were formed in response to past global climatic systems and are preserved in few parts of the World. Studying these can provide significant clues about the palaeoclimate at a regional and global scale. While most of the dunes in east and west coast of India (Tamil Nadu and Kerala) show the much younger age of deposition (Early to late Holocene), available radiocarbon dates for teri sands (Gardner 1981, Singhvi et al. 1986) show much older depositional age (Late Pleistocene). Many studies have been attempted in the past to study the origin and source of colouration of dunes using sedimentology and

geochemistry, but little is known about the chronology and its paleoclimatic significance of these dunes. Thermoluminescence dating of red dunes in comparable morphological and environmental settings was successfully applied in Sri Lanka (Singhvi et al. 1986), which shows the applicability of this technique in this area. Rock magnetic technique is an another proxy which is as climate proxy in sediments. In the red sand dunes, the ions oxides minerals are of major interest in our rock magnetic study as there origin are supposed to be controlled by apedogenic process which is again controlled by existing climates. Hence these proxies along with sedimentology, geochemistry and mineralogy will provide a unique opportunity to study the Late Quaternary climate change in the earth's history.

1.4 STUDY AREA

The study area is located along the southeast coast of Tamil Nadu between Tuticorin (8°42'28.70"N, 78°2'31.70"E) and Tirunelveli (8°19'57.64051"N,77°57'27.91272"E), extending ca. 13 km inland from the coast (Figure1.2). Teri deposits occur along the whole length of the coastline of extreme southeast coast Tamil Nadu (Jayangondaperumal et al. 2012). Three inland sampled sections were Servaikaran Madam (SKM), 8°42'28.70"N, 78°2'31.70"E; Kachanavilai (KCV), 8°33'51.9"N; 78°00'43.0"E; Edayan villa (TPV), 8°22'11.05830"N, 77°53'40.22456"E; and two near the coast, Thopu villa (THOP), 8°19' 57.64051"N; 77°57'27.91272"E and Muttom (MUT); 8°07'56" N; 77°19'84"E Both Inland Teri sands and coastal Teri sands were examined extensively.

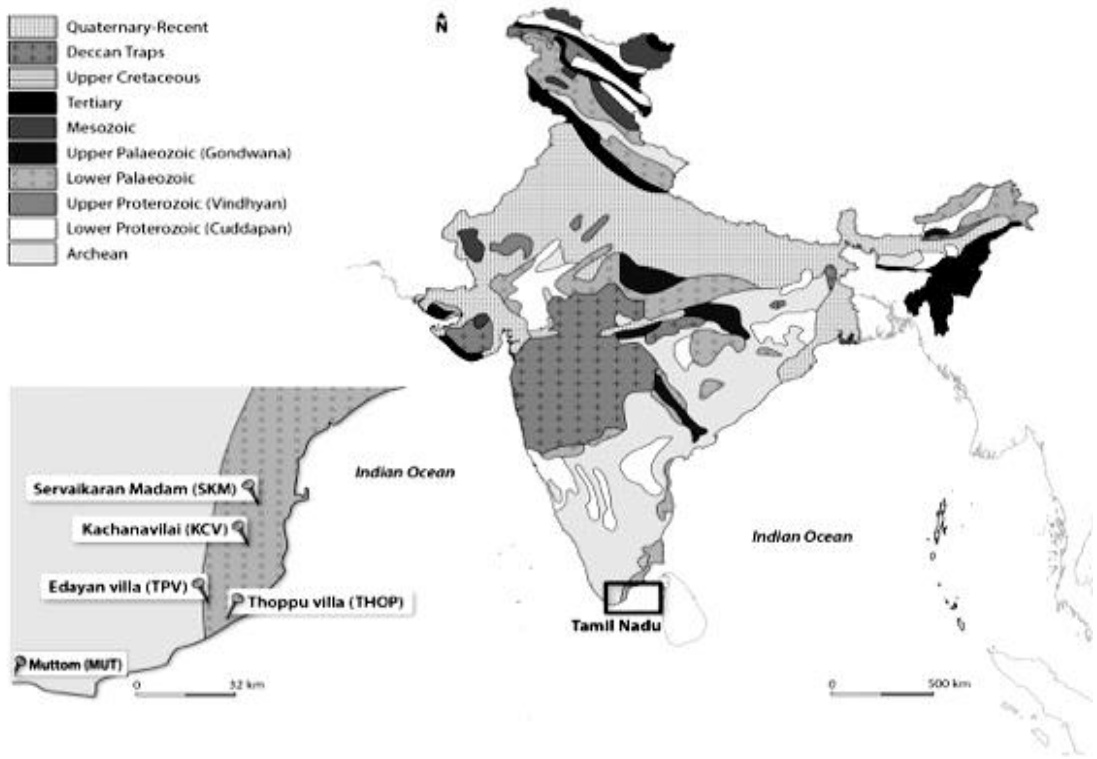

Figure 1.2 Location of samples collected

Jayangondaperumal et al. (2012) mentioned that formation of fluvial Inland Teri (IT) sediments during NE winter monsoon and reddening of IT occurred in the last 15 ka. During the Last Glacial Maximum (LGM), continental shelves were exposed with a vast reservoir of sediments with strong landward winds during (NE/E) winter monsoon, and sediments drifted inland until 11.4 ka to form coastal aeolian teri deposits. Coastal Teri reddening was occurring by in situ weathering which started during <11.4ka-5.6 ka during a humid climate.

1.5 REGIONAL CLIMATE

The climate is tropical in Muttom. In the winter, there is much less rainfall in Muttom than in summer. According to Köppen and Geiger climate, is classified as Aw. The average annual temperature in Muttom is 27.6 °C.

The average annual rainfall is 1093 mm. The driest month is January with 16 mm. Most precipitation falls in November, with an average of 194 mm. The warmest month of the year is May with an average temperature of 29.2 °C. In December, the average temperature is 26.0 °C. It is the lowest mean temperature of the whole year. The difference in precipitation between the driest month and the wettest month is 178 mm. The average temperatures vary during the year by 3.2 °C (climate-data.org).

The climate is also tropical in ThopuvillaandEdayan villa. In the winter, there is much more rainfall than in summer. The Köppen-Geiger climate classification is Aw. The average annual temperature in Thopuvilla and Edayan villa is 28.5 °C. The average annual rainfall is 729 mm. The driest month is January with 14 mm. Most precipitation falls in November, with an average of 213 mm. The warmest month of the year is May with an average temperature of 30.6 °C. In January, the average temperature is 26.2 °C. It is the lowest mean temperature of the whole year.The difference in precipitation between the driest month and the wettest month is 199 mm. The average temperatures vary during the year by 4.4 °C (climate-data.org).

1.6 REGIONAL STRATIGRAPHY

The primeval coastal deposits (Ovari Series) sit on Archaen granulitic rocks (Figure1.3), most of which are peninsular gneiss (garnet-sillimanite-graphite gneiss and charnockite gneiss (Jayangondaperumal et al. 2012). The coastal deposits are filled with Pleistocene and recent fluvial, fluvio-marine and marine deposits (Alappat et al. 2013). The teri sands cover an area of ~500 km^2 and thickness reaches 12 m (Gardner 1986). The Idindakarai Series overlies the Ovari Series and comprises terrigenous grains of gravel and sand size, and shell fragments of shallow marine origin (Jayangondaperumal et al. 2012). The marine shells gave U-series ages of ~112 to ~124 ka (Figure 1.2, Brückner, 1988, 1989) and therefore, define a

sea-level highstand during the last interglacial period (Jayangondaperumal et al. 2012). The Kanyakumari Series, which overlies the Idindakarai Series, consists of fossil deposits cemented together with calcium carbonate (Jayangondaperumal et al.2012). Above that overlies the Poochikkadu Series with calcrete and some marine sediments (Jayangondaperumal et al. 2012). *Helix vittata* is a land snail found all over the calcrete layer (Figure 1.3) with an age of 26,162–24,081 cal yr BP (21,000 ± 400 ^{14}C yr BP) and 31,244– 28,694 cal yr BP (25,000 ± 750 ^{14}C yr BP) (Jayangondaperumal et al. 2012). Inland teri sands (teri series) found in big patches, are dark in colour and discontinuous while coastal teri sands are continuous and light coloured. Marine deposits of Mandapam Series overlie the teri deposits (Jeyangondaperumal et al. 2012).

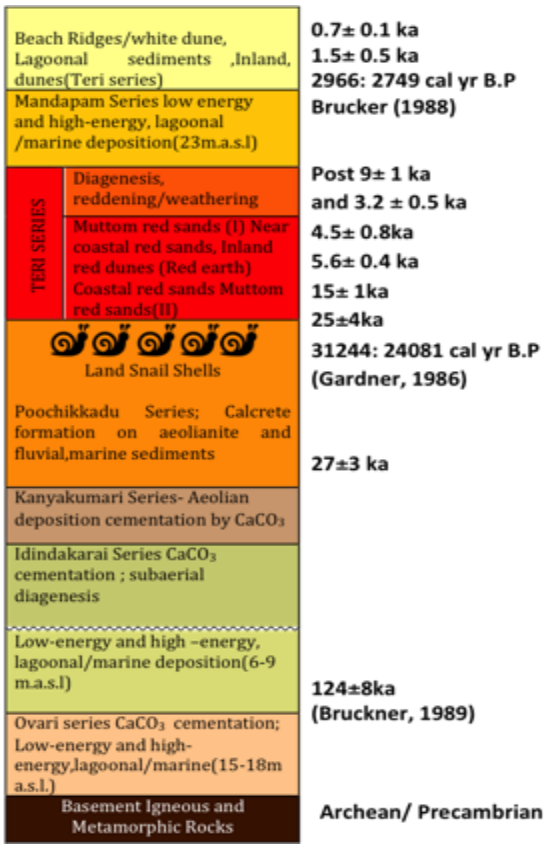

Figure 1.3 Regional stratigraphy from Jayangondaperumal et al. (2009) and some modified ages from Allapat et al. (2013).

In the shoreward direction, teri sands rest on either side of the crystalline basement, Ovari marine sandstone, aeolianite of Kanyakumari or the Poochikkadu Series (Figure 1.3; Gardner 1986, Joseph et al. 1997). Joseph et al. (1997), observing its texture, inferred that teri deposits were derived from the exposed continental shelf during a period of low relative sea level and that these sediments were transported by high landward winds. So the shelf is rich in heavy minerals like ilmenite, rutile, zircon, garnet, monazite and sillimanite. Chandrasekharan & Murugan (2001) suggest that these rich heavy minerals belong to the Precambrian.

1.7 GENERAL INFORMATION ABOUT STUDY AREA

1.7.1 Physiography, Temperature and Population

India is a tropical country and a land of diverse topography, soils, vegetation and climate. The study area is diverse nature with different coastal features. Sand dunes are present along the coast of Kanyakumari. The southern part of Kanyakumari coast is sandy beaches with heavy minerals. The general relief goes over to 15m above MSL. The south of Tiruchendur coast, consist of sandy beaches with heavy minerals. Sand dunes along the Tiruchendur coast rise up to a height of 67m. The coastal belt between Tuticorin and Tiruchendur has raised beaches with sandbars parallel to the coastline in a trend towards north to south direction. Sand dune and Terri dune complexes are present along the coast between Tiruchendur to Manappad.

Despite the rest of the world, the east coast of India experiences two monsoons. Oceanography of the Indian east coastal region is mainly controlled by the north-east (NE) and south-east (SW) monsoons. The equator-ward West India Coastal Current (WICC) during the summer monsoon, along the southwest coast, turns around Sri Lanka to the northeast

and flows into the Bay of Bengal as the southwest monsoon current (Vinayachandran et al. 1999). Along the study area, the wind speed during the southwest monsoon ranges from 36-60 Km/hour. During this period, the temperature is around 18- 28° C. The rainfall during the south-west monsoon is around 60-70 mm/month. The north-east monsoon starts from October and extends up to December. The wind speed during the north-east monsoon is ranged from 20-40 km/hour. However, during the cyclone, the wind speed may increase above 100 km/hour. Also, heavy rainfall (100-200 mm/month) accompanied by thunder and lightning occur during this period. During November to February, the climate is somewhat cool, but the temperature does not drop much, and it is mostly around 21° C.

The study area includes the part of three coastal districts of Tamil Nadu namely Kanyakumari, Tirunelveli and Tuticorin. The Kanyakumari district has a total population of 1,67,634. The rural population is 5,82,107 and urban population is 10,93,927. The Tirunelveli district has a total population of 27,23,988. The rural population is 1415742 and the urban population is 13,08,246. In Tuticorin district, the total population is 15,72,273. The rural population is 766823 and the urban population is 8,05,450.

1.7.2 Anthropogenic Activities and Natural Calamities

Recently various developmental projects like Koodankulam nuclear power plant, Sethu-samuthiram ship canal were started along the study area. The Sethu-samuthiram ship can project is a paramount one since it is an offshore project. Though India has a peninsular coast running to 3,554 nautical miles, it does not have a continuous navigational sea lane running within its territorial waters. Ships navigating from one side of the country to the other have to circumnavigate Sri Lanka due to the presence sandstone reefs, near the Rameswaram coast.

The Sethu-samuthiram project is an off-shore massive navigational channel of length 152.2 km, width 300 m and a depth of 12 m linking the Gulf of Mannar and Balk bay, which will connect the eastern and western parts of the Indian coast and thereby reduces time and fuel cost. About 80 million cubic meters of dredged sediment is dumped at nearby sites. Kudankulam Nuclear Power Plant is a nuclear power station under Indo-Russian collaboration which is currently under construction in the coast of Kudankulam in the east of Kanyakumari. Another power project is planned by coastal Energen Pvt. Ltd, an arm of the Coal & Oil Group of Dubai (C&O Group) is announced its plans to set up a 2,000 MW plant in Tuticorin district, Tamil Nadu. The plant aims to supply power to both industries and consumers and will bring down electricity generation cost. Several developmental projects and small-scale industries are functioning along the study area.

Indian coastal zone has a significant amount of heavy mineral deposits such as zircon, ilmenite, monazite, rutile, and sillimanite, which have wide applications in the field of the paint industry, nuclear sectors, pharmaceuticals, aviation, communication, electronics, water purification and oil refineries,etc. The Indian resources of placer minerals are 348 Million tons (Mt) of ilmenite, 107 Mt of garnet, 21 Mt of zircon, 18 Mt of Rutile, 8 Mt of monazite and 130 Mt of sillimanite. Indian resources constitute about 35% of world resources of ilmenite, 10% of rutile, 14% of zircon and 71.4% of monazite. India meets about 10% of the world requirement of garnet (Thomas & Baba 2005). The south Tamil Nadu coast of India, particularly from Navaladi to Periathalai coast, is rich in placer minerals. On-shore coastal sand mining is actively involved along these coasts. The inland Teri (red colour) sand dunes and beach placers have more amounts of mineral deposits. Currently, the beach sands are extracted and processed physically for exporting 100 % without any value addition.

The disaster can be defined as any disruption of human ecology, which cannot be absorbed by the adjustment capacity of the affected community with its own resources (Verma 1987). The disaster can be mainly classifiedinto two types. One is a natural disaster, and the other is a man-made disaster. Ganguly et al. (1993) insist that a determined human effort can wholly or to a great extent prevent man-made disaster, the

It does not hold good with respect to natural disaster, which have become a growing concern of mankind all over the world particularly during the last three decades. India being a vast country with a tropical monsoon type climate has all kinds of natural disaster prone areas except active volcanoes. The coastal area of southern Tamil Nadu is prone to flood, cyclone, earthquakes and sea erosion. Small to medium type cyclones are frequent during the monsoons in the last three decades. Although earthquakes, tsunamis or any other natural disasters are unpreventable, studying their impact on the coastal zone allows us to design and implement better strategies for mitigation activities. INSAT Disaster Warning System (IDWS) have been installed along the coastal Tamil Nadu and proved its worth during the last formed cyclones.

The recent Indian Ocean tsunami (26 December 2004) produced major changes on the Indian coast. The disastrous tsunami occurred in the Indian Ocean due to a devastating earthquake of magnitude Mw = 9.0 at 00:58:49 GMT (07:58 local time) on December 26, 2004, struck at 3.09' N, 94.26' E, near Indonesia (Figure 1.2). The tsunami had a great impact on the coastal areas of Indonesia, Sri Lanka, India and other neighboring countries. More than two hundred thousand people were killed making it the most devastating tsunami in the last forty years. Many beaches were entirely devastated by this tsunami.

Chandrasekar et al. (2005) and Mujabar et al. (2007) reported that the tsunami-induced a large amount of beach erosion and accretion along the study area. Channels were deepened by tsunami-induced currents and sometimes made shallow by transported and deposited sediments. The tsunami has devastated extensive stretches of coastal areas of the western side of Kanyakumari. The damage was more in areas, which are low-lying and flat devoid of any vegetation.

CHAPTER 2

REVIEW OF LITERATURE

2.1 SEDIMENTARY DYNAMICS

In order to determine sediment provenance clay mineralogy of 95 surface sediments samples of Aveiro shelf (covering the upper slope from Espinho to Averio and the continental shelf) have been analyzed and it had been also used to analyze provenance, dispersion and deposition is fine grained sediments. Using peak areas, a semi b quantitative x-ray a study of diffraction has been carried out about clay fraction (<2 micrometre).The major clay groups identified are kaolinite (average 30%), illite (average 59%), smectites (average 5%) and chlorite (average 5%). A terrigenous origin of these clay minerals can be supported by their presence in the suspended and bottom sediments of Ria de Averio margin and Douro River and also in the adjacent continental masses. However, the smectites minerals which are found near Averio Canyon may be of an authigenic origin. Douro River discharge through along shore currents are the main source of fine sediments to be studied. Other than this the supply sources are Ria de Averio lagoon discharge and coastal erosion. Kaolinite found in coarse grained deposits is probably related with relict supply process. The pattern of mineral distribution studied in the clay fraction suggeststhat the preferential offshore deposition and transport in lower energy environment of upper slope and outer shelf (Abrantes & Rocha 2007).

The successor of the international reference base for the soil classification (IRB) is the world reference base for soil receiver (WRB). The task of its is to apply IRB its principles of definition and linkages of it to the existing classes of the received FAO-UNESCO soil map of the world league (FAO 1988). The main objective is to provide background to received legend and scientific depth and to make sure that the latest knowledge relating to interrelationships in a worldwide soil reference system. The end aim is a well defined and described world reference base for soil resources that is accepted internationally by the community belonging to soil scientists it also shows us to facilitate the international use of pedological data, it is not only by the soil scientists but also by other users of the soil and the land (Spaargaren & Deckers 1995).

Big changes in the coercitivity of goethite and hematite grains in mineral assembling with other kind of origins mean that HIRM and S-ratio alone cannot simply be interpretedin terms of the relative and absolute changes, respectively, in the concentration of antiferromagnetic minerals. This problem can be however circumvented by using a new parameter the L-ratio which is defined as the ratio of two residual remaining after AF demagnetization of an IRM imparted in a 1T field with a peak AF of 100 mt and 300 mt ($IRM_{AF@300mT}/IRM_{AF@100mT}$). The absolute changes in the concentration of antiferromagnetic Material are represented by HIRM only when the L-ratio is relatively constant. The large fluctuate changes in the L-ratio point to significant changes on the coercively of antiferromagnetic minerals,which in turn, explains variations in sediments provenance. The L-ratio is an important parameter is environment magnetism due to the reason that it provide crucial ground-truthing for the long used S-ratio parameter and HIRM, as well as giving information concerning to the potential variations in the expertise of antiferromagnetic minerals (Liu et al. 2007).

In this work, we studied about traffic derived pollutants from primary sources road borders, surrounding areas and on roads (paved area). The study is mainly focused on the distribution, identification and concentration of pollutants and also in magnetic carrier. The magnetic parameters and its analyses suggest that the magnetic signal from the vehicle derived emissions can be controlled by a magnetic like phase. On estimating the grain size of magnetic materials revealed the presence of fine particles (0.1-5µm) that can be inhaled and are found dangerous to human health. The results of magnetic susceptibility (about $175*10^{-5}$ SI) reviewed a higher concentration magnetic enhancement in the central area of the tollbooth line that is related to higher traffic. In addition with that, the computation of magnetic materials was done on several road side soils along a length of 120km and 2-D counter map was generated using it, which revealed an higher magnetic values ($100\text{-}200\times10^{-5}$ SI) near the edge of the road.

The outcomes observed that the distribution of magnetic values indicates that magnetic particles exhausted by the vehicles cumulate and mainly concentrated within a distance of 1-2m from the edge of the road. In consequence with this the suitable indicates of traffic - related pollution is the magnetic susceptibility parameters can be used. The enrichment of come trace elements of non-magnetic studies such as cr, ba, zn, cu and pb that are also associated with traffic pollution. Furthermore, statistical correlation ship between the magnetic variables and the content of toxic trace metals support the usage of magnetic parameters as potential proxies for traffic related pollution in the study area (Marié et al. 2010).

Non-magnetic data can strongly correlate with particle size, which deems it accurately an correct thing as a particle size proxy and also as a reliable means for normalizing analytical data for particle size effects. The previous studies suggest that magnetic concentration parameters an another

way for normalizing these effects and given, the low cost, speed and sensitivity of the measurements may offer some more advantages over other kind of comported signals. In this work, contemporary sediments from a wide range of depositional environments has been analyzed with respect to their mineral magnetic concentration and characteristics in textural, to view that if the strength and the nature of relationship observed in previous studies are universal. Data of our magnetic parameters (XLF.XARM and SIRM) possess a relationship contrasting with the standard textual parameters for the sediments samples collected from estuarine (Gwendraeth Estuary), marine (carmarthen Bay) and fluvial (Rivers GwendraethFach and GwendraethFawr) settings .the magnetic concentrations of sediments from both the estuaries and marine environment are influenced highly by the contributions of magnetic properties of finer particle sizes; the sediments of GwendraethFawr river are affected by the contribution of magnetic properties of coarser size particle sizes, while those sediments obtained from the GwendraethFach river are not influenced significantly by any variations in properties relating textural. These outcomes indicate mineral magnetic measurements it has a potential considerably sedimentary environment, which in certain instances is useful for geochemical, sediment transport and sediment provenance studies. However, the data highlight before applying mineral magnet data as a particle size proxy (Booth et al. 2005).

2.2 ENVIRONMENTAL MAGNETIC MEASUREMENTS

The glacial erosion upper limit was represented by the sample of the soil analysis from the above and below trimlines. The weathering histories are demonstrated by last glacial maximum the lithology is responsible for conditioning of the contrast nature. The concentration-depend magnetic parameters are produced more at above trimline soil of basalt than the soil below the trimline which was due to the conversion to the magnetic forms

from the non magnetic iron bearing minerals. On the other hand parameters of the nonmagnetic will produce low value to the sand soil for the samples of above trimline, probably the ferrimagnetic minerals loss may be reflecting by the dissolution and oxidation. A new way for high level weather validation limited as the timelines of preglacial are stopped at the last glacial maximum(Walden & Ballantyne 2002).

The deflection of anthropogenic pollution is performed by the measurement susceptibility on top soil, which have been using for the last two year. A bartington susceptibility meter is used in most cases for the measurement of the field. However, still type is no standard protocol for such measurement carrying on in the field. Here, in this paper, the author aims to test the compatibility of different instruments setup, which have been being used and also the subjective influence factor. On a defined positions using Barrington MS2D instruments of four different types the measurement of field magnetic susceptibility are carried out for high and low values. It was very consistent the connection coefficient reached 97-98 % for the values measured using the Barrington MS2D. The results are verified by the two groups, mapped the test area independently without any restriction. However, under the too standard condition, which showed that it is suitable for magnetic sequencing of top soil (Schibler et al. 2002).

A soil geochemical survey was covered now in all over the Portugal for sample preparation, sampling and analysis a standard method is used for consistent data and high-quality achievement. The analysis of sample purposed for PH, 32 chemical elements, organic matter, and electrical conductivity. The identification of various chemical baseline levels is basic idea for that survey. The first Portugal soil geochemical atlas was produced due to the perfect compilation of the data. The atlas provides the information about chemical parameter, cumulative frequency curves, box plots etc and

spatial distribution maps and other environmental and geochemical information. This paper is about the soil atlas and it application example overview to obtain the reference value of the element this data base were very useful and also for achieving empirical formulae (Inácio et al. 2008)

The measurement of the soil susceptibility is interpreted based on the reference value knowledge. The reference value is chosen on the base of soil type we are using, In the current study, various soil 77 type,which formed on different parent material, are analysed. The soil pollution is estimated and excludes it since in the ground pollution and study this same data issued. The unpolluted soil susceptibility will vary on different soil types. In the analysis, the chosen samples get a high value of susceptibility. Where the intermediate value is for Cambisol and the lowest value obtained in water logged soils. On the comparison, the subsoil susceptibility depends strong on the parent material than a type of soil. To find the soils with unusual susceptibility thus comparability value provided by these studies can be very useful which could further extend to identify soil pollution (Hanesch & Scholger 2005).

The metallurgical dust and fly ashes are found to be enriched in ferromagnentic material from the mineralogically and magnetically studies on the collected sample of coal power plant fly ashes and metallurgical dust and samples from Ojcow National Park. The samples collected from the power plant area seem to have high magnetic susceptibility value, but the values are considered increased on the sample from Ojow national park which are nearly equal to the soils of the top horizons and that was taken as an anthropogenic origin evidences. The high susceptibilities of soil in adjacent areas and Upper Silesia are due to them (Strzyszcz et al. 1996).

This work mulls over the connection between's attractive properties and the substance of Cu, Zn, Cd and Pb in urban soils of Hangzhou, Eastern China. The attractive estimation demonstrates that urban top soils (0–5 cm)

have solid, attractive powerlessness and remanence. Attractive focus related parameters χ, ARM, IRM20 mT, Hard IRM and SIRM are found to increment in the request of modern arearoadsideresidential≈campuspublic parks, in this way showing that these attractive segments are connected with the mechanical exercises, car fumes and testimony of barometrical particulate. It was measured that the recurrence subordinate vulnerability (χfd) of urban soils is in an extent from 0.7% to 8.4%. The least χfd esteem with a mean estimation of 2.3% and 2.5%, separately, was found in the mechanical and roadside soils. The urban soils have the high substance of Cu, Zn, Cd and Pb. We concluded that the level of taintingwas expandedat the request of mechanical arearoadsidepublicparksresidential≈campus for Cu and Pb, and in the request of modern arearoadsideresidential≈campuspublic parks for Zn and Cd. Results showed a straight direct connection between's the attractive mineral focus related parameters and the groupings of Cu, Zn, Cd and Pb. It was found that the connection coefficients of the attractive parameters and overwhelming metal focus are high for Zn, medium for Pb, and low for Cu and Cd. This discovering proposes that the basic, quick and non-dangerous attractive estimation can be utilized as a pointer for the substantial metal defilement and intermediaries for the estimation of overwhelming metals content in urban soils (Lu & Bai 2006).

Presentation to metal-rich particulate contamination is connected with unfriendly wellbeing results. Specifically, lead has as of late been demonstrated to be harmful in youthful youngsters even at low levels already thought to be 'sheltered.' Lead harming from vehicle contamination has been tended to universally by evacuation of leaded petrol, however dangerous blood lead levels in youngsters keep on being accounted for in urban regions, the source recommended to be resuspended roadside soil, advanced in lead because of past leaded fuel use. Here, we utilize matched geochemical and attractive examinations of common biomonitors-kerbside tree leaves-and of

air test channels to look at contemporary wellsprings of particulate contamination, and demonstrate that co-related, fine (1 mm) lead-and iron-rich particles are transmitted as vehicle-inferred toxins. Higher and emphatically corresponded lead, iron and attractive remanence qualities were discovered closer to streets and out and about proximal instead of street distal sides of trees. Discriminatingly, most elevated poison qualities happened on tree leaves by tough instead of downhill street paths. The lead substance of the leaf particulates was related just with sub-micrometer, burning inferred round particles. These outcomes show that vehicle deplete outflows, as opposed to resuspended soil tidy, or tire, brake or other vehicle wear are the major wellspring of the lead, iron and attractive loadings on roadside tree takes off. Investigation of leaves at distinctive statures demonstrated that leaf particulate lead and iron focuses are most noteworthy at - 0.3m (i.e. little tyke stature) and 1.5–2m (grown-up head tallness) over the ground level; observing station gatherers put at 3m over the surface in this manner altogether under-assessment kerbside, close surface lead focuses. These outcomes show that helpless gatherings, particularly youthful youngsters, keep on being presented to fine, lead-and iron-rich, vehicle-inferred particular (Maher et al. 2008)

The aim of the research was to explain reasons of fluctuation in magnetic susceptibility of cement dust and the consequences for the environment. The research comprised measurements of magnetic susceptibility and Fe content in dust, and also in raw materials, additives, fuels, mixtures and clinkers used for cement production. The samples were taken in four cement plants located in Opole Province Žsouthern Poland. In addition to this, the influence of two production methods Ždry and wet. On magnetic susceptibility of dust and some aspects of ferrimagnetic minerals formation in the process of clinker burning were considered. It was proven that magnetic susceptibility of dust depends on raw materials and fuels but

especially on additives used for cement production, a method of production and the carbon monoxide content in gases from clinker rotary kilns. Statistically important linear correlations between magnetic susceptibility and Fe suggest that during clinker burning, ferrimagnetic minerals may be formed (Goluchowska 2001).

A point by point attractive investigation of three dirt profiles of Calcic Chernozem, LuvicPhaeozem, and OrthicLuvisol, depicted in the Soil Atlas of Bulgaria, was completed with a specific end goal to uncover the capability of attractive techniques for the portrayal of soil framing procedures and properties of pedogenic iron oxides. Thermomagnetic examination of weakness and SEM/EDX perceptions uncovered that the primary pedogenic mineral in each of the three dirts is fine grained superparamagnetic to single area maghemite. Warm dependability of this pedogenic stage up to temperatures of 500°C is uncovered by the fractional thermomagnetic investigations of defenselessness. Profundity varieties of attractive parameters and proportions point to the vicinity of stable single-area to pseudosingle space grains in humic skylines, the amount of which reductions strongly towards lower soil skylines. These attractive grain size changes are best communicated in OrthicLuvisol and reflect heightened procedures of translocation of substances descending (Jordanova et al. 2010).

We utilize bivariate scatter plots to represent varieties in chose rock attractive properties (low-field powerlessness anhysteretic and isothermal remanence) Neogene and Pleistocene remote ocean residue from 16 destinations in the Arctic Ocean, North Atlantic, tropical Atlantic and North Pacific Ocean, and the Arabian Sea. We will likely look at the stone's capacity attractive properties to separate the silt as per elements, for example, lithology, geological zone, and the prevailing method of terrigenous sedimentation, which at these destinations is by means of ice-rafting, by means of base

streams, or through eolian forms. Generally, connections between's dregs attractive properties and gross lithology are poor, and elements, for example, the source and transport way of terrigenous silt (and detrital attractive minerals), together with the activity of reductive diagenetic procedures, are the significant controls on the attractive properties. On the bivariate dissipate plots, destinations with real ice-rafted contributions tend to have high sedimentary ferromagnetic mineral fixations, moderately coarse Ferromagnetic grain-sizes, and scattered specimen point appropriations; interestingly, locales where we gather a critical base current supply of terdgenousmaterial have firmly assembled example point disseminations (Bloemendal et al. 1992).

The present's point study is to acquire a nitty gritty portrayal of fly fiery debris and adjacent anthropogenic soils from distinctive Bulgarian force plants, by utilizing coordinated rock attractive and traditional infinitesimal strategies. These consolidated systems, which empower a superior comprehension of the unpredictability of anthropogenic attractive stages, force the requirement for utilization of an interdisciplinary methodology in ecological studies. The joined utilization of both single grain and mass hysteresis estimations, consolidated with thermomagnetic examination and minute (optical, checking electron microscopy perceptions and vitality dispersive X-beam investigation) uncover the main considerations which control the attractive properties of the fly fiery remains. Optical magnifying lens perceptions on cleaned segments demonstrate that the complex inner structure (dendritic exsolutions) and specifically surface morphology of the fly slag particles are the explanations behind the watched critical disparity between the assessed attractive grain size and the physical grain size. Mass attractive concentrates show hysteresis parameters run of the mill for pseudosingle space and single area attractive states that are an aftereffect of superposition of the attractive reaction from particles with generally differing

grain size circulations. Attractive mineralogy found from the thermomagnetic examination is ruled by a magnetite-like stage, however in a few examples there is a noteworthy commitment to a stage with a lower blocking temperature of 500^{o}C, presumably showing the vicinity of substituted ferrimagnetics. The attractive mineralogy of the fly fiery debris is firmly identified with the kind of coals utilized by diverse force plants. The outcomes demonstrate a decent correspondence between fly fiery remains attractive powerlessness and aggregate Fe_2O_3 content which proposes the prevailing part of firmly attractive iron oxides. The attractive conduct of the anthropogenic soils is overwhelmed by the attractive sign from fly cinder contamination, in spite of the fact that commitments from pedogenic and lithogenic magnetite are likewise watched (Veneva et al. 2004).

2.3 MAGNETISM AND HEAVY METAL POLLUTION

As of late, the quantity of investigations of contamination and attractive intermediaries for natural contamination in created nations, particularly European and North American nations has steadily expanded from the 80's to date. Notwithstanding this pattern that demonstrates a positive enthusiasm for dealing with the earth and inquiring about into the ecological effect of a few human exercises, contamination studies in Latin American nations have been decreasing in number. Besides, investigations of attractive intermediaries for contamination are rare; specifically, investigations of this nature has been completed in Argentina in the course of recent years by Chaparro and colleagues. Investigations of attractive improvement in soils because of the copying component are talked about, and the consequences of smoldered soils influenced by flames of distinctive nature and characteristic soils are thought about, considering their attractive bearers. By thereby, this article bargains principally with the first investigations of attractive intermediaries for contamination led in an area in

Argentina. Soils, tidal pond and stream dregs from three ranges were examined. These territories contain La Plata, Chascom'us, and Tandil areas. The impact of contamination was explored in Tandil and La Plata, uncovering attractive upgrade and the vicinity of poisons just in Tandil soils. Then again, stream and tidal pond dregs were mulled over in La Plata and Chascom'us. Attractive bearers and the substance of some overwhelming metals were recognized and examined in both territories independently. Attractive parameters show unmistakable focuses and wide regions influenced by contamination. Besides, this attractive derivation is bolstered by the high substance of overwhelming metals, particularly lead and zinc. At last, another factual investigation of numerous connection examination concerning information from La Plata and Chascom'us ranges was attempted with a specific end goal to research the presence of a straight connection between sets of a few attractive parameters and a few substance variables (Marcos Chaparro et al. 2006).

Past attractive and geochemical investigations of stream dregs in the Northeast of Buenos Aires Province, in the Greater La Plata territory, have uncovered an abnormal state of follow components, particularly lead and zinc. Proceeding with these preparatory works, new examining destinations were considered keeping in mind the end goal to enhance and build the attractive mapping of this region. This a study's piece concentrates particularly on the attractive properties of residue from a cross-city stream. Such stream gets a variable poison load from urban, modern and diffuse sources. Focus subordinate attractive parameters, attractive transporters (para, against and ferrimagnetic) and their elements (e.g. milder or harder attractive bearer, grain size conveyance, and so on) have been ascertained utilizing attractive estimations. As per attractive parameters and substantial metal loads two fundamental unmistakable gatherings of sediment cores are recognized. The vertical appropriation of dregs uncovers a late anthropogenic impact,

potentially, fitting in with the last 20-40 years. Four out of all the attractive parameters (attractive helplessness, anhysteric remanent magnetisation, S-proportion and κARM/κ) were picked keeping in mind the end goal to examine their association with the substance of substantial metals. In every one of the cases, great positive relationships were gotten utilizing direct relapse. On the other hand, more huge connection variables were accomplished for grain size and attractive element subordinate parameters (κARM/κ and S-proportion) than for attractive focus subordinate parameters. Hence, the κARM/κ and the S-proportion appear to be the most important attractive parameters to portray the vertical and longitudinal circulation of overwhelming metals present in these stream silt. The nonsignificant relationship between substantial metals and focus subordinate parameters could be clarified considering the two's separation particular gatherings. The gathering having a place with the Coastal Plain demonstrates a reasonable straight pattern between substantial metals and attractive weakness and anhysteric remanent magnetisation (Chaparro et al. 2004).

As of late systems managing magnetometry have been proposed as a legitimate intermediary for evaluating the substantial metal contamination of soils. An aggregate of 113 topsoil tests was gathered from open stops and green strips along the edge of streets with high-thickness movement inside of the city of Isfahan, focal Iran. The attractive powerlessness (χ) of the gathered soil tests was measured at both low and high recurrence (χlf and χhf) utilizing the Bartington MS2 double recurrence sensor. As, Cd, Cr, Ba, Cu, Mn, Pb, Zn, Sr and V focuses were measured in the all gathered soil tests. Huge connections were found in the middle of Zn and Cu (0.85) and in the middle of Zn and Pb (0.84). The χfd estimation of urban topsoil fluctuated from 0.45% to 7.7%. Low mean estimation of χfd showed that the attractive properties of the specimens are predominately contributed by multi-area

grains, instead of by super-paramagnetic particles. Lead, Cu, Zn, and Ba indicated positive critical connections with attractive defenselessness, yet As, Sr, Cd, Mn, Cr and V, had no noteworthy relationship with the attractive helplessness. There was a critical relationship between's contamination burden record (PLI) and χlf. PLI was registered to assess the dirt natural nature of chose over whelming metals. In addition, the after effects of numerous relapse investigation in the middle of χlf and substantial metal focuses demonstrated the LnPb, V and LnCu could clarify pretty nearly 54% of the aggregate variability of χlf in the study region. These outcomes show the capability of the magnetometric routines to assess the overwhelming metal contamination (Karimi et al. 2011).

This paper discusses about the soil pollution due to combustion of coal with highly concentrated pyrite and metals. Fly ash is producedthrough combustion of fuel which is also rich in ferromagnetic materials. These also flow through the soil which can be identified using rock-magnetic methods. Magnetic susceptibility is proportional to concentration of materials. This paper explains the method used to monitor pollution due to airborne particles produced by combustion of coal. To determine contamination in soil magnetic mapping method is the most inexpensive method to map soil affected due to industrial pollution (Kapička et al. 1999)

Magnetic properties and pollution in Chascom are studied. The paper is mainly focussed on magnetic susceptibility, saturation, hysteric and isothermal remanentmagnetisation. In order to get results based on feature dependent magnetic parameter magnetic properties and chemical measurements are correlated. Results show that remanence correlate is up to 0.9094. Experimental results prove that magnetic phases are present in samples (Chaparro et al. 2005).

In this book different fractions such as,sand ,slit from black soil and alluvial soil showed traces of insoluble phosphate minerals belonging to plumbogummite group. An effective method to determine amounts of quarts and mica in the samples has been devised. Final results revealed that plumbogummite minerals were present in soil (Murti1970).

In this paper top soil across England's data are shared with data for soil type, concentration of bacteria for defining soil magnetism. In unpolluted areas magnetic soils have less magnetic substrate and more ultrafine super paramagnetic grains. In strong magnetic soils , magnetic bacteria are available in small amount. Minimum amount of samples show more values associated with magnetic particulars. The results showlink between secondary ferromagnetic minerals and a biological weathering, biological fermentation. The driving is Fe supply linked to climate (Dearing Hayet al. 1996).

This paper is focused on tracing , distribution and containments in soil along roadside using magnetic proxies. Gradient concentration and accumulation of possible pollutants in deep soil are also investigated. Pollution mapping is done by magnetic susceptibility. Strongly polluted areas have high susceptibility values influenced by traffic frequency. Magnetic signal in road side soil was due to magnetic-like phase (Hoffmann et al. 1999).

Concentrationof ferrimagnetic minerals are measured by magnetic susceptibility. In this paper the three field probers such as the Bartington MS2D and MS2F, Geofyzika KT-5 Kappameter to are used to measure magnetic susceptibility. Bartington MS2B probe and Geofyzika KLY-2 Kappabridge are instruments which are used for calibration. Samples were analysed and results showed that magnetic values of the samples were over 198% or they were underestimated by 42% when compared with MS2D probe. KT-5 Kappameter shows true susceptibility values referred to KLY-2 Kappabridge. Penetration of probes in soil is only up to a few centimetres.

MS2D probe reads 90% of susceptibility signal. KT-5 Kappamete at the first 2cm reads about 90%. MS2F probe reads almost all the signals in the 1cm range (Lecoanet et al.1999) .

On the biggest industrial centre of Estonia 531 samples were collected as a part of geochemical mapping under the project "Urban geochemistry of Tallinn" by NATO. Samples showed traces of magnetic susceptibility and other 40 elements. The studies objective was to narrow down the source of pollution and magnetic susceptibility. Correlation and factor analysis were used to magnetic susceptibility and elements found in soil. Higher values of magnetic susceptibility were foundin soil samples taken at maardu. The susceptibility was caused by geological and ferromagnetic minerals in rocks. Strong relation were found between magnetic susceptibility and CR and Pb in soils contaminated by pollutants from traffic and factories. To determine heavy metal pollution geochemical mapping and magnetic susceptibility were used (Bityukova et al. 1999).

In this paper Anthropogenic ferrimagnetics is studied in soil by means of temporal stability. Fly ash was used as pollutant and reactive medium was modelled using soil solutions. MSMS, FDMS were measured with different time periods. Independent of soil medium constant magnetic susceptibility values were obtained. non-stoichiometric maghemite phase eventually changed to stable phase. Temperature changes were also observed in some cases (Kapička et al. 2000).

Here we have the magnetic properties of salt-marsh soils exposed to intense atmospheric deposition of fly ashes from the iron industry in southeast France are discussed. The enhancement in the concentration of magnetic particles in the topsoil in this area is clearly observed. Low values of frequency-dependent susceptibility are characteristic of coarse multi domain grains and they were observed in surface samples. The anhysteretic remanent

magnetization saturation an hysteretic remanent magnetization ARM40 mTrSARM ratio versus isothermal remanent magnetization saturation isothermal remanent magnetization IRMy100 mTrSIRM. Ratio and the IRMy20 mTrSIRM ratio versus IRMy200 mTrSIRM ratio can be able to differentiate two different contamination emission sources. Magnetic methods used reflect not only the concentration of ferri magnetic minerals but also their grain size, thus the enabling discrimination of metallurgical dusts and fine pedogenic particles created in situ. The results suggest that pollution is not the only source but the pedogenesis also plays a role (Lecoanet et al. 2001).

Rock magnetic technique has been used to study pollution in different media. In this paper magnetic parameters are used as pollution indicators with relationship from heavy metals. The study was conducted on two different rivers in Tamilnadu to narrow down pollutants. Magnetic susceptibility, isothermal remanant magnetization were used to determine heavy metals in sediment samples. Samples were concentrated with ferrimagnetic minerals and some other magnetic carriers. Parameters revealed differences in samples between two rivers, such as magnetic susceptibility. PCoorda, PCA and RDA were also done which revealed relation between magnetic and chemical variables. concentration dependent magnetic were more related to this study than compared to other (Marcos Chaparro et al. 2008).

There is need for inexpensive method to conduct and test for pollution in surrounding environment due to industrial pollution. Soil magnetometry is a suitable method to test for pollution in some cases. For this method, knowledge of magnetite is needed. Magnetic materials are also produced by means of combustion fossil fuels in cars which is also a major factor. Magnetite, Fe_3O_4, can be easily used to outline areas affected pollution.

Anthropogenic pollution of magnetic mapping will be used to outline polluted areas in Czech republic and Germany (Petrovský et al. 2000).

In this paper, formation of lead phosphates in soil are accessed using thermochemical constants. The migration and fixation of lead in the environment is mainly controlled by interaction of lead and phosphorus. Calculations indicate that the solubility of lead phosphate is the limiting factor in lean ion in human body (Nriagu 1974).

2.4 MAGNETISM AND HEAVY METAL CHEMISTRY OF SOILS

Soil in Kathmandu have high magnetic susceptibility and isothermal remanence used to reduce environmental pollution. Magnetic susceptibility are one of the factors to define soil depth intervals in ranges, such as normal (10−7 m^3/kg), enhanced moderately (10−7–< 10−6 m^3/kg), enhanced highly (10−6 m^3/kg). Soils away from roads and industries are less affected by pollution and they fall into normal category. Soils close to road ways are highly polluted up to several centimetres. The concentration of pollution is higher on top and when it goes down it gradually decreases with moderate and on to normal category. Soil in urban areas have considerably moderate magnetic susceptibility. SIRM soil comprises of three components. (1)Soft 30-50mt (2) intermediate 120-180mt (3) hard 550-600mt. Suring daylight surface SIRM is mostly comprised of soft component meaning urban pollution has enriched magnetic like phase. Spectrometry of soil from samples reveal combination of copper zinc and Pb. Several metals are well correlated with magnetic susceptibility in Rani pokhari. At Ratna Park both magnetic susceptibility and SIRM have contribution of Zn, Pb and Cu and poor combination of Fe, Ni and Co. Polluted soil exhibit relationship with pollution index and elements such as Cu, Pb, Zn (Gautam et al. 2005).

In this paper method has been developed to identify fly ash originating from burning fossil fuels even at a long distance. But till now it has been difficult to find them. This technique uses particles measurement, microscopy and magnetisation. Ash from fossil fuel is in the form of spherical magnetite which is useful for this analysis. Particles are of high coercive than compared to other air bore particles. So the coercive gives an indication of fly ash. The fly ash concentration decrease with distance from source (Flanders 1999).

For mapping emission load over a territory soil magnetometry is used. This paper suggests that magnetic susceptibility is controlled by deposition of anthropogenic ferromagnetic particles. A map of top soil magnetic susceptibility has been compiled based on a study conducted on 460 sites. Higher values in magnetic susceptibility can be due to local pollution. Heavy metals of anthropogenic origin were present in top soil and correlation between Pb and magnetic susceptibility. Results show that magnetic mapping is a easy way to find levels of pollution in soils (Kapika et al. 2008).

This paper discusses about how good agricultural soils are developed on Pleistocene eolian sediments and how they are trapped in suburban and urban areas. Metal settlement in soil has been investigated in this paper. 331 samples were taken in Zagreb region, which were dissolved in aqua regia and were analysed for Cu, Fe, Pb and Zn with absorption spectroscopy. All samples showed average composition of materials. GIS is used to visualise spatial data and metals on topsoil is displayed. Statistical multivariate analysis are done by means of R-mode factor analysis. The top soil mainly comprises of Fe and Mn. Nickle is also a major contribution of top soil. The origin of metal due to various factors are also analysed in detail. The SAVA river has been exposed to pollution due to mining and industry. These areas have high concentration of Zn, Pb and Cd. The mapping shows a

clear relationship between human activities and concentration of metals in these area (Romic & Romic 2003)

Magnetic susceptibility -soil kappametry -test was done in the area of VSiKoSice. Test reveals higher concentration of heavy metal in soil. This method can be a quick and inexpensive method to detect heavy metals in top soil (Ďurža 1999).

In this paper according to heavy metal concentration anthropogenic impact can be evaluated. Metals such as Cu, Zn, Cd have affinity to create metallic bonds with materials of ferrous type. The aim of this study is to study magnetic and geo chemical investigation of road side urban soil in relation to environmental pollution of BeniMellal city. Samples were taken along 5km range of National road in BeniMellal, samples showed concentration of heavy metals on top soil. Soils taken near edge of the road showed high magnetic susceptibility. SEM coupled with RDX were used to discover pedo-lithogenic minerals and anthropogenic magnetic spherules. Presence of magnetite, hematite were validated by Mossbauer spectroscopy. Goethite are useful in absorbing foreign ions (El Baghdadi et al. 2012).

In this paper magnetic minerals in soil along Hangzhou City are measured. The SIRM and magnetic susceptibility's concentration decreased with distance from urban centre. Urban area soils had high concentration of Cd, Cu, Pb and Zn. Upper most soil had high concentration of heavy metals, magnetic susceptibility and its concentration decreased with its depth. Samples showed traces of SIRM, magnetic susceptibility, PLI. To detect environmental pollution, anthropogenic activities in growing urban areas, magnetic screening is an easy method (Lu et al. 2009).

Frequency dependent susceptibility are examined in this paper. This paper explains FDS in terms of behaviour of all upper paramagnetic grains. For a grain size of 0.01-0.025 pm range the FDS values were 14 to 17% and a max of 10-12% with a grain size of 0-0.03μm. Experimental and further studies support the model predictions with FDS percentage values relating to grain size within SP range. The concentration of SP grain in a sample can be estimated by mass specific term and FDS percentage. Presence of narrow distributions of ultrafine are caused by lower percentage of FDS percentage in soil. Paramagnetic and antiferromagnetic minerals present soils have low FDS percentage. Before these values can be applied to actual environment data, a prediction model is used to predict Sp grains in mixed grains (Dearinget al. 1996).

Geochemical analyses and minerals magnetic were carried out on surface sediments from India's continental shelf. The main need for this study is to analyze the environmental assessment about heavy metal concentrations and its effect in the coastal areas using techniques related to magnetic and also to understand on the factors controlling the metal distribution and of India. The relationship between heavy metals and anhysteretic remnant magnetization (XARM) can be detailed by the role of iron oxides contributing the link even though reinforced by the strong effect of XARM to be associated with the finer particle sizes. The higher value of magnetic susceptibility, SIRM and IRM20mt are associated with the coast presented in the earth shelf sediments suggest the existence of high ferromagnetic content, which is found to be derived from the weathering products of Deccan basalts . λ arm is as a normalize for particle size effect in which aluminum (Al) is always used. the relationship between heavy metal concentrations (Fe, Cu, Cr and Ni) and magnetic parameters showed a positive and strong correlation in the sediments present in earth coast (Alagarsamy 2009).

The advantage of magnetic techniques over the conventional methods is illustrated from a wide range of examples on the application of magnetic to environmental studies. Reconnaissance work could be done with the use of magnetic measurements from both the laboratory and field due to its flexibility and speed. Practical is within and between the lithosphere, atmosphere and hydrosphere by simple diagnosis as well as quantification of movement and transformation of magnetic minerals. The techniques of analysing mineral magnetic properties and intrinsic in addition with palomagnetic remanence, are described in subjects as diverse as hydrology, metrology, geophysics, ecology and sedimentology (Alagarsamy 2009).

In this paper the magnetic property of the tropics in Delhi is used to characterize the polluted areas in the terms of grains (magnetic domain) concentration and magnetic minerals which as a feature of other mutagenic pollutant concentration and toxic metals. The magnetic saturation remanence (MRS) and saturation magnetization is taken as a proxy for the ferromagnetic mineral concentration. However, the portrayal of anthropogenic magnetic a fraction from the lithogenic (geogenic) magnetic fraction was done by diamagnetic/paramagnetic contribution of soil along with the fact that the clean and fresh soil comprises higher diamagnetic and paramagnetic minerals than polluted. Predominantly, ferromagnetic minerals (maghemite and magnetite phase) dominates the top soils of Delhi. Significantly the highest concentration of ferromagnetic minerals is found in the industrial areas with negligible diamagnetic/paramagnetic fraction which leads to the contribution of anthropogenic .Densely populated areas and heavy traffic of Delhi provides a moderate to low soil pollution, whereas the green areas show lowest with higher diamagnetic/paramagnetic contribution. Pseudo-single domain (PSD) magnetic grain is dominated in Delhi though the industrial areas of Delhi show coarser multidomain (DM) grains when compared to stable single domain (SSD) in forest areas. Our study shows that the grain particles which

are fine does not reveal a significant link with the higher concentration of ferromagnetic minerals at least in the soils. The existence of the anthropogenically produced spherules and the lithogenic magnetic crystal in the forest soil in industrial areas and the higher concentration of the heavy metal in Delhi soil enhances our findings (Meena Maiti & Shrivastava 2011).

The study of this paper focuses mainly on magnetic susceptibility analysis and processing towards cost-efficient and fast semi quantification and discrimination of anthropogenic heavy metal loads in the soil. A set of soil cores, which from both "less polluted" and "polluted" forest soil are used to investigate spatial variability magnetic susceptibility close the steel mill located near Leoben, Austria. The test sites which are of ~10m^2 represents "site scale" dimensions. The statistical analysis on the magnetic data gives a boundary path showing the transformation from "polluted" to the deeper, "unpolluted" areas in the contamination of natural soil. The simplification of the complex variations of individual's curves was after the introduction of block master curve and it also represents magnetic susceptibility at "site scale". The requirement for linking the block master curve with the heavy metals is a magnetic susceptibility data from one soil core and few heavy metal data of two sub-samples from the same core. The applicable tool for semi-quantify anthropogenic heavy metal loads in the soil was optimizing produced by magnetic susceptibility data processing scheme (Blaha et al. 2008).

The measurements of magnetic susceptibility were performed on samples numbering upto 2000 of forest soils from the ortrava-karvina industrial region(Czech part of upper Silesian coal basia) and the Moravian-silevianbaskydy mountains and its area, podbeskydi.1200 samples from the same set is used to determine the concentration of related elements. The major sources for risk elements and magnetic particles are present in industrial

facilities (metallurgial industry and power plants) located in this region containing soils within the neighboring mountain areas and in the industrial region. A clearly correlated relationship is between magnetic susceptibility and zn,as,fe,cu and pb concentrations in soils. The magnetic susceptibility is inversely proportional to the distance from the sources. The behavior of the individual chemical elements during deposition and transport can be known from the studies by means of ratios of magnetic susceptibility values and concentration of elements. Magnetic susceptibility (Fe and Zn) materials correlated closely with metals were deposited along with the dust particles, whereas metals such as As, Pb and some trace amounts of Zn are able to create independent particles which tends to be components of long distance deposition and transport. The elevation of sampling site is being dependent by the concentrations of a Pb and also in some part Zn in soils. They are enriched in the uppermost part of the mountains. Other elements which on studies revealed that they don't have relationship with sources of air pollution nor even with the geomorphology of the area .It is seen that underlying sedimentary rocks comprising some concentrations of chemical elements such as v, Cr, Rb, Sr, U, Zr, Bi, Ti, Ca, and Mn (Matysek et al.2008).

Magnetic particulates in the earth, gathered from surfaces and specifically from the atmosphere, are reported. A critical rate of attractive material in numerous air-borne tests comprises of round magnetite from coal-smoldering utilities and from iron/steel fabricating with molecule distances across 2-10 pm which relate to normal coercive fields of - 100 Oe and remanence to immersion proportions of - =O.l. The measure of air-borne attractive material that settles to the ground differs conversely with separation from its source (Flanders 1994).

The Northern Iberian edge is a commonplace illustration of a mainland edge subjected to regular profoundly vivacious administration

(waves and tides) and getting inputs of mainland dregs by means of riverine releases. The central objective of this study has been to utilize dirt minerals as pointers of sedimentary progress in the open rack framework. The conveyances of mud mineral in the top layer of the sedimentary spread are demonstrated to be identified with their mainland sources, additionally mirror the impacts of winter tempests and long shore streams in deciding the pathways of dregs transport. The mineralogical sythesis of the material issuing from the waterways is fundamentally the same to the general mineralogical sythesis of the fine divisions of the seabed residue. Those stores that are straightforwardly affected by riverine releases have higher substance of kaolinite (20%), while those that are not have higher substance of illite (80%). The accessible information show no huge amounts of terrigenous particles are being released from the Spanish rias. Hence, we presume that physical procedures are controlling the mud mineral appropriations and that, notwithstanding commitments from the Minho River, the fundamental wellspring of fine detrital particles to the rack area is the Douro River release. These particles settle on the center rack, beneath the 60 m isobath. Amid tempest occasions these particles are re-suspended furthermore, advected northwards to the Galician rack or into more profound areas. Accordingly the appropriations of the dirts demonstrate there is a net transport of fine residue both northwards and off-rack (Oliveira et al. 2002).

Procedures of iron mineral authigenesis, diagenesis, and disintegration, in communication with essential inputs of iron minerals, act to deliver vertical separation of soil attractive properties. Along these lines, attractive iron oxides, in the same manner as other iron structures, might both react to and reflect soil shaping procedures. Examination of the level of noticeable and diligent attractive separation inside distinctive soil materials can give bits of knowledge into the nature and heading of particular arrangements of soil procedures. Proof of clear relationship between attractive

variety and discrete sorts of soil environment additionally has connected hugeness, in a few zones of ecological study: for instance, the watched attractive variety can be utilized to separate between individual soils and soil skylines, for the reasons of soil looking over, residue "labeling" and following, and experimental demonstrating of source-silt linkages. This paper reports the utilization of mineral attractive methods to portray the iron oxide arrays inside of soils of differing sort and provenance. The impact of diverse pedogenic administrations havebeen researched through estimation of a scope of attractive parameters (counting attractive powerlessness, recurrence subordinate weakness, and anhysteretic what's more, immersion remanences). In opposition to current pedologieal thought, yet as per other, attractively based, studies (e.g., Mullins), the vicinity of magnetite/maghemite (commonly of superparamagnetic-single space grain size) inside of soils has been found to be a to a great degree far reaching wonder. Its contemporary neoformation inside of the dirt environment is induced. In any case, the information of misleadingly produced ferrimagnetic material is demonstrated for one of the attractively "upgraded" soils analyzed here, and the likelihood of unessential wellsprings of magnetite in topsoils ought to be considered some time recently pedogenic procedures of attractive upgrade are derived.

From the information introduced, segregation of mechanically determined attractive particles seems conceivable, on the premise of their low levels of recurrence ward defenselessness (Xm), low anhysteretic remanence (ARM), and separation from the better, dirt estimated (< 2 Fm) parts of the dirt. Not the arrangement but rather the dynamic disintegration of ferrimagnetic minerals is demonstrated for soils influenced by the procedures of gleying and podsolisation. Eluvial skylines of podsolised profiles exhibit verging on aggregate loss of recognizable attractive substance; varieties as the iron reprecipitated in the hidden illuvial layers may reflect contrasts in the pedological qualities of these skylines. Inside gleyed (waterlogged) soils,

procedures of magnetite disintegration have all the earmarks of being grain size-particular; special lessening of those grains of ultrafine (superparamagnetic) and fine (single area) attractive grain size is shown. Where soil shapes a noteworthy giver to catchment residue loads, this has criticalness in the territory of source-silt demonstrating. Soil got from for all time wet or exceptionally filtered catchment ranges is unrealistic to add to tops in the attractive substance of saved dregs; further, just those erosional procedures that work at a quicker rate than those of attractive consumption will have the ability to deliver crests in silt ferrimagnetic focuses, for example, have been seen inside of the verifiable attractive record(Maher 1986).

Biometic study was done in rome to study pollution based on magnetic properties of tree leaves. Magnetic properties of different tree leaves were compared. Results showed that leaves of ever green tress showed higher magnetic intensities than compared to other species. Leaves of ilex and Platanus are commonly available and are used to monitor traffic pollution over two different periods, one in October 2001 and the other in August 2002. There was a strong difference in magnetic susceptibility from the leaves collected in traffic areas and green areas. Samples from road side, rail was showed larger magnetic particles than compared to samples collected from green areas. The results show that tree leaves can be used to monitor and identify air pollution in urban environments (Moreno et al. 2003).

In this paper, how soil is influenced by ironworks is studied. The research was carried out at five different places of which Ostrowiecwi_tokrzyski is explained in detail. Based on samples taken a magnetic susceptibility map was created. Magnetic susceptibility measurements such as isothermal remanent magnetization, geochemical analysis were also carried out. Ferromagnetic fractions are identified by SEM.

Heavy metal pollution was determined by this method (Rosowiecka & Nawrocki 2010).

Here, this study identified that England topsoil has increased the amount of magnetic susceptibility and the pollution like fly-ash is produced in it due to the anthropogenically presence. They studied this by taking samples from whole England for about 1176 sample which have taken in the 10km gap between each sample and at both high and low frequencies the magnetic susceptibility was tested using χ If and χfdr criteria the pollution presented in the soil is identified. The contaminated topsoil is positioned in the midlands, south-east around London, Merseyside, the north around the Manchester conurbations and West Yorkshire and Teeside. In the soils, heavy metal concentration is pushed above the background which will have good relation with magnetic susceptibility and other parameter of the magnetic (Hay et al. 1997).

Mineralogical, textural, micro faunal and geochemical data were learned along the OMEX core. The NW Iberian outer continental shelf Galicia Mud deposit KSGX40 was recovered off the Rio de Vigo. The record of the core is 4.8cal D.P, from bottom to the top, of a sedimentary sequence displaying a upward reducing in grain size. The core sediments are largely composed of quarts, siliciclastic, plagioclases, K-feldspars and physlosilicates which show a high continental influence on the zone(Martins et al. 2007).

The qualitative proxy identification is being viewed with the help of the environmental magnetism which is being distributed with the anthropogenic, which will be conducting the organic materials and heavy metals. In this generation there have been proposition of a quantitative magnetic proxy that is being used for viewing the temporal and spatial patterns in the specific area which is covered by all. The Korea and Seoul will

collect some of the samples on the roadside with the approximate range of 1353. Predominance is being identified by the electron microscopy and the thermo magnetic data, which is given by carbon bearing iron oxides, which is being indicated by the anthropogenic that will particularly originates the fossil fuel combustions. The anthropogenic is being quantified as a particulate of the apparent magnetic is being calculated as follows AMC Fe_3O_4 is being explained as seasonal dependences. The pollution initiation is majorly innovated through the south-western industries (Kim et al. 2009).

During the last 130ka period, the variability of southwest monsoon are found out using southern desert margin sequences of fluvial and acolian which are exposed by field stratigraphy, luminescence dating and sedimentology. In the period between 130-120 ka exist a sediments textural attributes and the sedimentary architecture, suggested the meandering river system result to developed conditions of southwest monsoon. During the 120-100 ka change over from a meandering to braid indicate a reduced precipitation phase bedded calcretes and flood fines presence during ~100-70ka suggested enhanced monsoon period with seasonality after that during 70-60 ka a phase of weal monsoon was observed. The increased south monsoon condition during the period <60-30 ka are indicated by paedogenesis and aggradations of regional flood plain. The dry climatic condition indicated by the initiation of a regionally extent Aeolian sedimentation and onset of flavio – aecolian sedimentation. These observation accords well with TOC (total organic carbon) data and moisture/vegetation control in the region on Aeolian sedimentation are suggested (Juyal et al. 2006).

The delegate structures can be preserved and it is being blinded with the malicious filaments and the cyanobacteria tolerate which is with the hydrological regimes. The rainfall can be controlled by the hydrological setup, and it can be served as bio meters, it is also distinguished in palaeonvironment

scenario and ecological shifts ranging which is being imitated from late Pleistocene at the earlier stage of the Holocene in the analysis of boreholes in the south Kerala basin. The various morphotypes of Rivularia which will be somewhat different which will be somewhat different which will be represented by the Rivularia sp and Gloeobacteria sp. That is variated at different levels in the sediment profiles and it will be reflected at its signatures of hydrological modifications that is being combined and enhanced with the wetland system. The cynobacteria is being same in the ayiramthengu and panavelly in the beginning of Holocene which is too small enough in its signal that is related with the precipitation. The beginning the earlier stage of Pleistocene and the Holocene section will have the cynobacteria which can be reflected and rejected in the rainfall and prevalence for a long term of dry space. The beginning and the middle period of the Holocene will get an turnover of cyanobacteria is being prolific, since it is because of the optimum rainfall, the beginning of Holocene or at the late period can have the size in big or to be small which is carbonised and also the little colouring of the morphotypes are grouped with those hydrological modifications, that will give an result as the high or low rainfall which can be declared in the beginning at the late Holocene. The cynobacteria will contain potential to determine the stabilization and adaptation with various eco and morphotypes with perfect space and time, the climatic change can be specialised with better biomarkers for the additional palaeodata (Limaye et al. 2010).

Using the energy values which is taken by the emission of radiation on transformations of nuclear given in the current evaluated nuclear structure data file (ENSDF). A few percent lower is used than used previously for the radiation factor of beta and gamma. A particle ranges based approach is used for the alpha dose-rate effectiveness and the values of the results are given (Adamiec & Aitken 1998).

In the south-east cost of India, In Vedaranniyan region of Tamilnadu on Cauvery delta region on costal dunes are noticed which are occurred in widespread for the better understand and to form the chronology of their formation those dune studied using optically stimulated luminescence (OSL) where the sedimentological studies are also combined. The widespread periodic dunes in the south east coast of Indian were formed on the recent time during the late Holocene due to variety of reason like the variation in the climatic condition and due to the land usage changes; those are resulted from the study of the dunes. The mobility of sand index shows that during past century dune were active in the Sothern part of Nagapattinam. In the northern Cauvery delta crests were active in Cuddalore region. The dune are suggested be formed from short region from their freshness and angularity and for the formation of the dune a sources proximal sand deposition is proposed. As result of the study demonstrated the India's south east coast sand dunes are sensitivity to the changes in the land use and climatic variations (Alappat et al. 2011).

During late Quaternary, the interlacing network of wetlands were evolved and endowed to the Kerala coast located in southwest region of India. The wetland lands presented around the Kollam district of Kerala shows the antecedent characteristics and is decorated on the sediments of Neogene. This wetland includes Holocene sediments deposit for the thickness of around 20.0-35.0m which contains good location evolution archives and climates changes. At about 8920±110BP the Holocene sedimentation was initiated and they are mainly represented by carbonaceous clay or sub-fossil wood/ peal. In the middle of Holocene brackish water is presented. The proposed model revels that many wetland bodies are evolved from the protoestuarine basins wetland bodies like Chelupola lake, Sasthamkotta lake, Kotta lake and Chittumalachira lake during the climatic optimum of Holocene, due to the

alluvial sediments progradation. The pre-Holocence Ashtamudi and Paravur estuaries upper arms are cut off (Padmalal et al. 2011).

The “old red sand” development formation environment on the south china coast is examined as per the laboratory works and field investigation. The “old red sands” on the south china are believed to be the sediments deposits of the aeolian during that period of time the level of sea were lower than the present time and under the wet and hot climate the laterization were took place. During the period of postglacial and interglacial time there was a high sea level. The hematite and goethite differential solubility is determined on 0.1M HCl at 85 degree Celsius. The calculation showed that limonitic goethite which is finely divided is thermodynamically unstable to plus water of hematite under all geological conditions. This indicates that the red sediment from the ancient times are believed to be originally in the colour of yellow. On the surface of the mars also the limonitic goethite will be thermodynamically unstable which is cleared from the analysed data (Wu & Wang 1998).

One of the periodically changing landform is the shoreline in coastal area, hence to understand the various dynamic features of coastlines and costal process in efficient manner a frequent monitoring and accurate detection of shorelines is required. This study is about th investigation of the coastline area between Tuticorin and Kanyakumari of south India for the shoreline changes, where after tsunami 2004 a continuous morphological and hydrodynamic changes occurs. To extract the data of the shorelines multi-data satellite data of Indian Remote Sensing (IRS) satellites is used. Using the ERDAS IMAGINE 9.1 software the data is processed and by using ArcGIS 9.2 workstation the data is analyzed. Many maps are developed based on the shoreline changes and the changes in the shore line are analysed by the survey of India toposheets. The current study indicates that during the period of

1969-1999 the accretion was main along the study. As per the recent study erosion is experienced by most of the coastal areas. On some coastal area shoreline reversal modification is indicated by the study. The headlands costal area experience both accretion and erosion. Though the erosion in the coastal area are occurred due to the anthropogenic activities and natural activities, the main reason is the sand mining in the coastal area than any other land. Hence in the seashore sand mining industries a sustainable management concept should be incorporated (Sheik & Chandrasekar 2011).

The lake level fluctuations and regional water table during the Holocene, over decades to centuries is revealed by the Lunkaransar dry lake sediments. Which is presented in the north western region of India. They are very shallow lake and in the holocenec period it is fluctuated often and then around 6300 carbon- 14 years ago it rose abruptly. During 4800-14 year ago the lake got dried completely. The wet period overlapped with intense dune period at the end. The harrapan – Indus civilization started and grown in the region 1000 years after Lake Dryed during arid climate and with the lacustral phase it never synchronous(Enzel 1999).

On the India east coast area, along from cap comorion to Rameswaram a high ride level is present which exposes an pack stone and sandstone bed of Holocene , intertidal fossil and hermatypic coral colonies bearing grain stone and of a hate Pleistocene high stand . it is free from hate quaternary seismogenic movement indication since it being a passive margin boundary .this area is used to describe small changes occurring in the sea levels during the Holocene high stands and late Pleistocene .In the area Holocene high stand sea level indicators occurs, and also along Godavari delta fringes further north (Banerjee 2000).

The dry land and deserts science were truly changed by the luminescence dating and it is revised the today’s sedimentary conventional

interpretation records and stratigraphic correlations. on the global desert paleoclimatology this contributes a key questions ,also in the desert luminescence age meaning and it is also deliver a review about Aeolian sand records of luminescence date. The paleoclimatology of dry land changed to quantitative science from a qualitative science for which the luminescence dating played a major role on it. In the past, Aeolian sedimentation occurred in the frequent interval of time and for short duration of time that was the key inference. During the specific climatic changes an accentuated Aeolian aggradations occurred, by an transport, optimal combination of sediment supply and by erosion the changes timing is determined for desert paleoclimatology, New development method are outlined by the reviews (Ashok et al.2008).

Here in these paper new methods is proposed for calculation optical ages by using the light sensitive component of partially bleached sediment. During the subscriber measurement for the bleach of laboratory at simulation a technique called partial differential bleach is used. The methods are proposed based on results of on this. Simulated luminescence of infrared from the diverse depositional environment fine grain sediments. From the result optical dating shown that on the poor bleached sediments the results are improved, on the primary stage this technique is used to applicable of silt-sized sediments where an for single grain dating is not applicable (Lang, n.d.).

In the central Sri Lanka, on the Horton plains national park. From mire at ca 2200 ma a.s.l a 6m long core was subjected to chronostratigraphic, litho and bio analysis since, it seen to be consist of mixture of classic articles and organic matter. The pollen spectra proposed, semi – and condition and a community of species plants from >24000 up to 18,000 calyr BP are connected with weak south west monsoon (SWM) the monsoonal require change are due to the result of the fluctuating between the humid condition

and relatively dry condition in during late Pleistocene time. The expansion of upper moonstone rain forest (UMRF) resulting from the semi-humid climate, which is caused by the onset of the monsoon. The two dry climatic events avoided the SWM strengthening, each two dry climate last ca 1000 years .pre humid event characterised the early Holocene. Which is followed by a hyper humid event is influenced by a further SWM strengthening. The semi and climatic condition makes marks a mark by trend for the middle Holocene. The SWM rains are strengthened again by this late Holocene (Premathilake & Risberg 2003).

The late quaternary evolution is discovered while addressing two hole are collected from the meeting point of the Kallada River with Ashtamudi Lake in India's southwest coast region for sedimentological and palynological analysis .from the two samples, one of the sample taken at pangod finds, at the base there is a fining upward sequence (Nair et al. 2010).

The preceding 40 kyr BP until 28 kyr BP, a general decrease in $^{\delta}13$ C of - 19 to - 18 for every mil. At around 16 kyr BP a sharp inversion in $^{\delta}13$ C to a top of - 14.7 for each mil shows an unmistakable power of c4 veggie lover connected with bone-dry conditions, conceivably amid or soon after the last Glacial most extreme. A wet stage at around 9kyr BP (the Holocene ideal) with strength of c3 vegetation sort is watched, while bone-dry conditions are re-built up amid 5-2 Kyr BP with a general predominance of c4 vegetation. New information don't bolster the event of a soggy stage matching with the medieval warm period (at 0.6 kyr BP) as proposed earlier. overall, the atmosphere and vegetation in the high elevation locales of the southern Indian tropics appear to have reacted to past worldwide climatic changes, and this is reliable with different proofs from India and other tropical dis (Rajagopalan et al. 1997).

A weathered store in South China is far reaching on the waterfront zones of Fujian and Guangdong territories, China. This store comprises of somewhat solidified, medium-to fine-grained sands, and is portrayed by its shades of red, chestnut red, light rosy cocoa or dull yellowish orange, and is normally called "Old Red Sand". The vulnerability in its arrangement age has been a noteworthy deterrent to the investigation of this sort of store. In this paper, optically animated radiance (OSL) strategies were utilized to date the "Old Red Sand" residue from Jinjiang, Fujian Province, China. The impact of the geochemical conduct of uranium and thorium in dregs amid compound weathering on estimation of yearly measurements was explored. The outcomes demonstrate that the adjustment in yearly measurement because of weathering represents a noteworthy issue for the optical dating of such weathered residue. The optical dating of these weathered stores will create mistaken ages if normal yearly measurement amid internment can't be accurately assessed. For the profiles mulled over, the OSL dates acquired on tests from the upper part don't speak to the internment age of the examples. It is exceptionally likely that they are thought little of because of the aggregated radioactive components as an aftereffect of concoction weathering. It is reasoned that adjustments in yearly dosage because of concoction weathering must be considered when dating comparable residue in South China. With a point by point examination of the OSL dating results, the marine's order porches around there was recommended. The most reduced porch was shaped at ~3.5 ka and the second patio was dated to ~74 ka. The age of the most elevated porch may not be built up precisely, but rather is surmised to be more seasoned than the obvious OSL date of ~77 ka as is the Paleolithic curios from it (Zhang et al. 2008).

In this study hills from south east India were dated utilizing optically invigorated radiance (OSL) to reproduce the depositional history. A belt of rises has created parallel to the coast in the middle of Pondicherry and

Karikal in Tamil Nadu, south east India. In the region in the middle of Cuddalore and Porto Novo the hill belt is 5 km wide. A transect from the coast to the most western ridge inland was explored. Changes in the ecological conditions are recorded in the rises. They show components including unconformities, alters in the course of sheet material, erosional elements, water departure structures and remainders of human settlements. The OSL results demonstrate that solid changes in the natural conditions happened around 100 and 300 years prior. The last occasion stamps additionally the end of settlement in this spot. The settlement period began around 1500 years before hand. The times of sand versatility and adjustment of the area surface by soil arrangement correspond with changes in the precipitation record of India. The examined hills likely reflect vacillations in the storm movement amid the most recent 3500 years in south east India (Kunz et al. 2010).

Red colouration in dune sands results from the presence of ferric oxide which is derived from the weathering of iron-bearing minerals. There are five basic requirements for reddening to occur: 1) an iron source; 2) availability of a minimum amount of moisture; 3) oxidizing interstitial conditions; 4) sediment stability; and 5) sufficient time to allow the build up of iron oxides. Climatic conditions are favourable for reddening in both the arid and wet tropics, but the length of time required to attain a given state of redness is likely to be greater in the arid tropics. Reddening in temperate humid climates is very slow and may not occur at all in cold climates. Stability and subjection to pedogenetic rube faction greatly accelerates the rate of reddening in dune sands. Actively moving dune sands may redden very slowly but the maximum degree of redness which can be attained is probably limited by abrasion during aeolian transport. The time required for reddening cannot be regarded as an independent variable but is dependent on

temperature, moisture availability, sand mineralogy, degree of stability, and significance of aeolian dust input (Gardner & Pye 1981).

To examine the applicability of the magnetic mapping for the purposes of heavy metal pollution of urban soil in large region two types of soil namely fluvisols and anthrosols are collected from different environmental conditions such as suburb and industrial area in central China, Wuhan. Chemical analysis and magnetic measurements indicated heavy metal concentrations and elevated magnetization of topsoils in the industrial area. Saturation isothermal magnetization (SIRM), magnetic susceptibility and anhysteretic remanent magnetisation (ARM) of fluvisols are found to be much higher than those in the anthrosols, but it is contrary for frequency- dependent susceptibility, it strongly shows that the soil magnetism depends upon soil type/condition. Predominant magnetic carrier found at topsoils of industrial area is multi-domain magnetite/pseudo-single domain. Energy dispersive X-ray examination/environmental scanning electron microscope of the magnetic extracts from the topsoils provide abundant spherical shaped particles of diameter 10-50 lm which are seemed to be rich in iron-oxides, and can be used for the nearby industrial activities (e.g., steel work and power generation). There exists a significant correlation between concentrations of Cu, Pb, Zn, Hg Tomlinson pollution load index and magnetic concentration-related parameters (e.g., v, ARM and SIRM). The results on the discussion showed that the magnetic proxy mapping of the soil pollution is a fast, inexpensive and effective tool for the delineation of heavy metal pollution. However, magnetic properties interpretation for a such a kind of purpose must be done on a site-specific basis, taking on a account the possibilities of pedogenic depletion/enhancement under some specific soil condition (Yang et al. 2012).

Reliable stratigraphic markers were formed from the organic deposits derived from the mangrove swamps within the Late Quaternary sequence of Kerala-Konkan Basin. Such deposits were found for three generations. With a few dates beyond the radiocarbons the older one was dated 43,000-40,000yr B.C., and the Late Holocene (<4000 14C yr B.P.) and the latest ones date from Middle Holocene to latest Pleistocene (10,760–4540 14C yr B.P.). The analyses confirmed by Pollen say that mangrove forests provide the most deposits. Excess rainfall correlated with peat accumulation on the period 40,000-28,000 BC yr, which is 40-100% greater than the modern values, of the Asian summer monsoon. The low occurrence of mangrove was calculated between 22,000 and 18,000 BC yr B.P which can be attributed to prevailing aridity or/and reduced precipitation which is associated worldwide with Last Glacial Maximum, because that the exposure layers and ferruginous surface are commonly found in this period. High rainfall was found in 11,000-4000 BC yr B.P. as the mangrove reached the growth of around 11,000 C yr B.P. but with periods of punctuated weaker monsoons. The results show that after 5000 or 4000 C yr B.P. the monsoon will reduce gradually leading to drying of marginal marine mangrove ecosystems (Kumaran et al. 2005).

The outcome provided above, and the consistency which is recorded overall, closely provide feasibility of dating the red-sand beds. In the Sri Lankan context these results, based on available data, tend to support two or more episodes of dune formation. The TL dates also shows that the sea level in that region which cannot be explained solely on glacio-eustacy and quite probably was subsequently affected by either the regional tectonics or had a geoidal component or both. This will be the aim of an extensive programme now in progress. Archaeologically the TL dates unambiguously assign geometric microliths on age of ca. 25,000 years much older than the age range of 4000-8000 years B.P. as believed so far (Singhvi et al. 1986).

In TL dating methods based on quartz inclusions it is necessary to take into account the attenuation of the beta radiation by the grains. The beta dose-rate experienced by the inclusions can be determined directly by replacing the grains by similar sized grains of a more sensitive TL phosphor. A more convenient method is to determine first the infinite-matrix dose-rate, and then apply a correction factor for attenuation that will depend on the size of the quartz grains. As the stopping-power values for the quartz grains and the clay matrix are almost identical, the attenuation factor for a grain will be equal to 1minus the absorbed-dose fraction or self-dose that would result if the grain had a content of radionuclides equal to that of the matrix. Attenuation factors may be obtained, therefore, by calculating absorbed dose fractions to grains embedded in clay. Absorbed fractions of the dose contributed by beta particles, internal conversion electrons and Auger electrons from 40Kand the 232Th and 238U series were calculated for spherical quartz grains with diameters ranging from 0.005 to 10.0 mm. The calculation was based on the tables of absorbed-dose distribution around point isotopic beta sources compiled by Berger (1971, 1973) in conjunction with the scaling procedure developed by Cross (1968). Finally, combined absorbed fractions for the three nuclide groups were obtained for two typical abundances of radionuclides using the conversion factors given by Bell (1977) as weight factors (Mejdahl 1979).

Magnetic susceptibility was applied in many recent studies mapping as tool for the monitoring of preliminary pollution using the Barington MS2 Meter. A standard procedure was introduced in the previous paper for which the compatibility for set-ups of different instruments and subjective (human) influences was tested (Stud. Geophys.Geod.46 2002 43).Long term reproducibility was tested on this procedure. For this purpose, the magnetic susceptibility is measured in two fields West Austria on a regular grid of 10_10 km and 129 sites located in North. The results of the

measurement were distributed normally; in 94% cases there magnitude lies within the instrument biases. For sites located away from the pollution source the susceptibility was found to be constant. Repeatability was affected by the following factor: positional precision of navigation, in homogeneities within the place measured, plant cover and anthropogenic activity, different equipment sets used. The samples of magnetic susceptibility of soil reference materials taken from the in situ measured sites correlated with the readings measured in the field. The proposed method comprises both repeatability and sensitivity and for delineating polluted areas it can be applied as a large data set acquisition (Boyko et al. 2004).

This paper reproduces the microscopic fluctuations and their effects on the doses distribution is quantified in quartz. Here, they computed the dose to quartz grain according to the hotspots spatial configuration within the beta range of maximum sphere and averaged all possible configurations for achieving distribution of dose rate. The distribution of dose is exchanged positively. For such distribution the net effect is calculated as a function of concentration of potassium. For the samples well bleached with the potassium content, the results suggested that (a) zero doses grains receiving probability is negligible, (b) doses distribution is large. They suggested a concept of reduced dose trough percentile distribution function analysis. This study shows that the from a single grain paleodose distribution the ages can be computed, which is indicated by the paradigm shift (Mayya et al. 2006).

From this study and the other researches it is indicated that long-term grouping of the U polluted environment results in U is precipitated under Oxic condition as Fe-Free U (VI) and also U (VI) Oxide phase is reducing under microbially reduction condition and U structural incorporation in host Phases of other mineral. In the aqueous system, those Mechanisms delay the

U transportation. The Other studies aim to U incorporation into mineral Phases of crystalline in natural samples (Duff et al. 2002).

This paper is about the purification of the quartz for the luminescence dating for which they using a magnetic separation method. For this study they using 15 years old equipment called “Frantz Magnetic Barrier Laboratory Separator Model LB-1”. It can be used in normal neon light or under subdued orange lights; the separator is located in the light-tight room (Porat 2006).

2.5 INFERENCES FROM LITERATURE REVIEW

Till now then from the review of literature, the study of texture for various teri sands were analyised and also researchers inferred the terideposits, which derived from the exposed continental shelf for a period of low relative sea level and theyobserved the sediments which are transported in high landward winds. The teri sands which is rich in heavy minerals like ilmenite, rutile, zircon, garnet, monazite and sillimanite are analysed for there magnetic and chemical properties. In this thesis we study and analysed the relation between the teri sand deposits and their characteristcs due to the climate such as dry and wet and the presence of the hematite and magnetite in terissand. The chemical paratmeters also analysed for their size and impacts. To have a clear cut analysis between the climatic changes and the magnetic and geochemistry of the sands is proposed in this study.

CHAPTER 3

METHODOLOGY

3.1 INTRODUCTION

This chapter deals with the various methods employed in the collection, processing and analysis of sediments samples used for this investigation. The present investigation consists of different phase and explained in following flowchart (Figure 3.1).

3.2 SAMPLING

Using small earthmovers, various trench sections were made to collect samples. Approximately less than 1 m of loose sand was on the topsoil. Samples were collected at 10 cm intervals, along vertical profiles, and collected samples were carefully packed in plastic bags and labeled. Five profiles were made in different areas by coastal and near coastal deposits. In a few areas, it was a serious challenge to make trenches because, due to the loose sand and high wind energy, the trench was closed in a minute. But finally after a lot of trials, it was possible to reach various depths.

The samples were analysed for sediment logical sedimentogical techniques, geochemical studies, magnetic studies, X-ray diffraction and geochronological dating using optically stimulated luminescence (OSL) technique. Textural studies on the sediments were performed for sand, silt and clay distributions (Ingram 1970).

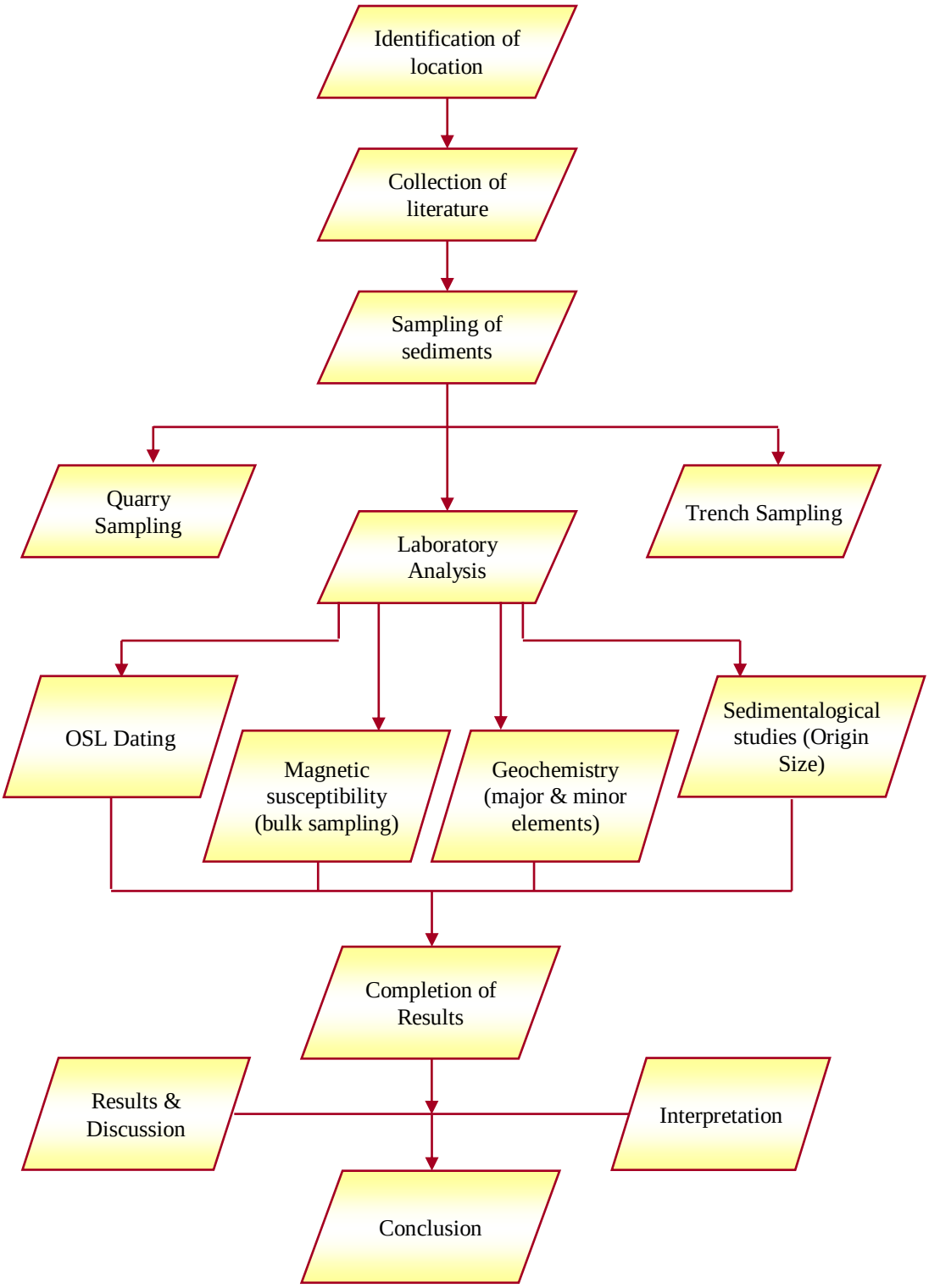

Figure 3.1 Methodology Flowchart

Determination of calcium carbonate ($CaCO_3$) was performed following the procedure of Loring & Rantala (1992). Grain-size analysis was done with the mechanical sieve shaker using a set of sieves with mesh size ranging from 18 – 325 ASTM. In microns it ranges from 1000 to 44microns.

3.3 PREPARATION OF SAMPLES

The samples were dried in hot air oven at 60°C to remove the moisture. From the dried samples, 100 gm of the samples were taken by repeated coning and quartering to ensure the uniformity and avoid errors in analyses of heavy mineral separation.

3.3.1 Pre Treatment of Samples for Particle Size Analysis

The pre treatment of the samples included the following steps:

i) Clay fraction removal: the samples were soaked in water with a pinch of sodium hexametaphosphate ($(NaPO_3)_6$) for a night, and then were washed in water (+4 phi value) to remove the clay fractions. The samples were dried and weighed, and the weight loss was taken as the weight of clay.

ii) Organic matter removal: the samples were soaked in hydrogen peroxide (H_2O_2) overnight, and the samples were washed in water (+4.00 phi value) until a clear column of water without any turbidity was obtained. The samples were then dried and weighed, and the weight loss was taken as the weight of organic matter.

iii) Carbonate removal: the samples were treated with 1:9 hydrochloric acid (HCl) to dissolve and remove the calcareous shell fragments present in the sediments. After proper washing

and drying, the samples were weighed, and the weight loss was taken as the weight of carbonates.

iv) Iron removal: the samples were soaked with 1:9 nitric acids (HNO_3) for a night, and were then washed (+4.00 phi value) in water until a clear column of water was obtained. The samples were then dried and weighed and the weight loss was taken as the weight of Fe.

v) Sieving: though the grain size may influence heavy mineral composition, usually fine to medium grained sands yield the optimum heavy mineral assemblages. Sieving was carried out in ASTM at ½ Φ interval (Figure 3.2). The sieve sets, stacked in descending order of their sizes, were shaken using a mechanical sieve shaker continuously for about 20 minutes. During sieving proper attention was given to minimize the sand loss from the sieve sets. The sieve materials were collected separately for weighing. Weight of individual fractions was tabulated for further granulometric studies. The sieved sands of 80, 100 and 120 meshes were separately kept for heavy mineral studies. The geochemistry data was obtained in the Department of Geology, Anna University, Chennai, India.

Figure 3.2 Sieve Shaker shaker

3.4 ENVIRONMENTAL MAGNETISM

In environmental magnetism, palaeoclimate studies use the magnetic characteristics of sediments and soils to identify the climatic conditions that prevailed during their deposition or formation. It is possible to use magnetic climate proxies because firstly, iron is an important component in all rocks and their weathering products, and secondly, iron(hydr)oxide formation is strongly dependent on climatic factors such as rainfalland temperature (Maher1998). Unfortunately, the magnetic signal alone is not always adequate for palaeoclimate reconstruction, and additional methods are needed to improve the interpretation of the magnetic parameters as climate proxy. Ideally, a method that can differentiate between maghemite and magnetite within soils.

3.4.1 Brief Memoir of Environmental Magnetism

The important role of iron oxides in soils was for a long time not recognized for two main reasons: they occur in low concentrations, and they are often amorphous and very fine grained. This makes it difficult to detect iron oxides in soils. The first report of soil hematite and goethite dates back to 1939, when Alexander et al. (1939) identified these minerals with X-ray diffraction (see also: Cornell & Schwertmann 1996). It was not until 1951, however, that maghemite was identified in a soil for the first time by van der Marel (1951). This result was confirmed by Le Borgne in 1955, who attributed the increase in magnetic susceptibility in the topsoil to pedogenic formation of maghemite through forest fires (Le Borgne 1955). His work is also the first report on magnetic enhancement within a soil profile, and it was not until the late1970s that the importance of this discovery was fully understood. At this time, Mullins (1977) published a paper on the significance of magnetic susceptibility in identifying pedogenic and lithogenic ferromagnetic minerals in soils. By then, it was generally realised that soils and sediments contain magnetic material that has been subject to transport, deposition or in situ transformation, and that the magnetic mineral composition of natural materials is influenced by environmental processes in the atmosphere, lithosphere, biosphere and hydrosphere. The first explicit description of environmental magnetism as a distinct field was in 1980 by Thompson et al. (1980). One of the landmark studies in this new field was the work of Heller & Liu (1982. 1984). They were the first to successfully construct a palaeomagnetic time-scale for the Chinese loess-palaeosol sequences. They used the information from their palaeomagnetic study to show that the pattern of magnetic susceptibility variation with depth in a Chinese loess-palaeosol sequence was in broad agreement with the oxygen isotope record in marine sediments, and that the high susceptibility layers (the palaeosols) were formed during interglacial stages. After this landmark study,

many others started investigating how the magnetic signal in sediments is linked to climate. A more elaborate overview of the field is given by several authors, including the books of Thompson & Oldfield (1986) and Maher & Thompson (1999), as well as the reviews of Verosub & Roberts (1995), Heller & Evans (1995) or Dekkers (1997).

3.4.1.1 Magnetic properties related to grain size, mineralogy and concentration

To understand the influence of environment on magnetic minerals, one first has to develop methods to describe mineralogy, grain size and concentration of magnetic minerals in natural samples. Several mineral-magnetic parameters have been identified as being either dependent on mineralogy, grain size, concentration or on a combination of these characteristics. A list of parameters and ratios used in environmental magnetism for this research is given in Table 3.1. Here, we will briefly discuss them. For a more detailed overview we refer to Thompson & Oldfield (1986) or Maher (1986).

3.4.1.2 Magnetization and magnetic susceptibility (χ)

The magnetization (M) is defined as the magnetic moment per unit volume and is measured in amperes per meter (Am^{-1}). It may be natural or induced laboratory.

3.4.2 Magnetic susceptibility (χ)

The magnetic susceptibility parameter is particularly important in the field of the environmental magnetism, it can be defined as a measure of how an object is magnetized in a magnetic field, ie, its "magnetizabilidade".

Table 3.1 Parameters and ratios used in environmental magnetism

Symbol	Parameter description	Dependent on/Indicative of
X	Mass specific susceptibility (m^3/kg)	Concentration of ferromagnetic grains and grain size
X_{fd}	Frequency dependent of susceptibility (%)	grain size
SIRM	Saturation isothermal remanent magnetization (=M_{rs}) (Am^2kg^{-1})	concentration, grain size
M_s	Saturation magnetization (Am^2kg^{-1}) or (Am^{-1})	Concentration
Bcr	Remanent coercive force (mT)	grain size, mineralogy (ferromagnetic vs antiferromagnetic)
B_c	Coercive force (mT)	grain size, mineralogy (ferromagnetic vs antiferromagnetic)
$IRM_{0.3T}/SIRM_{IT}$	S-value (-)	Mineralogy (ferromagnetic vs antiferro)
M_{rs}/M_S & B_{cr}/B_c	Day plot (-)	grain size (specifically for (titano-) magnetite
T_C	Curie Temperature (˚C)	mineralogy
T_M	Morin Transition temperature (˚C)	mineralogy(hematite)
T_V	Verwey transition temperature (˚C)	mineralogy(magnetite)
$IRM_{77\text{-}293\ K}$	Isothermal remanent magnetization (from 77 to 293 K) (Am^2kg^{-1})	grain size, mineralogy
ARM	Anhysteretic remanent magnetisation (Am^2kg^{-1}) or (Am^{-1})	concentration of SD ferromagnetic minerals
X_{ARM}	ARM susceptibility (-)	concentration of SD ferromagnetic grains
X_{ARM}/χ	Susceptibility ratio (-)	grain size
ARM/SIRM	Magnetization ratio (-)	grainsize, concentration of SD remanence carrying particles
SIRM/ χ	Ratio of saturation IRM to susceptibility (10^3 Am^{-1})	concentration, grain size, mineralogy grain size
χ /M_S	Ratio of susceptibility to saturation magnetization (mA^{-1})	

It allows us to obtain data on the ease with which a material is magnetized and thus have an idea of the concentration of magnetic minerals in the sample. It can be determined by in rocks, dirt dust, sediments and soil samples of 0.1 to 100 g. The magnetic susceptibility can be considered in mass due to the magnetized body or, alternatively, expressed in terms of its volume (Hunt et al. 1995).

The volume susceptibility, K has no units and is given by the relation:

$$M = KH$$

The specific mass susceptibility, χ, is expressed in m^3kg^{-1} and is defined by

$$\chi = K / \rho,$$

where ρ is the density of the material.

Magnetic susceptibility usually reflects the content of magnetic minerals of the sample; a high susceptibility indicates a high content of magnetic minerals (Thompson et al. 1980, Maher 1986, Verosub & Roberts, 1995). It is a useful tool to quickly identify ferro- and ferrimagnetic minerals (which have a high susceptibility, see Table 3.2). Since the susceptibility of diamagnetic minerals is very small and negative, and that of paramagnetic minerals is also small (but positive), they usually represent a very small fraction of the sample susceptibility. The susceptibility signal will thus be dominated by the ferri- and ferromagnetic minerals provided their concentration is large enough (> 1 wt%) (Mullins1977). However, there are certain settings, for example marine limestones and marls, in which the concentration of the ferri- and ferromagnetic minerals are very low. In these materials as much as ~50% up to even ~90% of the susceptibility signal originates from diamagnetic or paramagnetic minerals. The susceptibility not only reflects concentration of magnetic minerals, but can also express grain size. Super paramagnetic (SP) grains with a grain size close to the single-domain (SD) boundary have extremely high susceptibility (up to ~ 20 times the value of the SD grains of the same mineral) (Mullins 1977, King et al. 1982, Maher 1988, Banerjee et al. 1993, Sun et al. 1995, Verosub & Roberts

1995). This makes susceptibility a good indicator for the presence of (large) SP grains.

Table 3.2 Chemical formula, magnetic behavior and typical susceptibility values (at room temperature) for a number of common minerals

Minerals	Chemical formula	Magnetic behavior	χ ($10^{-8}m^3kg^{-1}$)
Magnetite	Fe_3O_4	ferrimagnetic	57000
Maghemite	γ-Fe_2O_3	ferrimagnetic	57000
Hematite	α-Fe_2O_3	antiferromagnetic	60-600
Goethite	α-FeOOH	antiferromagnetic	70
Pyrite	FeS_2	paramagnetic	30
Quartz	SiO_2	diamagnetic	-0.6
Feldspar	(Ca, K, Na, Al) silicate	diamagnetic	-0.5
Clay minerals	e.g. illite, kaolinite	dia/paramagnetic	2 to 100
Calcium carbonate	$CaCO_3$	diamagnetic	-0.5

3.4.3 Isothermal Remnant Magnetization

This type of magnetization results from exposure of the sample to a magnetic field at a constant temperature; this temperature usually corresponds to the ambient temperature. The magnitude of magnetization depends on the intensity of the applied field. This dependence may be demonstrated by laboratory by subjecting a sample to increasing field intensity and the magnetization measuring, after each application. The maximum value of magnetization that can be obtained is called the remnant magnetization saturation isotherm (MRI). The field to which this magnetization is obtained depends on the composition and size of magnetic grains.

3.4.4 Laboratory Equipment

The equipment used in environmental magnetism studies belong basically three categories: susceptibility-meters susceptibilímetros, magnetizer sand magnetometers. These devices allow respectively to quantify the ease with which the material is magnetized, for magnetizing the samples subsequent measurements and, finally, measuring the natural or laboratory induced magnetizations. These equipment Constitute what Thompson and Oldfield (1986) call "environmental magnetic kit ".

3.4.5 Susceptibility Meter

Also called scales or susceptibility bridges, these devices measure the magnetic susceptibility of materials in the laboratory or in the field (Figure 3.3). In susceptibility meter, an electromagnetic circuit detects variations in inductance when a sample is placed inside a solenoid. In this work a magnetic susceptibility meter, AgicoKappabridge KLY-4S model (Czech Republic) equipped with the Sumean software was used. The susceptibility of bridges operating at two frequencies is particularly useful in environmental studies with soil samples. For measurement of magnetic susceptibility variation with temperature susceptibility are used scales coupled to a furnace (Figure 3.3).

(a) (b) (c)

Figure 3.3 Susceptibility Meters: a) Meter, b) frequency sensor, c) susceptibility meter (Spinner/ static)

3.4.6 Magnetizer

The basic operation of such devices consists of a coil capable of generating a pulsed field. To magnetize samples, they can be used also electromagnets that are somewhat slower than the coils (Maher et al. 1999). Fields direct, uniform, intensity up to 1 mT may be easily produced on a reel in the form of a solenoid. The field inside the solenoid is equal to μ_0Ni, where N is the number of turns per meter EIA intensity of the current in Amperes. The field is constant inside the solenoid (Thompson & Oldfield 1986) (Figure 3.4).

3.4.7 Magnetometers

The Magnetometer detects the magnetic field surrounding the sample space, allowing to measure measuring the intensity and direction of the magnetization.

Figure 3.4 Molspin magnetizer

Must be sensitive enough to measure magnetic moments that can vary by a factor on the order of a million, because sediments, soil and dust can contain magnetic minerals in very different concentrations. The fluxgate magnetometer of the "fluxgate" (Figure 3.5) used in many laboratories pale

magnetism, constitute a right choice to work in the field of environmental magnetism.

Figure 3.5 Molspin Spinner magnetometer

They are reliable and easy to use. The magnetometers "fluxgate" an axle (Figure 3.5) measure the intensity of the magnetic field in a specific direction; the magnetometers "fluxgate" tri-axial, more versatile, are composed of three orthogonally arranged sensors allowing to measure the intensity of the magnetic field in the x, y and z. Thus, one can determine the magnitude and total magnetic field direction.

3.4.8 X-ray Diffraction Analysis(XRD)

The mineral composition was determined in unrented powder mounts for bulk sample analysis. XRD measurements were made with X'Pert3 MRD (XL) equipment at LaboratórioNacional de Energia e Geologia,; I.P. (Figure 3.6). The samples, which are used for magnetic measurements was the same samples that were used for XRD.Because because the samples were don't get destructed or get affected by the magnetic measurements. Samples were carefully picked with variation shown during

the magnetic susceptibility analysis. So by this we do not get missed any information from the samples.

Figure 3.6X'Pert³ Powder

Before proceeding any further, selected samples gets done coning and quartering to ensure they are homogeneous to evade even minimal errors during the XRD analysis. The estimates of the mineral abundances were based on subsequent peak intensities. For the semi-quantification of the identified principal clay minerals, peak areas of the specific reflections were calculated and weighted (Lapa & Reis 1977). High Score plus software were used to correct the intensities and to correlate between each sample. Pan analytical X'Pert3 MRD (XL) is 200 times the precision and faster than the old models.

3.5 OSL ANALYSIS

3.5.1 Introduction to Luminescence Dating

Luminescence dating is a form of geochronology that measures the energy of photons being released. In natural settings, ionizing radiation (U, Th, Rb & K) is absorbed and stored by sediments in the crystal lattice. This stored radiation dose can be evicted with stimulation and released as luminescence.

The calculated age is the time since the last exposure to sunlight or intense heat. The sunlight bleaches away the luminescence signal and resets the time 'clock'. As time passes, the luminescence signal increases through exposure to the ionizing radiation and cosmic rays. Luminescence dating is based on quantifying both the radiation dose received by a sample since its zeroing event, and the dose rate which rate, which it has experienced during the accumulation period. The principal minerals used in luminescence dating are quartz and potassium feldspar.OSL dating age range for various sediments are given in Table 3.3.

Table 3.3 OSL dating age range for various sediments

DEPOSITS	AGE RANGE (years)
GLASS/ VOLCANIC ASH	10-250,000
LOESS	8000-416,000
FLUVIAL	MODERN-400,000
COLLUVIUM/ALLUVIUM	100-150,000
EOLIAN	10-70,000
PALOEDISCHARGE -A&C HORIZONS	3000-190,000

3.5.2 Applications of Luminescence

3.5.3 Types of Luminescence Dating Techniques

- Photo-Transferred (PTTL)
- Thermal (TL)
- Optically Stimulated (OSL)
- Green Light (GSL) - Feldspar & Quartz
- Infrared (IRSL) - K-Spar

- Blue Light (BSL) - Quartz
- Red Light (RSL) - Volcanic Feldspar & Quartz

3.5.4 OSL Dating Principles

Luminescence dating is based on solid-state properties of mineral grains that allow them to record their exposure to radiation. The recorded radiation exposure can be measured by stimulating the sample with light of one wavelength and monitoring the emitted luminescence at another wavelength (optically stimulated luminescence, OSL). The intensity of luminescence is a function of the absorbed natural radiation dose. If the rate of natural irradiation of the grains is constant and can be determined, then dividing absorbed dose by dose rate gives a radiation exposure age, according to:

$$\text{Age, } T(a) = \frac{\text{Equivalent natural dose, } D_e \text{ (Gy)}}{\text{Annual dose rate, } R(\text{Gy/a})}$$

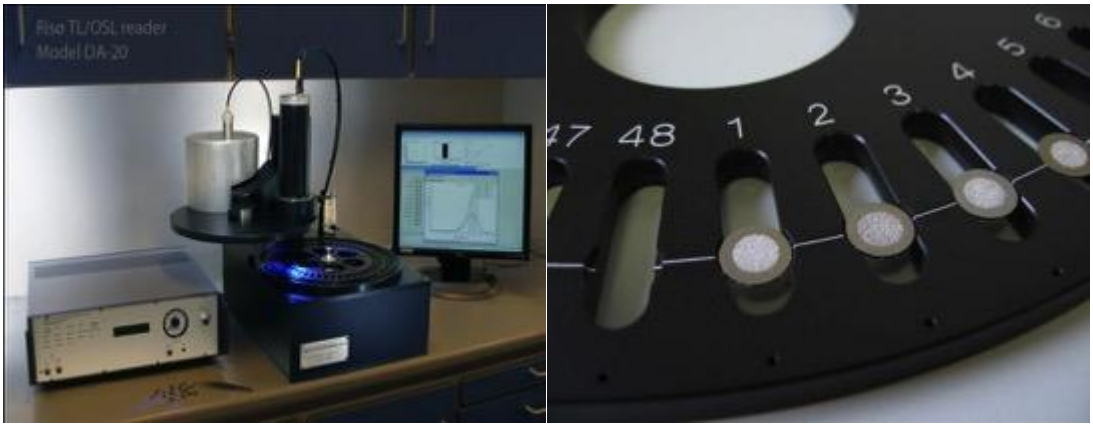

Figure 3.7 Instrument used for OSL dating

The equivalent natural dose (D_e) absorbed during burial may be determined from the response of the OSL signal to radiation. Most often the so-called single aliquot regenerative-dose (SAR) procedure is used to determine the D_e. The technique of luminescence dating is well established for age-dating sediments on Earth. There is an abundance of published examples throughout the terrestrial geologic literature describing successful applications of the technique. Thus the age of the sediments is more or less approximately identified using optically stimulated luminescence method. Instrument used for OSL dating is depicted in Figure 3.7.

3.5.5 Leica Viva GS12

Leica Viva GS12 is used to track accurately coordinates of sampled areas via GPS. Leica comes with two devices one, base station acting as theodolite and the other as free station. The base station is set at a particular place with known sea level and the free station is positioned at points to measure the change in vertical and horizontal plane.

Figure 3.8 Leica Viva GS12

Leica uses RTK data processing, which will provide precise results, with the two available frequencies it can track up to 60 satellites simultaneously. The Figure 3.8 shows the Leica Viva GS12. It's lightweight, wireless operation and fast initialization makes it easier to set it up almost anywhere. It can provide better results in the presence of obstacles such as trees and under extreme temperatures (-40^{o}C to +65^{o}C). Its smart check algorithm improves acquisition and operating speed of the device, providing accurate results in a short period. The communication ports include USB, Bluetooth, which makes it easier to share data with other devices.

CHAPTER 4

GEOMORPHOLOGY OF SOUTH EAST COAST OF TAMILNADU

4.1 GENERAL

The coastal geology deals with structure formation such as rock, cliffs, sea weed and sediments deposited on coastal region (Eric Bird 2007). The coastal land marks and communities can be preserved by knowledge of coastal geomorphology. The beaches, cliffs, sand dunes and salt marshes are formed based on forces acting up on them both natural and man-made. Coastal geomorphology helps in relating land forms with sediments and rocks along the coastal lines. Coastal geomorphology is a subsidiary of geomorphology, which focuses on area influenced by water bodies.

This chapter presents geology and coastal geomorphology of Kanyakumari, Tuticorin region of south India. The study of this coastal area comprises of vegetated wet lands, non-vegetated wet lands, coastal lands and water bodies.

4.2 GEOLOGY OF THE COAST

The crystalline rocks along with sandy materials are deposited along the Kanyakumari to Tuticorin area. Rocks with concentration of crystallized minerals, without any glassy materials are called as crystalline rocks. Depending on the rock formation along the coast, the beaches are

grouped into marine calcareous, crystalline rocks and coralline. The cliffs present near Kanyakumari are crystalline in nature along with presence of sandstone and lignite seams. The warkhali beds are similar to bed formation of Cuddalore in Tamilnadu. The material sediments of Manappad have composition of sandstone. The reefs along the Periathalai coast parallel to the shore line. The reef is a combination of calcareous rock, which is common along the coast of Kanyakumari and Rameswaram. The red color sand sheets locally know as Teril is fond along the coast of Navaladi, ovary, Periathalai. The formation is found in a short distance from shore, they form high mounds, and ridges composed of piles of red dunes. The formation is mainly a combination of clay dust and fine grains of iron ore.

Combination of quartz, feldspar, mollusc shells form marine calcareous sandstones. They are mainly found in areas of Manappad and Tiruchendur zones. The sand stones rise several meters above the tide level. The coastal lines From Tiruchendur to Tuticorin comprises of sediments such as grained limestone and gritty sandstone and pebbles. These combinations of sediments are known as Panamparai sandstone. Depending on the sediments along the beach, sandy beach can be classified into calcareous, siliceous, sea weed rich, mineral rich, muddy beach. Muddy beaches are mainly found in Tamiraparani River and Punnakayal coast.

4.3 COASTAL GEOMORPHOLOGY

4.3.1 Vegetated Wet Lands

a)Mangroves: mangroves are typically found along the shores. Some of these trees also grow on sand, peat and coral rock. They can survive in salt water where other plants will not survive. There are over eighty species of mangroves, sixty of which are mainly found along the coastal areas, twelve are found in America. Mangroves grow in all shapes and sizes from small

bushes to several meters. Mangroves cannot grow in low temperature regions. Tides and coastal currents influence mangrove distribution to islands. Mangrove occupy a total of 4250 sqkm in India. These mangroves are considered depraved due to tidal slope and siltation. mangroves are well present in Pichavaram, Muthupet. The Pichacavaram is a swamp extending from vellar to coleroon estuaries. Mangroves are well adjusted with the ecosystem-providing habitat for fish and wild life present in the beach. Depending on the coastal areas where mangroves are present, they provide habitat to the local wild life. Seventy five percent of fishes and prawn found in Australia are habitat of mangrove ecological system.

b)Salt marsh vegetation: a marsh is a transitional inter tidal between land and saline water. The salt marshes are found along the coast of Tuticorin and Punnakayl. The seawater brings nutrients from the sea. These nutrients settle at the roots of these bushes. This natural occurrence improves bio diversity greatly.

4.3.2 Non -Vegetated Wet Lands

a) Sandy Beaches and Beach Cusps: Sandy beaches are formed by accumulation of sediments deposited by the waves and longshore drift along the coast. The size of sand and nature of wave also determine the slope of the beach. The sediments along the beach are in varying sizes and are well sorted. There are two type of beaches namely, dissipative and reflective. One type of beach has rock's along the coast and the other has a marine plain. The third type, which is the intermediate, has narrow sediment barriers along the coast. Beaches along the coast of Kanyakumari and Tuticorin fall under the category of sandy beaches. The coast of Tuticorin, Kayalpattinam, Ovari, Navaladi, Idinthakarai, Tuticorin and Perumanal has well-developed beaches. The width of Tuticorin beach varies from 20-50 m. The beach has a combination of minerals, quartz, coral and algal fragments. The coast along Koodankulam

near ovary zone has well developed beach cusps. The cusps are formed by combination of various grades of sediments in arc pattern. Pebbles and embayment contain finer grain sediments, which form horns. The cusps are all in equal size and have a regular pattern.

Figure 4.1 Beach Cusps along the Kudankulam

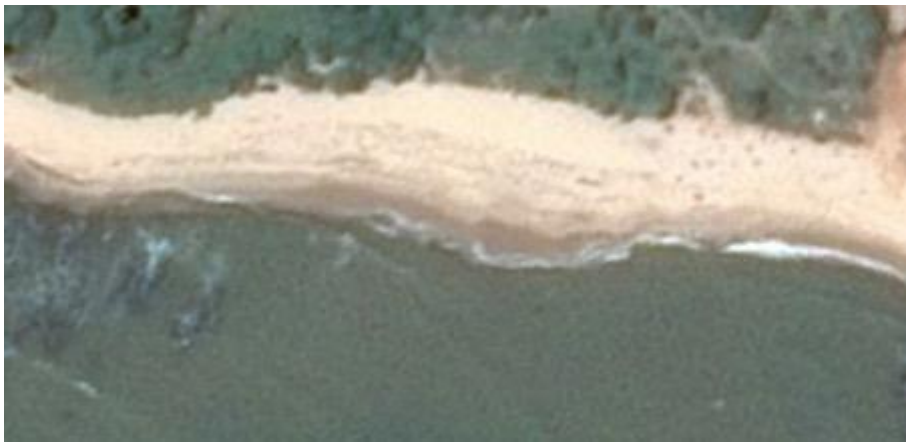

Figure 4.2 Sandy Beaches along Navaladi coast

Figure 4.3 Spits and Mud Flats along Tuticorin Coast

Figure 4.4 Sand Bars and Spits along Punnakayal Coast

b) Sand Bars and Spits: a sand bar is a piece of land, which extends over water at seas. The sand bar is formed by combination of sand and silt. The size of the composition depends on the force of wave acting up them. The study area, along the Tuticorin coast has sand bars, spits and mudflats trending 4km from the main shore. Small bars are observed along the coast of Punnakayal. These bars grow in size when there is rainfall mainly during northeast monsoon season. The sediment deposition along the bars makes

them larger. They undergo dynamic changes both in size and direction along the coast. A spit is a land with two surfaces above water and the rest below. One surface will be along the coast and the other at sea. A split is formed by long shore drift, which transfers sediments through water along the beach. The currents, which form the split, are formed by longshore drifts, which aids in sediment deposition along the coast. A tongue shaped spit is present in Tuticorin with a 2km expansion. The spit has one end connected with main land and the other end, Tombolo, which is presently used for port operations. The spits along the Tuticorin coast are formed by long shore currents and the sediments from Thambraparani river. Another spit is also recorded along the Manappad coast. It is formed by discharge of sediments from during monsoon from Karamaniyar river.

c) Mud flats: mud flats are formed by deposition of mud along the coastal lands by tides or rivers. They are typically found in areas such as bays and lagoons. Mud flats are exposed layer of bay mud formed by deposition of estuarine silts, clay. Most of the mud flap formations are along the tidal coast lines which are very useful in preventing coastal erosions. They are visible approximately two times a day. Mudflats are under constant impedance by rising sea level all over the world.

Figure 4.5 Mud flats

Figure 4.6 Spit

Figure 4.7 Sand dunes

Figure 4.8 Sand dunes

Mudflats are along the coast of Punnakayal and Tuticorin. Well developed mudflats are located along Thambraparani estuary and Koramballam Creek river. Mudflats here comprise mainly of alluvial soil.

d) Marine Terrace and Head Lands: Marine terrace are flat areas found along the base of sea cliff formed by the action of waves. The platforms main composition is sand. They are formed by coastal erosion, rise, and fall of sea level. The marine terrace along the Tuticorin coast is formed by combination of quartz, shell fragments and calcareous cement. A bay is defined as something, which is surrounded by land on three sides whereas a headland is vice versa of bay, it is surrounded by water on three sides. Bays typically appear as normal sea beaches whereas headlands have high breaking waves and intense erosion. Weak rocks such as sand and clays are eroded leaving strong rocks (chalk, limestone) forming headland.

4.3.3 Shore Lands

a) Sand Dunes: sand dunes are formed along beaches where waves constitute to accumulation o f sand along beach and wind, which blow sands on to the inlands. The hill of sand is formed by Aeolian process. As the sand is blow toward the inland the sand are caught by vegetation along the beach and this repeated process will cause the dunes t develop along the

coastal lines. The ovary coast have dunes of about 50m, coast of Navaladi, ovary and Tuticorin has sand dunes locally known as Teril. These dunes have mixture of sediments with little vegetation. Teri dune is formed by combination of red colour sand and silt of Aeolian origin. The southwest monsoon wind blows the dust from red loam to the teri dunes which results in sediment deposition along these coasts. These dunes are formed along the coastlines resulting in vegetation and used as filters for water. In recent decade, these teri dunes are used for cultivation as well.

b) Beach ridges: a beach ridge is a ridge deposited along the coastline. Its main composition is sand and sediments from underlying beach materials. The ridges are discontinuous and in varying size along the coastlines. The ridges in Tuticorin are separated by swales and saltpan. Beach ridges have a composition of sand, gravel and shingle formed by the action waves along the shores of beach.

c) Salt Marsh and Salt Pan: salt marsh is a type of marsh dominated by salt tolerant plants. Salt marshes are a productive habitat of ecological system, which has often been treated as wastelands. The tidal waves bring in nutrients from the sea to the coastal lines where these marshes are present. These nutrients help in improving the bio diversity of the planet.

Saltpans are places where the water settled on a small area like a pond, the water that does not drain leaves behind minerals after they are evaporated. The study area has many saltpans along Tuticorin, Punnakayal coast. Salt panes usually shine white under the sun.

4.3.4 Water Bodies

a) Estuaries and Creeks: Estuaries are places where the tides meet the streams. They are valuable because they bring in nutrients during the

monsoon rains. So several fish varieties such as prawns, lobsters, mussels are found in significance, which provide breeding grounds. The rivers like Hanuamn Nathi, Karamaniar river form estuarine environment, which is helpful in renewing marine resources.

b) Swales: Swales are low elevation areas located between dunes and are formed in areas where water table is high. They are also called as dune slacks and interdunal wetlands. Swales are formed in Tuticorin and ovary coasts. They are used for rainwater harvesting which helps in recharging aquifers and wetland plants.

4.4 CONCLUSION

In this chapter, the geomorphology of south east coastal areas of Tamilnadu starting from Kanyakumari to Tuticorin area is studied for their character in terms of Sandy Beaches and Beach Cusps, Sand Bars and Spits, mud flats, Estuaries and Creeks, Swales, Sand Dunes, Beach ridges, Salt Marsh and Salt Pan and Marine Terrace and Head Lands. The above geomorphology character of the study are helps in relating land forms with sediments and rocks along the coastal lines and also we study the water bodies, since the Coastal geomorphology influenced.

CHAPTER 5

RESULTS AND DISCUSSION

5.1 INTRODUCTION

The climate study in earlier days is carried out with Paleoclimatology before the invention of various climate study measurement instruments. The instruments record the only tiny fraction of past Earth climate data. So the evaluation of climatic variation, comparing with the previous data leads to incompetent evaluation. In the Paleoclimatology proxy data is used for the evaluation of climatic change. The proxy record of data's is related to the climate changeability based on the climate-dependent of a natural phenomenon for more accuracy. In Paleoclimatology, climate dependent can be evaluated with sand dunes.

In coastal and continental regions, red and orange dune sand occurs. The red colouration and its origin play a vital role in palaeoenvironmental studies regarding the dating of sand dunes. In some red sands, the inherited colour occurs due to red parent sediments or rocks. Whereas the other red sand colour may also occur due to downwind transportation. During the movement of enormous active dunes, the larger part of the sand body remains for hundreds of years. During the hundred years, the chemical change occurs and forms iron oxides. A chemical change in iron-bearing minerals creates airborne dust. However, many pieces of research pointed out the redness and their limitation by transportation and abrasion Anton & Ince (1986) and Wasson (1983a) also proved that field evidence does not support the

reddening with time. Since the reddening occurs due to arid conditions and also destabilised sands under semi-arid and humid conditions. Now current active red sand areas are stabilised during wet periods of Quaternary with experience of pedogenetic rube faction. Pye classified four groups of pedogenetic red beds. (a) Red latosols, are red soils bleaches, except for a2 horizon (b) Red podsols are available in humid regions (c) Red Desert, which exhibit weak horizon differentiation (d), Red Mediterranean are clay-rich soils that are reddish brown in colour.

The changes in wind strength, rainfall & evaporation rates affects the coastal dune activity, still the other changes like sea level, marine sediment also affects the coastal dune. From the various studies of coastal dunes, the relationship between sea level changes and the coastal dunes are derived from the data collection of many different areas proves that dunes can form during high and low sea level stands and marine transgressions and regressions.

In the identification of date, dune sediments are carried out with luminance techniques for past three decades. The luminance dating of dune date is calculated based on light energy emission from mineral crystal during the exposure to ionizing radiation if minerals are heated then it is called thermo luminance (Huntley 1982) or from a laser source to ionize is called as optical luminance (1985). In the natural decay process of radioisotopes in the surrounding sediment produces the free electrons in the crystal which are trapped within lattice defects.

The asymptotic relationship is obtained from the amount of stored light energy to the length of exposure to ionising radiation & eventually all the electron traps are filled. Dating is based on the assumption that exposure to the sunlight during the grain transport empties the electron traps ‘Zeroing' the luminance ages during the burial electrons traps inside filling up

progressively again with lime. Figure 5.1 shows the normalised value variation in depths for sand, clay, $CaCO_3$, Fe. The normalise values are calculated in % from the sample. The normalised value of sand% is more up to 220 cm, and after that, there is a decrease from 230cm. The clay% values are of negligible till 220cm and whereas from 240cm, there is a drastic change and the change prolongs throughout the profile. The $CaCO_3$ % values fluctuates from 0cm to 130 cm. The Fe% values vary at 600 cm depth, and there is no change above that.

The noramalised value in percentage is calculated based on the equation below:

Normalize the sample percentage =(Sample Percentage-total sample average)/standard deviation of sample percentage

5.2 SERVAIKARAN MADAM (SKM) - SAND, CLAY, $CaCO_3$ AND Fe VARIATIONS

In this section the sample percentage are normalized as shown in Figure 5.2. Sand % is higher till 220 cm and gradually decreased from 230 cm. Also, in this section, clay (%) values are almost negligible until 220 cm, and there is a drastic change from 240 cm and remain throughout the profile. While for $CaCO_3$ (%) its values fluctuate from 0 cm to 130 cm. The Fe (%) seems to have no particular fluctuation along the profile except at 600 cm depth.

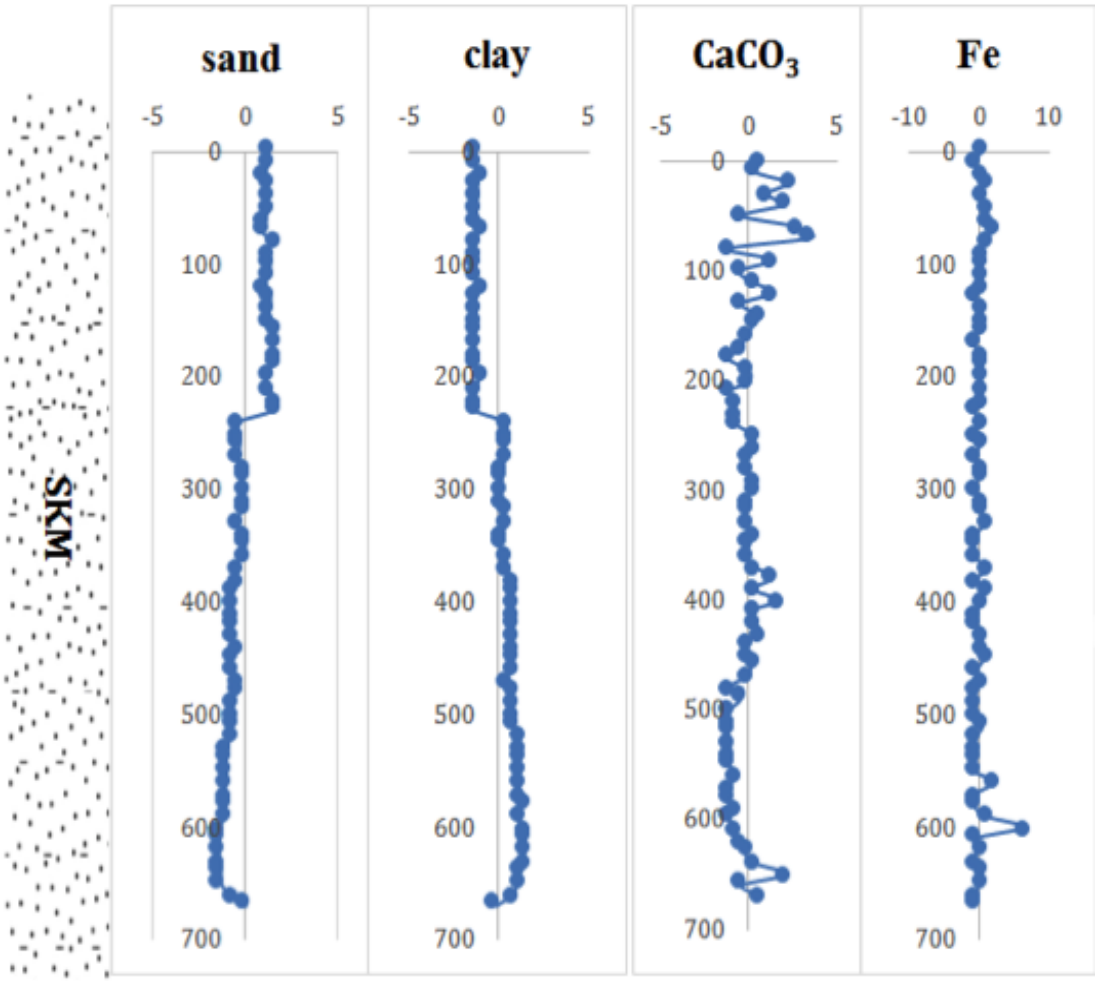

Figure 5.1 Down core variation of sand, clay,$CaCO_3$, and Fe (normalized values) in SKM

5.2.1 Sediment Compositions of SKM

The Table 5.1 shows the results of samples which were pre-treated before the sieving analysis. The following samples contain sand, organic matter, calcium carbonate and iron content in the study area.

Table 5.1 Sediment compositions of Servaikaran madam (SKM)

SERVAIKARAN MADAM (SKM)							
Depth(cm)	**Sample Weight (g)**	**Sand %**	**Silt %**	**Clay %**	**$CaCO_3$ %**	**OM %**	**Fe %**
0	100.02	93.94	0.15	3.45	0.66	1.33	0.47
10	100.03	94.85	0.19	3.21	0.57	1.04	0.13
20	100.03	90.45	0.36	5.71	1.29	1.78	0.42
30	100.02	91.82	0.46	4.68	0.83	1.58	0.63
40	100.02	92.38	0.38	4.82	1.18	0.87	0.37
50	100.01	94.74	0.33	3.64	0.31	0.38	0.60
60	100.03	91.09	0.44	4.81	1.50	1.35	0.81
70	100.01	88.95	0.50	5.95	1.79	1.84	0.98
80	100.02	96.13	0.25	2.51	0.00	0.47	0.64
90	100.01	93.80	0.21	3.42	0.96	1.21	0.40
100	100.53	95.51	0.20	3.18	0.26	0.46	0.39
110	100.53	93.99	0.34	3.90	0.50	0.93	0.33
120	100.42	91.44	0.24	5.14	0.97	1.85	0.37
130	100.13	95.68	0.32	3.08	0.30	0.54	0.08
140	100.1	94.18	0.30	3.94	0.62	0.69	0.27
150	100.19	95.41	0.48	2.88	0.54	0.30	0.39
160	100.35	96.18	0.13	2.60	0.36	0.44	0.28
170	100.43	95.88	0.23	3.14	0.29	0.35	0.12
180	100.15	96.77	0.20	2.51	0.00	0.20	0.31
190	100.42	96.46	0.19	2.16	0.43	0.26	0.50
200	101.52	91.82	0.65	5.84	0.46	0.78	0.45
210	100.14	95.28	0.35	3.43	0.02	0.46	0.46
220	100.28	96.76	0.11	2.35	0.15	0.20	0.43
230	100.32	96.87	0.09	2.58	0.14	0.19	0.13
240	100.53	74.23	0.33	23.70	0.18	1.25	0.31
250	100.45	74.38	0.37	24.12	0.56	0.43	0.14
260	100.4	75.03	0.30	23.51	0.48	0.30	0.38
270	100.26	74.12	0.27	24.34	0.40	0.71	0.17
280	100.2	76.29	0.20	21.75	0.39	0.93	0.43
290	100.18	76.48	0.25	21.70	0.55	0.73	0.29
300	100.41	77.15	0.30	21.01	0.51	0.83	0.19
310	100.2	78.00	0.40	20.78	0.37	0.06	0.39
320	100.32	75.58	0.44	22.90	0.38	0.30	0.39
330	100.16	73.46	0.31	24.68	0.36	0.52	0.66

Table 5.1 (Continued)

SERVAIKARAN MADAM (SKM)							
Depth(cm)	**Sample Weight (g)**	**Sand %**	**Silt %**	**Clay %**	**$CaCO_3$ %**	**OM %**	**Fe %**
340	100.24	77.98	0.32	20.62	0.50	0.41	0.17
350	100.23	78.66	0.32	19.93	0.46	0.52	0.10
360	100.2	75.40	0.26	23.06	0.38	0.80	0.09
370	100.12	72.16	0.28	25.70	0.59	0.48	0.79
380	100.21	71.89	0.25	26.54	0.96	0.14	0.21
390	100.64	70.31	0.20	27.19	0.53	1.07	0.69
400	100.58	69.70	0.23	27.27	1.06	1.35	0.39
410	100.32	70.39	0.23	28.08	0.49	0.56	0.26
420	100.4	69.41	0.28	28.89	0.58	0.59	0.25
430	100.12	69.12	0.31	28.89	0.69	0.61	0.37
440	100.24	71.36	0.28	26.87	0.35	0.64	0.51
450	100.3	69.56	0.26	28.14	0.44	1.02	0.59
460	100.19	70.40	0.24	27.68	0.51	0.91	0.26
470	100.4	73.41	0.30	24.91	0.38	0.70	0.31
480	100.26	71.36	0.90	27.69	0.00	0.03	0.03
490	100.42	70.98	0.65	27.50	0.27	0.40	0.21
500	100.32	68.85	0.60	29.98	0.04	0.43	0.11
510	100.39	68.42	0.55	29.83	0.01	0.69	0.50
520	100.28	68.06	0.88	30.81	0.00	0.07	0.19
530	100.35	66.71	1.06	32.08	0.04	0.10	0.01
540	100.64	65.70	1.03	33.08	0.06	0.05	0.07
550	100.16	66.26	1.11	32.41	0.03	0.12	0.06
560	100.27	65.89	0.18	32.55	0.19	0.10	1.10
570	100.69	63.89	0.89	34.74	0.01	0.29	0.19
580	100.3	63.38	0.93	35.30	0.04	0.28	0.08
590	100.64	65.04	0.96	33.19	0.10	0.07	0.63
600	100.61	61.25	0.66	35.21	0.03	0.27	2.59
610	100.33	61.44	1.07	37.08	0.13	0.16	0.12
620	100.4	61.01	1.29	36.72	0.21	0.46	0.31
630	100.79	61.43	1.45	36.50	0.34	0.26	0.02
640	100.11	62.38	2.35	33.71	0.57	0.55	0.44
650	100.42	62.24	3.14	32.45	1.26	0.63	0.28
660	100.24	67.76	2.87	28.34	0.31	0.49	0.23
670	100.58	79.04	2.37	17.73	0.72	0.05	0.09

In this trench sand % is higher from 0-230 cm depth of this deposition, and it scores with 96.87% at 230 cm of the soil. From 230 to

670 cm there is a sudden decrease in sand % and an increase in clay %of the deposition. The clay scores at highest at 610 cm of 37.08% in the soil. Silt % is negligible till 600 cm and a marginal increase from 600 to 670 cm in silt%. The highest percentage of silt is 2.87% at 660cm. The organic matter and $CaCO_3$ are small. The trench shows high organic matter percentage of 1.84% at 70cm depth. The $CaCO_3$ percentage is of a maximum peak with 1.79 % at same 70 cm depth. The Fe % is very less; negligible these irons are available as a coating of the each mineral grain that is available. The trench shows high Fe content of 2.59% at the depth of 600cm.

5.2.2 Heavy Mineral Analysis in SKM

Table 5.2 displays the fine size of all heavies distributed in the samples.

Table 5.2 Heavy mineral composition of SKM

SERVAIKARAN MADAM					
Depth(cm)	**HM %**	**Depth(cm)**	**HM %**	**Depth(cm)**	**HM %**
0	6.29	240	11.75	480	10.89
10	5.54	250	10.27	490	10.78
20	6.97	260	10.10	500	10.60
30	5.14	270	10.15	510	10.52
40	6.65	280	10.64	520	10.39
50	5.08	290	10.74	530	10.56
60	6.21	300	11.23	540	9.85
70	7.80	310	10.92	550	9.68
80	3.84	320	11.55	560	9.45
90	5.08	330	9.70	570	9.68
100	3.65	340	10.88	580	9.38
110	4.64	350	11.22	590	9.87
120	4.21	360	10.59	600	9.65
130	2.35	370	10.04	610	10.01
140	5.29	380	9.40	620	10.24
150	2.68	390	9.44	630	10.86
160	4.19	400	10.66	640	11.11
170	3.75	410	10.33	650	11.60
180	4.86	420	10.94	660	13.91
190	6.14	430	10.99	670	15.21
200	7.44	440	11.00		
210	4.85	450	11.89		
220	4.45	460	10.98		
230	4.94	470	10.79		

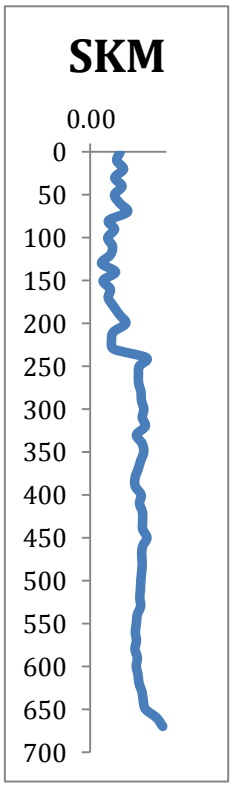

5.3 KATCHANAVILLAI (KCV) - SAND, CLAY, CaCO3 and Fe VARIATIONS

From KCV sample, the normalised percentage values are shown in Figure 5.2. The sand % values fluctuate till the depth of 220cm which explains the dynamic, high wind currents prevalent in the area and below the depth the sand values reduces. The decrease in sand implies an increase in clay $CaCO_3$ % and whereas there is no fluctuation of Fe % along the profile.

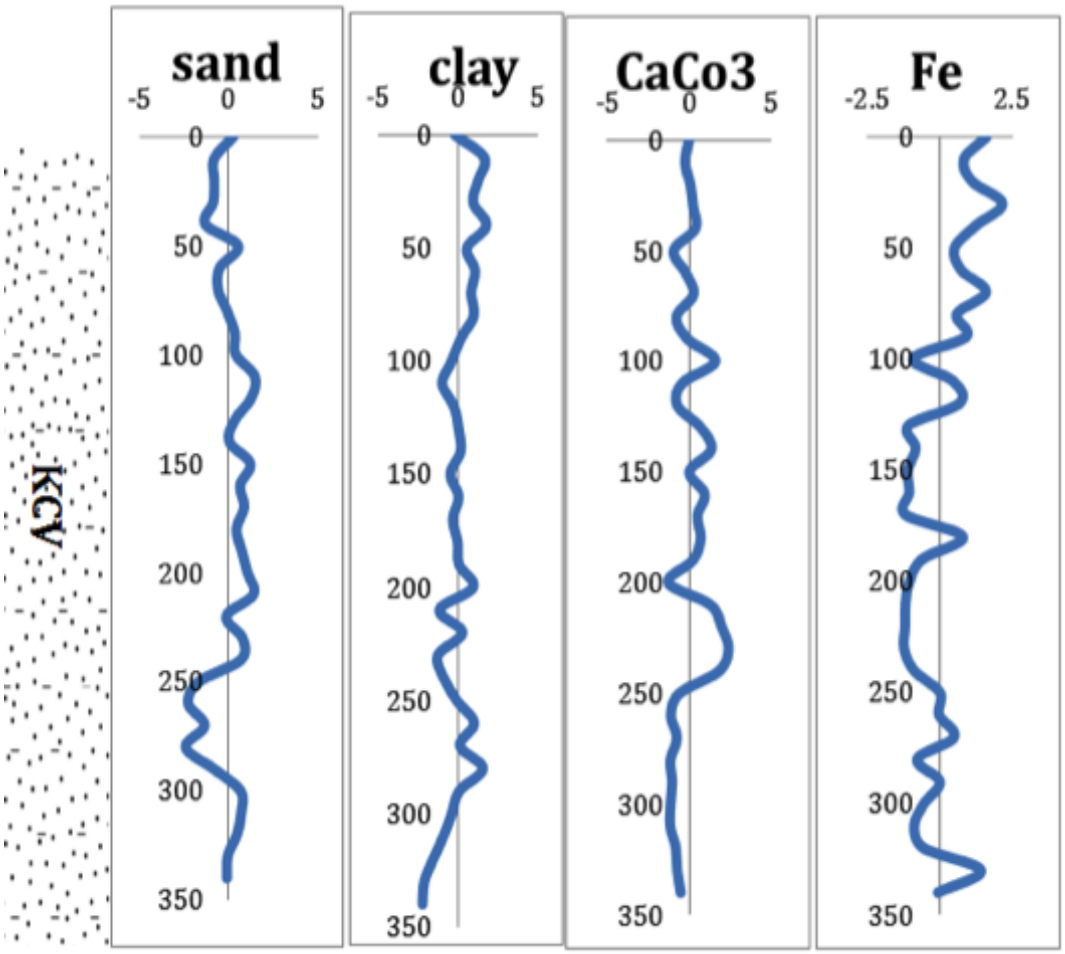

Figure 5.2 Down core variation of sand, clay, $CaCO_3$, and Fe (normalized values) in KCV

5.3.1 Sediment Composition of KCV

The level of Sand % is more, and there is no much change in concentration throughout the sample section. Its level is higher at 210 cm with 88.27% of the soil. In sand %, 0 to 80 cm and 250 to 300 cm depth the sand % is less to the normality. However, clay% is different to the sand %. The clay percentage is at 40 cm of 11.03% in the soil. Silt % is minimum up to 240 cm and marginal increase from 250 to 340 cm in silt%. The silt % is 4.25% at 260cm that is high. The organic matter and $CaCO_3$ are in a negligible amount. The trench shows high organic matter percentage of 0.31% at 340cm depth. The $CaCO_3$ percentage shows a maximum peak of 3.42 % at 230 cm depth. The Fe % is very less and negligible, and these irons are available as a coating on mineral grain that is available. The below Table 5.3 shows the vertical distribution of sand, clay, $CaCO_3$ and Fe.

Table 5.3 Sediment compositions of Katchanavillai (KCV)

Sample No	Sand %	Clay %	Silt %	OM %	CaCO3 %	Fe %
KCV-1	87.02	9.33	1.45	0.03	1.66	0.78
KCV-2	85.81	10.91	1.32	0.20	1.47	0.57
KCV-3	85.82	10.59	1.49	0.04	1.71	0.64
KCV-4	85.76	10.32	1.40	0.11	1.84	0.92
KCV-5	85.25	11.03	1.41	0.03	1.94	0.68
KCV-6	87.32	9.97	1.42	0.01	0.96	0.48
KCV-7	86.17	10.42	1.57	0.04	1.50	0.54
KCV-8	86.05	10.19	1.41	0.03	1.85	0.77
KCV-9	86.62	10.35	1.59	0.04	1.09	0.50
KCV-10	87.10	9.65	1.31	0.02	1.58	0.59
KCV-11	87.16	9.17	1.00	0.08	2.85	0.10
KCV-12	88.35	8.65	1.30	0.08	1.35	0.47
KCV-13	88.13	9.27	1.03	0.11	1.12	0.53
KCV-14	87.11	9.53	1.29	0.11	2.18	0.06

Table 5.3 (Continued)

Sample No	Sand %	Clay %	Silt %	OM %	CaCO3 %	Fe %
KCV-15	86.77	9.63	0.99	0.18	2.66	0.12
KCV-16	88.07	9.09	1.16	0.17	1.66	0.05
KCV-17	87.44	9.53	0.75	0.17	2.36	0.06
KCV-18	87.69	9.22	1.20	0.07	2.03	0.03
KCV-19	87.20	9.48	0.85	0.06	2.18	0.56
KCV-20	87.54	9.55	1.05	0.10	1.82	0.18
KCV-21	87.89	10.31	1.03	0.08	0.72	0.07
KCV-22	88.27	8.49	0.78	0.13	2.61	0.03
KCV-23	86.56	9.73	0.81	0.17	3.12	0.03
KCV-24	87.59	8.41	0.89	0.07	3.42	0.02
KCV-25	87.47	8.73	0.96	0.10	3.00	0.11
KCV-26	84.86	9.42	4.23	0.09	1.22	0.35
KCV-27	84.20	10.37	4.25	0.15	0.84	0.34
KCV-28	85.23	9.59	3.66	0.11	1.12	0.48
KCV-29	84.04	10.84	4.23	0.06	0.81	0.13
KCV-30	85.82	9.56	3.39	0.13	0.90	0.35
KCV-31	87.46	9.17	2.42	0.03	0.82	0.20
KCV-32	87.51	8.71	2.80	0.16	0.81	0.11
KCV-33	87.24	8.17	3.37	0.09	1.06	0.20
KCV-34	86.66	7.68	3.93	0.05	1.13	0.73
KCV-35	86.60	7.58	4.07	0.31	1.28	0.33

5.3.2 Heavy Mineral Analysis of KCV

From samples, the heavies are concentrated at 120 mesh. The heavies are of a fine size and graphically represented along with the Table 5.4 From the table, heavies in all the samples. The heavy mineral content is maximum up to 14.04 % at the depth of about 190 cm and minimum at about 300 cm depth with 5.15%.

Table 5.4 Heavy mineral composition of KCV

DEPTH vs HM%			
Depth (cm)	**HM%**	**Depth(cm)**	**HM%**
0	12.45	180	12.53
10	11.89	190	14.04
20	10.89	200	13.53
30	11.36	210	13.05
40	11.61	220	12.56
50	11.47	230	12.36
60	11.37	240	13.66
70	11.7	250	11.91
80	12.03	260	11.78
90	11.74	270	11.47
100	11.57	280	11.39
110	11.61	290	10.53
120	13.07	300	5.15
130	12.75	310	5.28
140	13.25	320	7.57
150	13.15	330	8.61
160	12.45	340	9.1
170	11.45		

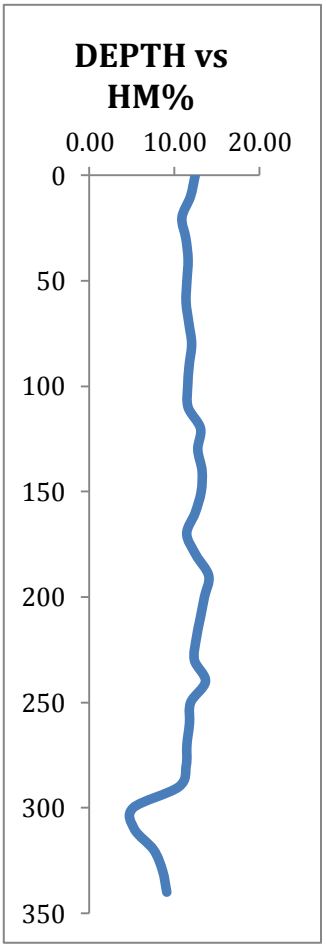

5.4 EDYAN VILLA (TPV)- SAND%, CLAY%, CaCO3% & Fe% VARIATIONS

For TPV samples, Fig.8 shows the graphical representation and normalised values of Sand, clay, $CaCO_3$ and Fe are consistent with moderate fluctuations towards the depth of 370 cm because of the $CaCO_3$ cementation. However, the sand and clay (%) remain more or less uniform with minor fluctuation sat the depth of 50 cm. Fe (%) is constant and high-value changes at (350 cm) due to $CaCO_3$ cementation.

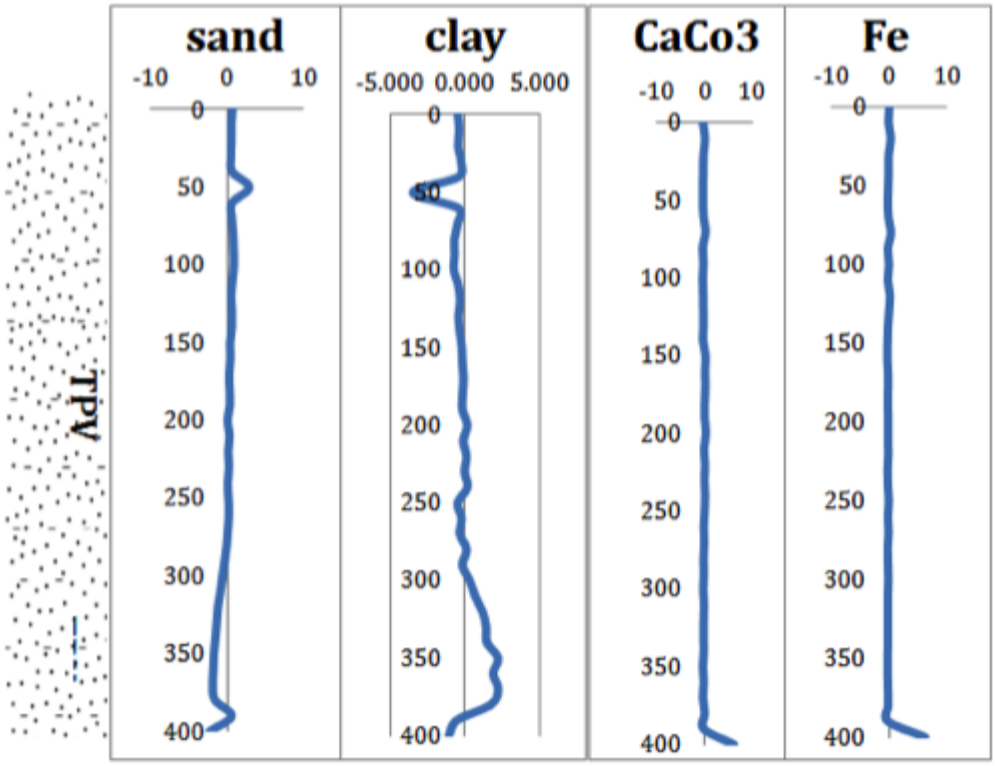

Figure 5.3 Down core variation of sand, clay, $CaCO_3$, and Fe (normalized values) in TPV

5.4.1 Sediment Compositions of Edyan Villa (TPV)

Table 5 shows sediment composition of Edyan villa. Sand% is high without more difference, higher at 50 cm with 98.91% of the soil. Whereas for clay%, the rating is opposite to the sand %. The clay highest rate is at 370 cm with 28%. Silt % is low up to 250cm, and there is a marginal increase from 250 to 400 cm. The highest score of silt % is 2.23% at 370cm. The organic matter and $CaCO_3$are in a negligible amount. The trench shows high organic matter percentage of 4.27% 290cm depth. The $CaCO_3$ percentage shows a maximum peak of 9.97 % at 400 cm depth. The Fe % is very less and negligible, but there is a sudden increase of 9.97% at depth 400 cm.

Table 5.5 Sediment compositions of Edyan villa (TPV)

EDAYAN VILLA							
Depth (cm)	**Weight (gm)**	**Sand %**	**Silt %**	**Clay %**	**OM %**	**$CaCO_3$ %**	**Fe %**
0	50.00	84.12	0.45	14.80	0.02	0.07	0.61
10	100.00	83.35	0.33	15.24	0.02	0.75	0.36
20	100.00	83.36	0.32	14.91	0.12	0.28	1.05
30	100.00	83.05	0.61	15.84	0.00	0.20	0.39
40	100.00	83.93	0.60	15.05	0.03	0.09	0.39
50	77.97	98.91	0.39	0.13	0.21	0.10	0.27
60	100.00	84.00	0.51	14.90	0.28	0.24	0.15
70	100.00	83.73	0.24	14.75	0.06	0.93	0.33
80	100.00	84.80	0.41	13.73	0.02	0.03	1.07
90	100.00	85.29	0.50	13.80	0.10	0.23	0.15
100	100.00	85.57	0.42	13.53	0.02	0.02	0.50
110	100.00	84.21	0.63	14.96	0.02	0.15	0.14
120	100.00	83.13	0.40	15.52	0.03	0.20	0.80
130	100.00	83.87	0.36	15.03	0.03	0.27	0.51
140	100.00	83.75	0.66	15.42	0.02	0.08	0.17
150	100.68	82.28	0.23	16.10	0.44	0.93	0.07
160	100.53	82.47	0.30	16.31	0.20	0.76	0.02
170	100.85	81.47	0.24	16.68	0.55	0.87	0.23
180	100.81	81.84	0.30	16.40	0.61	0.70	0.20
190	100.29	82.13	0.35	16.30	0.44	0.66	0.18
200	100.23	80.09	0.31	17.92	0.44	1.02	0.28
210	100.72	81.77	0.48	16.58	0.57	0.46	0.22
220	100.53	80.62	0.47	17.68	0.28	0.76	0.29
230	100.46	81.30	0.43	17.04	0.65	0.59	0.07
240	100.69	80.20	0.33	18.01	0.56	0.80	0.15
250	99.04	80.83	1.32	14.75	2.25	0.66	0.43
260	99.48	81.24	1.15	16.03	1.24	0.36	0.18
270	99.34	80.31	1.30	15.44	2.30	0.52	0.37
280	98.71	79.42	1.43	17.73	1.31	0.27	0.11
290	99.14	77.64	1.48	16.33	4.27	0.40	0.19
300	99.41	75.74	1.65	18.70	3.79	0.18	0.32
310	99.44	73.71	1.87	20.50	3.75	0.46	0.16
320	99.10	71.68	1.96	22.90	3.46	0.36	0.17
330	99.46	70.65	1.98	24.07	3.32	0.32	0.21
340	99.17	69.45	2.13	24.34	4.14	0.38	0.17
350	99.29	68.20	1.97	27.96	2.31	0.04	0.12
360	99.17	67.70	2.27	26.41	3.84	0.35	0.12
370	99.38	67.07	2.23	28.00	3.12	0.07	0.21
380	98.99	69.24	2.07	25.61	2.70	0.71	0.28
390	99.24	83.53	0.90	14.51	0.65	0.36	0.18
400	98.71	64.33	1.58	11.86	1.03	9.97	11.77

5.4.2 Heavy Mineral Analysis in TPV

In all samples, the heavies are more concentrated in the 120 mesh. All the heavies are of a fine size it's graphically represented along with the Table 5.6 showing distribution of heavies in all the samples. The heavy mineral content overall does not have too much fluctuations in the depth, maximum up to 17.56 % at the depth of about 230 cm and is minimum at about 400 cm depth with a percentage of about 5.23%.

Table 5.6 Heavy mineral composition of TPV

EDYAN VILLA			
Depth (cm)	**HM%**	**Depth(cm)**	**HM%**
0	7.58	210	17.16
10	16.05	220	17.09
20	15.41	230	17.56
30	15.76	240	16.89
40	15.33	250	15.95
50	11.99	260	15.82
60	14.95	270	15.11
70	14.35	280	14.49
80	15.75	290	14.09
90	14.33	300	12.56
100	15.2	310	12.86
110	15.05	320	11.66
120	15.82	330	11.32
130	16.01	340	11.49
140	16.53	350	11.06
150	16.69	360	9.55
160	16.45	370	9.91
170	16.25	380	11.91
180	16.6	390	6.61
190	15.8	400	5.23
200	17.04		

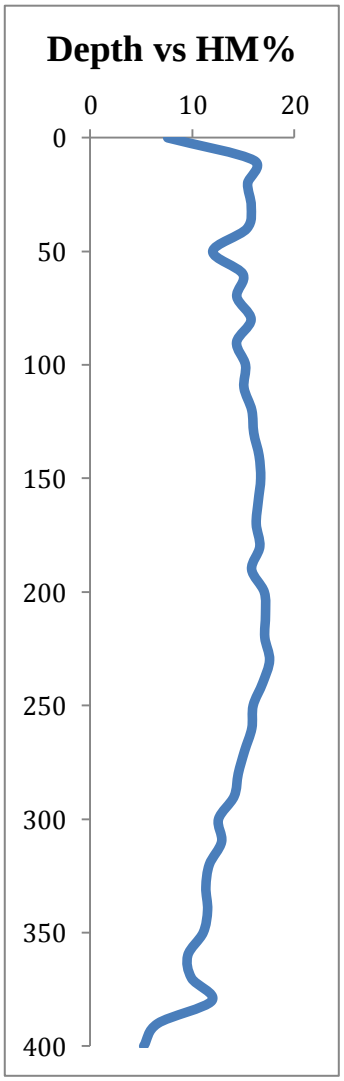

5.5 THOPPU VILLAI (THOP)SAND, CLAY, $CaCO_3$&Fe VARIATIONS

The THOP, section shows the heterogeneous deposition from (220-330 cm) in (Figure 5.9).The heterogeneous deposition forms due to shell fragments and calcrete cementation. However, the sand % show high fluctuation due to the near coast. In a depth of 550 cm sand % increases and $CaCO_3$ (%) decreases and C values increase. Clay, shows a steady increase during downfall variation of sand %. Fe (%) show no big fluctuation though out the section.

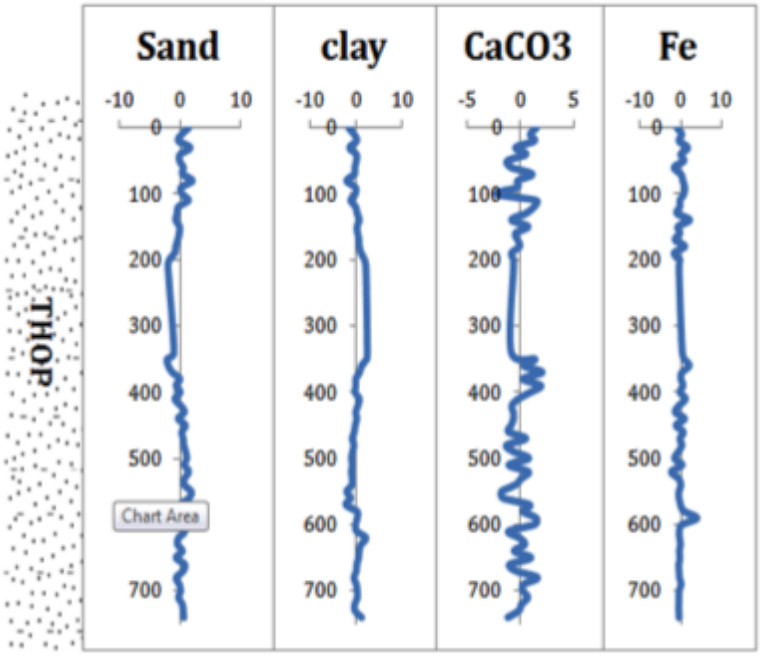

Figure 5.4 Down core variation of sand, clay, $CaCO_3$, and Fe (normalized values) in THOP

5.5.1 Sediment compositions of Thopuvillai (THOP)

In THOP trench, sand % percentage is higher and no much difference throughout the section it is high at 550 cm with 97.22% of the entire soil. Whereas clay% rates different to sand %. The clay is higher at 210

cm with11% in the ground. From the depth figure, at 220-330 cm, 1.3m of fossil ferrous deposition is found. At this 1.3 m section, the geochemical analysis is not possible due to the presence of samples in boulders. So at 1.3 meters of deposition. The analysis is skipped small Silt % found throughout the section. A negligible amount of organic matter is present in the trench. The highest silt % is 1.12% at 600cm. The high organic matter of 1.91% was at 360cm depth. The $CaCO_3$ and Fe % are negligible till 210 cm depth, a sudden increase from 340 cm depth. $CaCO_3$ shows a peak of 8.70 % at same 370 cm depth. The Fe % is a maximum of 9.92% at same 400 cm depth. In Table 5.7 percentage of various minerals are shown.

Table 5.7 Sediment compositions of Thopuvillai (THOP)

THOPPUVILLAI							
Depth (cm)	**Weight(Grm)**	**Sand %**	**Silt %**	**Clay %**	**OM %**	**CaCO3 %**	**Fe %**
0	100.20	90.71	0.50	8.12	0.30	0.29	0.08
10	100.21	89.82	0.44	9.08	0.27	0.26	0.13
20	100.22	89.40	0.48	9.50	0.24	0.28	0.10
30	100.22	90.89	0.29	8.30	0.14	0.19	0.19
40	100.20	89.64	0.44	9.43	0.13	0.24	0.12
50	100.22	89.54	0.53	9.44	0.19	0.15	0.15
60	100.22	90.02	0.42	9.18	0.16	0.17	0.05
70	100.20	89.92	0.42	9.13	0.14	0.27	0.12
80	100.22	91.16	0.31	7.81	0.38	0.20	0.14
90	100.20	89.75	0.45	9.27	0.17	0.20	0.16
100	100.21	89.87	0.43	9.27	0.18	0.10	0.15
110	100.22	90.68	0.27	8.47	0.18	0.29	0.11
120	100.22	89.42	0.62	9.30	0.27	0.28	0.11
130	100.21	89.26	0.67	9.57	0.18	0.24	0.08
140	100.20	89.07	0.45	9.95	0.15	0.17	0.21
150	100.20	89.54	0.38	9.56	0.18	0.25	0.09
160	100.22	89.51	0.39	9.65	0.15	0.19	0.11
170	100.20	89.33	0.38	9.91	0.12	0.20	0.06
180	100.20	89.07	0.38	9.92	0.26	0.21	0.16
190	100.22	88.92	0.43	10.23	0.20	0.17	0.05
200	100.20	88.26	0.51	10.83	0.11	0.18	0.11
210	100.20	88.08	0.46	11.09	0.09	0.18	0.10
340	77.46	77.31	0.38	8.17	0.34	5.39	8.41
350	72.54	72.40	0.88	7.86	1.68	7.91	9.27

Table 5.7 (Continued)

360	73.37	73.22	0.99	5.52	1.91	6.73	11.6
370	76.27	76.11	1.01	4.62	1.24	8.70	8.32
380	81.72	81.55	0.60	2.82	0.51	6.63	7.89
390	79.01	78.85	0.47	2.83	0.55	8.54	8.75
400	82.04	81.87	0.40	2.45	0.35	7.44	7.48
410	78.11	77.95	0.76	4.44	0.76	6.18	9.92
420	82.18	82.00	0.82	3.83	0.75	5.46	7.14
430	85.01	84.82	0.67	2.79	0.87	5.61	5.24
440	80.58	80.42	0.66	3.29	0.54	5.63	9.46
450	85.74	85.56	0.56	2.55	0.27	5.39	5.67
460	83.11	82.94	0.47	2.11	0.44	5.11	8.94
470	84.11	83.93	0.38	1.20	0.13	6.95	7.41
480	84.52	84.33	0.35	1.99	0.19	4.90	8.24
490	85.88	85.71	0.32	1.33	0.21	5.70	6.74
500	86.65	86.48	0.27	0.90	0.12	7.27	4.97
510	84.99	84.82	0.30	1.25	0.14	5.12	8.37
520	88.10	87.91	0.22	0.88	0.23	7.22	3.54
530	85.17	84.98	0.44	1.17	0.16	6.49	6.77
540	84.84	84.65	0.42	1.09	0.17	5.85	7.82
550	100.20	97.12	0.67	0.62	0.20	1.34	0.06
560	100.20	96.14	0.88	1.08	0.24	1.60	0.07
570	100.20	91.85	1.08	0.51	0.35	5.61	0.61
580	100.20	90.51	0.93	1.86	0.36	4.60	1.75
590	100.20	84.10	0.91	1.90	0.57	6.62	5.91
600	100.20	89.43	1.12	1.69	0.37	6.35	1.05
610	100.20	94.19	0.96	1.82	0.48	2.39	0.17
620	100.20	91.34	1.01	2.93	0.35	4.09	0.28
630	100.20	90.97	0.91	2.34	0.34	4.88	0.57
640	100.20	93.11	1.00	2.13	0.33	3.25	0.18
650	100.20	90.35	1.04	2.07	0.35	5.81	0.39
660	100.20	94.19	1.02	1.83	0.37	2.55	0.04
670	100.20	93.46	0.90	1.78	0.22	3.54	0.10
680	100.20	90.34	0.80	1.49	0.34	6.81	0.23
690	100.20	91.71	0.85	1.78	0.21	4.66	0.80
700	100.20	92.37	0.80	1.88	0.22	4.61	0.13
710	100.20	91.40	0.93	1.91	0.33	5.33	0.11
720	100.20	93.08	0.68	1.59	0.23	4.37	0.05
730	100.20	93.45	0.58	1.62	0.34	3.96	0.05
740	100.20	93.77	1.04	2.42	0.37	2.29	0.12

5.5.2 Heavy Mineral Analysis in THOP

At 120 mesh, the heavies are more concentrated in all the samples. The heavies are of fine size graphically represented with Table 5.8. The heavy mineral has more fluctuations at depths, a maximum of 10 % at the depth of about 560 cm and minimum at about 520 cm depth with 2.16%.

Table 5.8 Heavy mineral composition of THOP

THOPUVILLAI			
Depth	**HM%**	**Depth**	**HM%**
0	6.71	450	6.02
10	6.73	460	4.92
20	7.36	470	4.34
30	4.96	480	3.52
40	6.5	490	3.52
50	6.55	500	2.61
60	6.42	510	3.18
70	5.86	520	2.16
80	5.08	530	3.96
90	6.06	540	4.21
100	6.65	550	9.2
110	5.03	560	10.01
120	3.93	570	9.1
130	3.55	580	8.52
140	6.92	590	7.61
150	6.02	600	8.29
160	6.26	610	8.38
170	5.66	620	8.17
180	6.93	630	7.76
190	6.17	640	7.6
200	6.89	650	7.38
210	6.75	660	7.2
340	4.68	670	7.27
350	7.53	680	7.71
360	7.58	690	7.01
370	7.84	700	6.96
380	9.05	710	8.26
390	7.41	720	7.07
400	8.33	730	7.09
410	7.19	740	8.07
420	8.46		
430	7.61		
440	6.57		

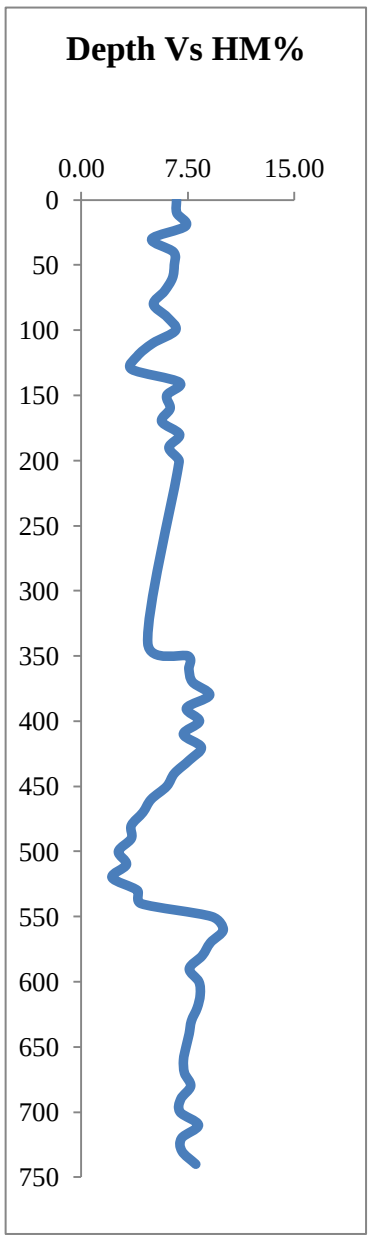

5.6 MUTTOM (MUT) SAND%, CLAY%, CaCO3% and Fe% VARIATIONS

In the Muttom (Figure 5.5) sand (%) is less until 400 cm and then from the depth of 430 cm, there is an increase in sand % and a decrease in Clay (%) values. Clay seems to have a steady rise when there is a downfall in the variation of sand %. $CaCO_3$,(%) OM, (%) and Fe (%) have related fluctuation till 180 cm. Particularly Fe (%) and $CaCO_3$ (%) have similar fluctuations throughout the profile.

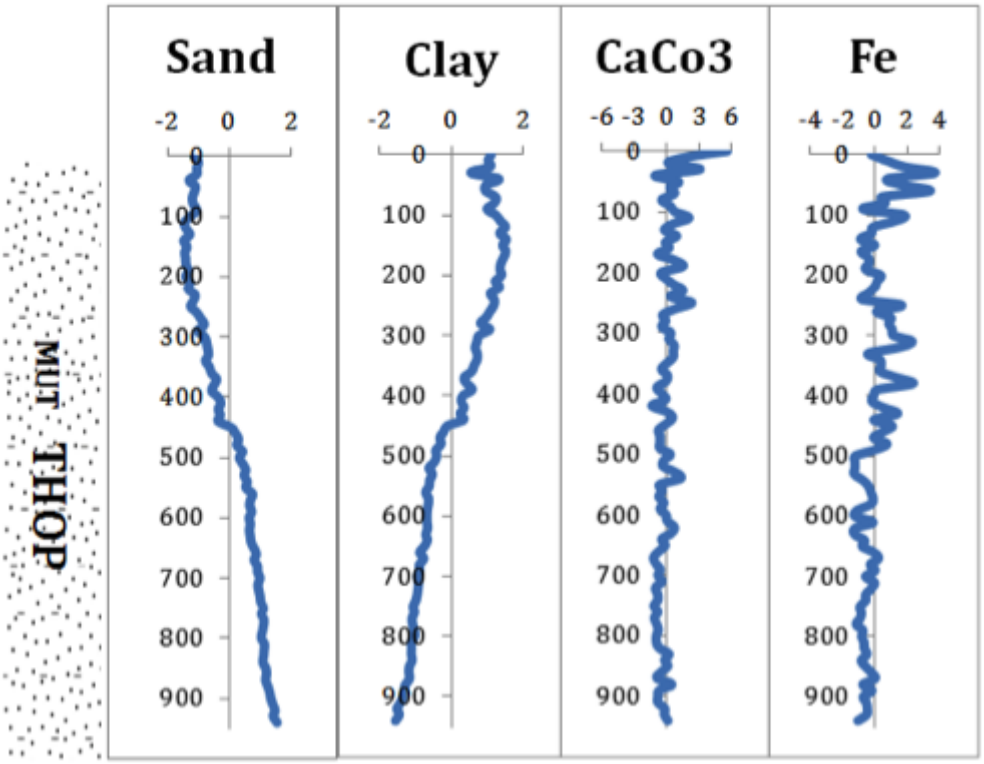

Figure 5.5 Down core variation of sand, clay, $CaCO_3$, and Fe (normalized values) in MUT

5.6.1 Sediment Compositions of Muttom (MUT)

In Muttom area samples are pretreated before the sieving analysis. Table 5.9 shows the Sand, Organic matter, Calcium Carbonate and Iron

content in the study area. The sand % percentage is low than clay % till 450 Cm depth, and clay % gets gradually lower from the depth 450 cm. However, clay% values are opposite to the sand %. The sand is highest at 940 cm of 85.76% in the soil %. The clay% is highest at 140 cm of 37.31% in the soil. Silt % is very low in the entire region. The maximum silt % is 0.97% found at 510cm. The organic matter is small. The high organic matter is 3.08% at 60cm depth. The $CaCO_3$ and Fe % are negligible till 210 cm depth, a sudden increase from 340 cm depth. $CaCO_3$ has a maximum peak of 2.59 % at same 0 cm depth. The Fe % has a maximum peak of 1.43% at 30 cm depth.

Table 5.9 Sediment compositions of Muttom (MUT)

Depth cm	Sand %	Silt %	Clay %	OM %	CaCo3 %	Fe %
0	63.61	0.36	34.04	0.17	2.59	0.33
10	64.81	0.46	33.37	0.21	1.25	0.60
20	64.41	0.22	33.83	0.82	0.64	0.90
30	64.44	0.20	29.68	5.47	1.69	1.43
40	62.33	0.09	35.68	2.21	0.21	0.61
50	64.03	0.29	33.00	2.27	0.98	0.86
60	63.66	0.16	32.86	3.08	0.70	1.35
70	63.19	0.14	35.05	1.18	0.85	0.50
80	63.52	0.16	34.75	1.46	0.43	0.57
90	64.35	0.47	33.17	2.20	0.70	0.18
100	62.70	0.46	35.04	1.06	0.87	0.89
110	61.15	0.14	36.05	2.21	1.33	0.74
120	61.55	0.34	37.13	0.41	0.80	0.35
130	62.58	0.41	35.89	0.91	0.52	0.33
140	60.95	0.39	37.31	1.13	0.92	0.13
150	61.78	0.43	36.54	1.07	0.55	0.38
160	61.19	0.46	37.20	1.05	0.66	0.15
170	61.46	0.67	36.76	1.23	0.29	0.27
180	61.54	0.25	36.16	2.15	0.85	0.29
190	62.21	0.29	35.96	1.09	1.13	0.23
200	61.48	0.56	36.30	1.75	0.41	0.49
210	62.63	0.52	34.94	2.01	0.56	0.43
220	62.12	0.44	35.80	1.41	0.81	0.38
230	63.93	0.37	33.89	1.40	1.12	0.27
240	63.50	0.25	34.72	1.51	0.72	0.16

Table 5.9 (Continued)

250	62.80	0.49	34.64	0.97	1.42	0.86
260	64.46	0.30	33.78	0.94	0.89	0.42
270	65.49	0.31	33.03	0.64	0.46	0.66
280	66.39	0.69	31.76	0.53	0.56	0.63
290	64.64	0.64	33.75	0.37	0.43	0.69
300	66.49	0.40	31.44	1.03	0.73	0.71
310	67.01	0.35	31.00	0.73	0.66	1.04
320	67.31	0.37	30.59	0.90	0.83	0.81
330	67.52	0.37	31.02	0.52	0.81	0.27
340	66.75	0.77	30.99	0.92	0.81	0.47
350	67.80	0.78	30.36	0.45	0.60	0.50
360	68.31	0.63	29.83	0.88	0.42	0.48
370	69.67	0.69	28.20	0.64	0.62	0.77
380	68.99	0.61	28.84	0.63	0.56	1.05
390	68.39	0.71	29.98	0.63	0.27	0.43
400	70.14	0.64	27.95	0.99	0.43	0.37
410	70.82	0.61	27.59	0.47	0.56	0.34
420	70.15	0.68	28.21	0.71	0.10	0.54
430	70.69	0.59	27.35	0.54	0.59	0.78
440	70.13	0.51	28.10	0.63	0.79	0.37
450	73.47	0.44	24.59	0.75	0.57	0.69
460	74.70	0.26	23.80	0.80	0.32	0.53
470	75.51	0.45	22.97	0.66	0.37	0.37
480	75.02	0.60	23.25	0.51	0.37	0.60
490	76.61	0.50	22.14	0.22	0.37	0.38
500	75.69	0.65	22.25	1.08	0.71	0.05
510	76.58	0.97	21.79	0.30	0.50	0.04
520	77.41	0.73	20.63	1.06	0.47	0.04
530	77.01	0.24	21.37	0.87	0.88	0.03
540	77.84	0.30	20.77	0.17	1.05	0.18
550	77.46	0.97	20.68	0.51	0.36	0.28
560	79.21	0.16	19.91	0.13	0.45	0.32
570	78.70	0.15	20.53	0.10	0.33	0.36
580	78.47	0.12	20.47	0.37	0.50	0.32
590	78.98	0.15	20.25	0.33	0.37	0.08
600	78.37	0.13	20.18	1.07	0.57	0.04
610	78.68	0.11	20.19	0.33	0.61	0.36
620	78.40	0.10	20.34	0.58	0.84	0.04
630	78.61	0.09	19.93	0.95	0.75	0.03

Table 5.9 (Continued)

640	78.84	0.15	20.28	0.29	0.42	0.21
650	79.54	0.13	19.60	0.20	0.54	0.17
660	80.25	0.13	18.65	0.50	0.33	0.37
670	79.64	0.13	19.48	0.33	0.16	0.45
680	80.57	0.12	18.59	0.35	0.23	0.31
690	80.60	0.10	18.62	0.08	0.37	0.39
700	81.17	0.15	18.10	0.19	0.30	0.23
710	80.69	0.15	18.37	0.15	0.44	0.38
720	80.87	0.10	18.27	0.40	0.22	0.32
730	81.22	0.12	18.09	0.18	0.29	0.23
740	81.43	0.10	17.77	0.34	0.30	0.23
750	82.10	0.12	17.22	0.38	0.17	0.13
760	81.60	0.08	17.46	0.60	0.30	0.15
770	82.30	0.10	16.94	0.48	0.18	0.13
780	82.12	0.10	17.08	0.53	0.25	0.06
790	81.84	0.10	17.45	0.26	0.31	0.18
800	81.53	0.10	17.55	0.61	0.25	0.16
810	82.41	0.10	16.81	0.38	0.25	0.20
820	82.31	0.10	16.84	0.36	0.35	0.21
830	82.18	0.10	16.76	0.24	0.66	0.25
840	81.94	0.09	17.00	0.51	0.52	0.15
850	82.77	0.10	16.38	0.06	0.62	0.23
860	82.94	0.11	16.28	0.08	0.41	0.33
870	82.72	0.10	16.41	0.26	0.27	0.39
880	83.27	0.10	15.57	0.33	0.76	0.18
890	83.79	0.06	15.20	0.45	0.34	0.34
900	84.11	0.18	14.99	0.36	0.30	0.19
910	84.61	0.08	14.48	0.43	0.30	0.24
920	85.21	0.08	13.75	0.34	0.53	0.25
930	84.73	0.06	14.21	0.42	0.52	0.24
940	85.76	0.05	13.40	0.21	0.63	0.09

5.6.2 Heavy Mineral Analysis in MUT

The heavies are more concentrated at 120 mesh. All the heavies are of a fine size and graphically represented along with the Table 5.10. The heavy mineral content does not have too much variation in the depth,

maximum up to 10 % at the depth of about 560 cm minimum at about 520 cm depth with 2.16%.

Table 5.10 Heavy mineral composition of MUT

MUTTOM					
Depth (cm)	**HM%**	**Depth**	**HM%**	**Depth**	**HM%**
0	12.03	420	16.82	840	20.20
10	12.12	430	16.50	850	20.77
20	12.11	440	16.44	860	21.27
30	12.17	450	17.80	870	22.58
40	11.24	460	17.66	880	22.55
50	11.91	470	18.09	890	23.15
60	12.04	480	18.25	900	22.49
70	11.32	490	17.70	910	21.71
80	11.47	500	18.53	920	21.07
90	11.50	510	18.35	930	20.37
100	11.58	520	18.45	940	19.12
110	11.78	530	19.19		
120	11.38	540	18.40		
130	11.55	550	18.71		
140	11.54	560	18.90		
150	11.55	570	18.94		
160	11.35	580	18.85		
170	11.68	590	18.28		
180	12.06	600	18.73		
190	11.84	610	18.98		
200	12.53	620	19.01		
210	12.44	630	18.63		
220	12.84	640	18.60		
230	12.69	650	17.88		
240	13.14	660	18.75		
250	13.72	670	18.46		
260	14.01	680	18.37		
270	14.65	690	18.25		
280	14.09	700	17.66		
290	14.50	710	18.20		
300	14.93	720	18.83		
310	14.90	730	18.62		
320	15.47	740	18.18		
330	15.41	750	18.37		
340	15.37	760	18.81		
350	14.18	770	19.19		
360	14.51	780	18.51		
370	15.45	790	18.57		
380	16.33	800	18.73		
390	15.08	810	18.63		
400	16.33	820	19.13		
410	16.36	830	19.51		

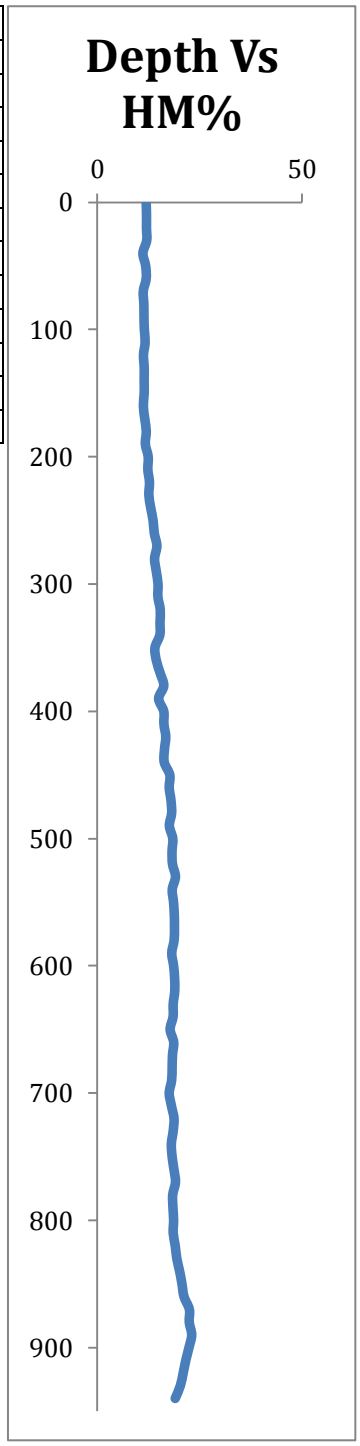

5.7 ENVIRONMENTAL MAGNETISM

Soil magnetic parameters are relatively quick and easy to obtain, compared to geochemical, sedimentological and paleontological data. The geochemical, sedimentological and paleontological data's are collected after an extended period with more processing whereas soil magnetic parameters are relatively quick and easy to obtain. Soil magnetic parameter should be used carefully to identify the variety of climatic and environmental change (Maher & Thompson 1999).

The teri sand colour and the particularity of origin in the location plays the critical problem in identifying the changes. Traditionally, the level of reddening relates to antiquity (Folk 1976, Walker 1967). However, later studies have shown that colour and age were not related. The level of dune reddening increases due to loss of ferromagnetic minerals by the process of hydrolysis (Walker 1967, Van Houten 1968, Berner 1969). With cyclic precipitation & temperature being the primary factors for dune reddening (Folk 1976, Gardner & Pye 1981, Pye & Tsoar 2009).

Many studies done on teri sand's revealed the color, sedimentology, geochemistry, paleoclimate and economic importance. (Gardner & Pye 1981, Gardner & Martingell 1990, Joseph et al. 1999, Chandrasekharan & Murugan 2001, Joseph et al. 2002, Joseph & Thrivikramji 2005, Thrivikramjiet al. 2008, Jayangondaperumalet al. 2012;). Recent research (Singhvi et al. 1986, Zhang et al. 2008, Jayangondaperumal et al. 2012) proved that dune aggradations extensively using dates of teri sands. The analyzes of Teri sand with new dimensions of environmental magnetism such as Magnetic

Susceptibility, Isothermal Remanent Magnetization (IRM) measurements and geochemistry data. For dates of teri sands Magnetic

susceptibility and IRM, values are used in environmental magnetism, due to the advantage of non-sample destruction during analysis and possibility of reuse for other studies (Lourenço et al. 2012).

To identify the concentration and type of natural magnetic carriers in the sample magnetic parameters are measured and analyzed. Maher (1986) mentioned the importance of drying the samples at low temperature, before analysis to avoid any possible changes in mineralogy. The particular or mass susceptibility, χ (measured in m^3/kg units) is the ratio of the material magnetization, J, (per mass unit) to the weak external magnetic field, H: $J=\chi H$. The magnetic susceptibility reflects the composition of sediments with a frequent contribution from ferromagnetic minerals, which has higher susceptibility values than paramagnetic and diamagnetic minerals, such as clay or quartz (e.g., Verosub & Roberts 1995, Dekkers 1997, Maher & Thompson 1999, Evans & Heller 2003).

The sample acquires remanence when exposed to a direct magnetic field at ambient temperature is called Isothermal Remanent Magnetization (IRM). IRM curves are used to estimate the characteristic coercivity of ferromagnetic structures. The trend of the IRM curves depends on the relative concentration of low-coercivity, magnetite-type, minerals and high-coercivity, hematite-type, minerals (e.g. Thompson and Oldfield, 1986). The IRM acquired in the magnetic field of one tesla (T) is defined as Saturation Isothermal Remanent Magnetisation (SIRM). IRM is imparted at fields of 0/ 12.5/ 25/ 50/ 75/ 100/ 150/ 200/ 250/ 300/ 500/ 700/ 900 mT and up to 1000 mT and backfield is imparted up to 1000 mT. The relative contribution of antiferromagnetic minerals, Hard IRM, is found using the formula HIRM $=0.5 \times (SIRM + IRM_{-300}\,mT)$ (e.g. Alargarsamy2009), where $SIRM= IRM_{1\,T}$ (Lourenco et al. 2012) calculated. HARD% (= HIRM/SIRM × 100) is also

determined (Lourenco et al. 2014). S-ratio parameters were used to determine the relative contribution of hematite versus magnetite by dividing each IRM value with the corresponding value from the SIRM (S_{-100} = $|IRM_{-100\ mT}/SIRM|$ and S_{-300}=$|IRM_{-300\ mT}/SIRM|$) (Thompson &Oldfield1986, Maher & Thompson 1999, Evans & Heller2003).

5.7.1 Magnetic Susceptibility Analysis for SKM, KCV, TPV, THOP & MUT

The geochemical data magnetic susceptibility graph is shown for different trenches to get an idea, how susceptibility values change along with geochemical analysis for different depth.

I) SERVAIKARAN MADAM

Table 5.11 shows the susceptibility values. The values are fluctuating till 350 cm depth and below 350 cm onwards the graph remains almost equal or not much changed. The highest susceptibility values of SKM is at the 9th sample is 100.49 (*10^{-8} m^3/kg) at the depth of 80 cm and scores lowest susceptibility at SKM at 24 sample, 33.57(*10^{-8} m^3/kg) at 230 cm in depth.

Table 5.11 Susceptibility variations within SKM profile with graph

Samples	Depth cm	χ (x 10-8) m^3/kg	Samples	Depth cm	χ (x 10-8) m^3/kg
SKM1	0	43.92	**SKM35**	340	79.81
SKM2	10	60.00	**SKM36**	350	66.15
SKM3	20	58.17	**SKM37**	360	74.35
SKM4	30	73.49	**SKM38**	370	70.87
SKM5	40	78.42	**SKM39**	380	71.07
SKM6	50	54.92	**SKM40**	390	74.42
SKM7	60	66.12	**SKM41**	400	76.06
SKM8	70	59.60	**SKM42**	410	76.21
SKM9	80	100.49	**SKM43**	420	77.08
SKM10	90	66.18	**SKM44**	430	72.43
SKM11	100	62.69	**SKM45**	440	76.10
SKM12	110	54.98	**SKM46**	450	74.68
SKM13	120	62.84	**SKM47**	460	78.40
SKM14	130	85.16	**SKM48**	470	77.69
SKM15	140	69.66	**SKM49**	480	69.98
SKM16	150	88.30	**SKM50**	490	72.56
SKM17	160	85.30	**SKM51**	500	74.35
SKM18	170	68.67	**SKM52**	510	70.16
SKM19	180	63.02	**SKM53**	520	75.18
SKM20	190	67.14	**SKM54**	530	71.44
SKM21	200	52.51	**SKM55**	540	72.65
SKM22	210	70.61	**SKM56**	550	69.39
SKM23	220	65.27	**SKM57**	560	72.80
SKM24	230	33.57	**SKM58**	570	75.68
SKM25	240	78.45	**SKM59**	580	71.29
SKM26	250	68.67	**SKM60**	590	71.51
SKM27	260	64.58	**SKM61**	600	70.94
SKM28	270	66.42	**SKM62**	610	77.11
SKM29	280	65.14	**SKM63**	620	71.57
SKM30	290	72.61	**SKM64**	630	72.22
SKM31	300	65.65	**SKM65**	640	70.16
SKM32	310	76.72	**SKM66**	650	71.96
SKM33	320	59.33	**SKM67**	660	75.59
SKM34	330	75.43	**SKM68**	670	73.19

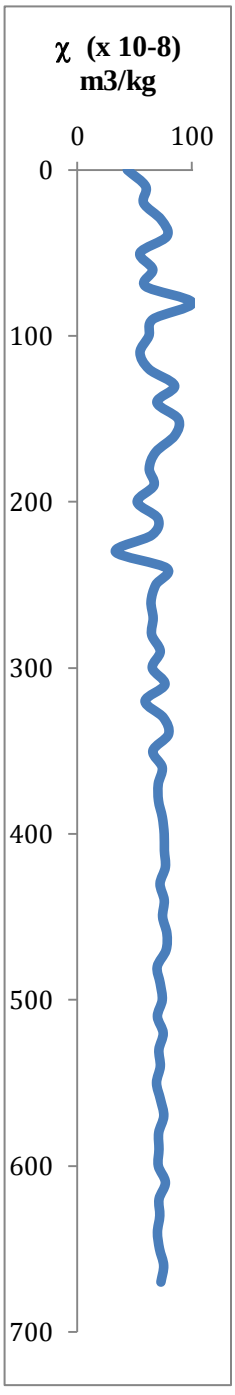

II) KATCHANAVILAI

Table 5.12 shows the susceptibility values which fluctuates till 300 cm depth and from above 300 cm, sudden decrease in susceptibility value in the depth. The highest susceptibility value of KCV 1st sample is 62.26 (*10^{-8} m^3/kg) at the depth of 0 cm, and lowest susceptibility of KCV 31 sample is 20.84 (*10^{-8} m^3/kg) at 300 cm in depth.

Table 5.12 Susceptibility variations within KCV profile with graph

Specimen	Depth cm	χ(x 10^{-8}) m^3/kg	Specimen	Depth cm	χ(x 10^{-8}) m^3/kg
KCV1	0	62.26	**KCV25**	240	54.88
KCV2	10	56.15	**KCV26**	250	41.52
KCV3	20	55.08	**KCV27**	260	44.05
KCV4	30	55.81	**KCV28**	270	43.02
KCV5	40	59.60	**KCV29**	280	43.35
KCV6	50	53.94	**KCV30**	290	42.37
KCV7	60	52.91	**KCV31**	300	20.84
KCV8	70	52.54	**KCV32**	310	20.91
KCV9	80	57.57	**KCV33**	320	21.78
KCV10	90	51.58	**KCV34**	330	29.03
KCV11	100	49.97	**KCV35**	340	32.81
KCV12	110	50.43			
KCV13	120	55.45			
KCV14	130	45.51			
KCV15	140	49.98			
KCV16	150	48.61			
KCV17	160	48.82			
KCV18	170	47.62			
KCV19	180	53.07			
KCV20	190	44.70			
KCV21	200	49.09			
KCV22	210	48.75			
KCV23	220	51.00			
KCV24	230	48.34			

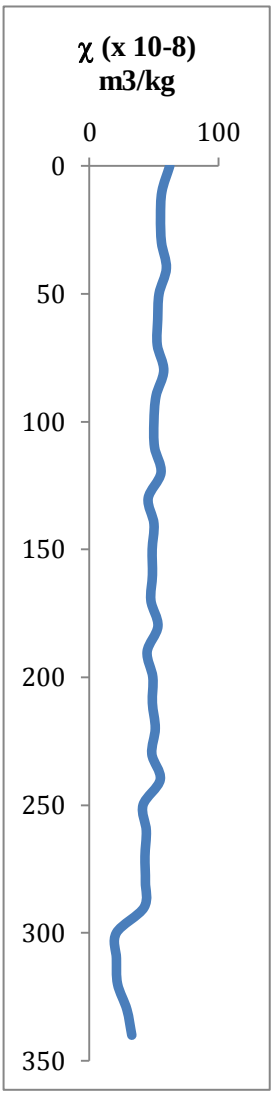

III) EDYAN VILLA

The Table 5.13 shows the susceptibility values (table12) are quite fluctuated up and down towards till 350 cm depth and from 350 cm there is a sudden decrease in susceptibility value in the depth. The highest susceptibility values score at TPV 33 sample is 69.34 (*10^{-8} m^3/kg) at the depth of 320 cm and scores lowest susceptibility at TPV 41 sample is 11.31(*10^{-8} m^3/kg) at 400 cm in depth.

Table 5.13 Susceptibility variations within KCV profile with graph

Samples	Depth	χ (x 10-8) m3/kg	Samples	Depth	χ (x 10-8) m3/kg
TPV1	0	57.41	**TPV22**	210	60.54
TPV2	10	54.45	**TPV23**	220	62.65
TPV3	20	52.10	**TPV24**	230	61.24
TPV4	30	52.11	**TPV25**	240	62.30
TPV5	40	56.72	**TPV26**	250	58.17
TPV6	50	54.35	**TPV27**	260	57.57
TPV7	60	54.85	**TPV28**	270	60.13
TPV8	70	55.31	**TPV29**	280	60.53
TPV9	80	56.57	**TPV30**	290	64.43
TPV10	90	59.66	**TPV31**	300	62.02
TPV11	100	61.41	**TPV32**	310	61.61
TPV12	110	60.90	**TPV33**	320	69.34
TPV13	120	54.70	**TPV34**	330	67.24
TPV14	130	58.08	**TPV35**	340	68.35
TPV15	140	55.85	**TPV36**	350	67.40
TPV16	150	56.53	**TPV37**	360	67.54
TPV17	160	57.99	**TPV38**	370	67.18
TPV18	170	55.74	**TPV39**	380	59.06
TPV19	180	60.38	**TPV40**	390	32.26
TPV20	190	60.95	**TPV41**	400	11.31
TPV21	200	61.19			

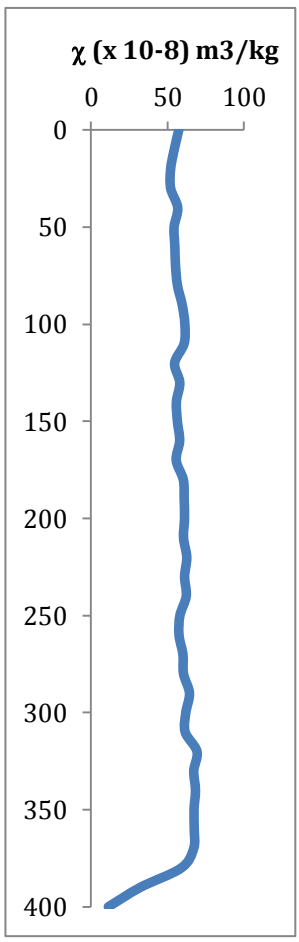

IV) THOPUVILLA

In THOP sample section Table 5.14, the section has been divided into four levels due to the height, so the level repeated samples names. The

susceptibility values are quite fluctuated up and down towards till 210 cm depth and from 210 cm there is a sudden decrease in susceptibility value in the depth. Again the susceptibility values get higher at the depth 550 cm. The highest susceptibility values score at THOP 9 sample is 55.16 (*10^{-8} m^3/kg) at the depth of 320 cm and scores lowest susceptibility at THOP 1 sample is 11.67 (*10^{-8} m^3/kg) at 220 cm in depth.

Table 5.14 Susceptibility variations within THOP profile with graph

Sample	Depth cm	χ(x 10^{-8}) m^3/kg	sample	Depth cm	χ(x 10^{-8}) m^3/kg	sample	Depth cm	χ(x 10^{-8}) m^3/kg
thop1	0	50.60	**thop1**	340	25.98	**thop14**	680	34.16
thop2	10	52.49	**thop2**	350	30.93	**thop15**	690	34.78
thop3	20	48.99	**thop3**	360	32.34	**thop16**	700	33.44
thop4	30	49.02	**thop4**	370	31.34	**thop17**	710	33.65
thop5	40	47.95	**thop5**	380	32.18	**thop18**	720	31.91
thop6	50	49.38	**thop6**	390	28.47	**thop19**	730	33.08
thop7	60	50.00	**thop7**	400	34.47	**thop20**	740	36.36
thop8	70	53.37	**thop8**	410	31.44			
thop9	80	55.16	**thop9**	420	29.31			
thop10	90	49.14	**thop10**	430	29.26			
thop11	100	49.10	**thop11**	440	27.89			
thop12	110	46.81	**thop12**	450	27.04			
thop13	120	46.82	**thop13**	460	22.49			
thop14	130	47.25	**thop14**	470	20.09			
thop15	140	45.69	**thop15**	480	24.53			
thop16	150	41.49	**thop16**	490	19.22			
thop17	160	46.31	**thop17**	500	19.22			
thop18	170	49.51	**thop18**	510	21.08			
thop19	180	47.06	**thop19**	520	18.47			
thop20	190	47.28	**thop20**	530	24.63			
thop21	200	49.66	**thop21**	540	21.95			
thop22	210	48.57	**thop1**	550	40.17			
thop1	220	11.67	**thop2**	560	38.36			
thop2	230	22.22	**thop3**	570	39.75			
thop3	240	14.28	**thop4**	580	39.36			
thop4	250	19.82	**thop5**	590	44.74			
thop5	260	30.81	**thop6**	600	40.46			
thop6	270	16.74	**thop7**	610	35.42			
thop7	280	31.90	**thop8**	620	34.76			
thop8	290	23.10	**thop9**	630	36.05			
thop9	300	36.41	**thop10**	640	35.69			
thop10	310	31.94	**thop11**	650	34.78			
thop11	320	28.73	**thop12**	660	33.07			
thop12	330	30.91	**thop13**	670	27.90			

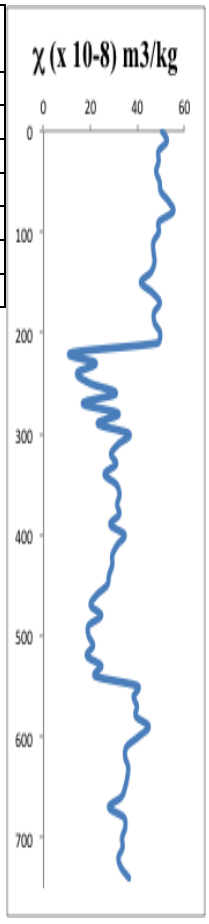

V) MUTTOM

The Table 5.15 shows the sample section is one of the biggest sampled section. The susceptibility values are quite fluctuated up and down towards till 400 cm depth and from 400 cm there is a gradual decrease in susceptibility value in the depth. The highest susceptibility values score at MUT 40 sample is 83.76 (*10^{-8} m^3/kg) at the depth of 300 cm and scores lowest susceptibility at MUT 95 sample is 5.66 (*10^{-8} m^3/kg) at 940 cm in depth.

Table 5.15 Susceptibility variations within MUT profile with graph

Specimen	Depth (cm)	χ(x 10^{-8}) m^3/kg	Specimen	Depth (cm)	χ(x 10^{-8}) m^3/kg
M1	0	47.60	**M29**	280	34.56
M2	10	42.66	**M30**	290	21.64
M3	20	37.35	**M31**	300	20.77
M4	30	40.89	**M32**	310	22.62
M5	40	35.17	**M33**	320	20.96
M6	50	38.59	**M34**	330	20.60
M7	60	37.27	**M35**	340	29.55
M8	70	33.31	**M36**	350	78.80
M9	80	21.05	**M37**	360	33.12
M10	90	29.00	**M38**	370	19.85
M11	100	29.79	**M39**	380	18.53
M12	110	34.79	**M40**	390	83.76
M13	120	29.56	**M41**	400	24.63
M14	130	29.75	**M42**	410	19.13
M15	140	44.47	**M43**	420	18.27
M16	150	52.77	**M44**	430	17.11
M17	160	41.75	**M45**	440	17.06
M18	170	74.05	**M46**	450	13.58
M19	180	71.88	**M47**	460	14.36
M20	190	49.80	**M48**	470	13.56
M21	200	28.27	**M49**	480	13.49
M22	210	26.34	**M50**	490	13.17
M23	220	28.79	**M51**	500	14.35
M24	230	47.15	**M52**	510	13.32
M25	240	26.64	**M53**	520	12.46
M26	250	22.91	**M54**	530	13.46

Table 5.15 (Continued)

M27	260	30.09	**M55**	540	13.08
M28	270	21.60	**M56**	550	12.79
M57	560	12.69	**M77**	760	8.93
M58	570	11.82	**M78**	770	8.91
M59	580	11.32	**M79**	780	9.11
M60	590	12.04	**M80**	790	9.06
M61	600	11.57	**M81**	800	9.01
M62	610	10.96	**M82**	810	8.39
M63	620	0.61	**M83**	820	8.57
M64	630	11.61	**M84**	830	9.23
M65	640	11.79	**M85**	840	8.56
M66	650	10.36	**M86**	850	9.80
M67	660	10.03	**M87**	860	7.29
M68	670	10.24	**M88**	870	7.47
M69	680	9.73	**M89**	880	8.39
M70	690	9.77	**M90**	890	6.55
M71	700	10.14	**M91**	900	5.83
M72	710	10.63	**M92**	910	5.98
M73	720	9.68	**M93**	920	5.78
M74	730	9.62	**M94**	930	6.45
M75	740	9.97	**M95**	940	5.66
M76	750	8.74			

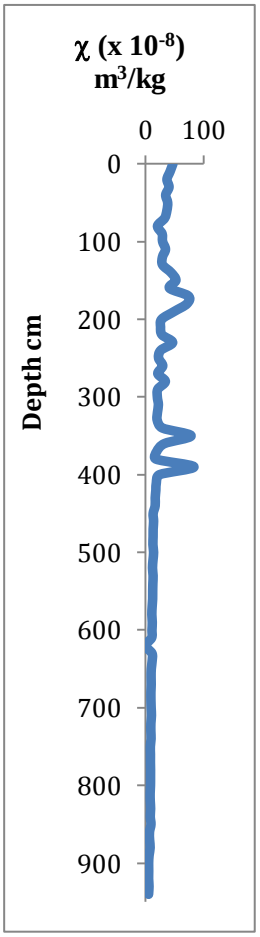

5.7.2 Magnetic Parameters with Each Profile

The χ, SIRM, S-ratios, SIRM/χ and HIRM% variations in the different sampling sites for some representative samples of each section is shown in Table 5.16. For THOP, the magnetic susceptibility values range between 11.67 and 55.16 × 10^{-8} m^3kg^{-1} (mean= 36.46) and the SIRM between 0.557 and 3.007 × 10^{-3} $Am^{-1}kg^{-1}$ (mean= 2.104). For KCV the magnetic susceptibility values range between 21.78 and 62.26 × 10^{-8} m^3kg^{-1} (mean= 49.25) and the SIRM between 3.452 and 8.228 × 10^{-3} $Am^{-1}kg^{-1}$ (mean= 7.105). For SKM the magnetic susceptibility values range between 33.57 and 100.49 × 10^{-8} m^3kg^{-1} (mean= 70.14) and for SIRM between 0.926 and 3.221 × 10^{-3} $Am^{-1}kg^{-1}$ (mean= 1.916). Finally, for TPV the magnetic

susceptibility values range between 11.31 and 67.40 × 10^{-8} m^3kg^{-1} (mean= 54.25) and the SIRM between 1.042 and 7.774 × 10^{-3} $Am^{-1}kg^{-1}$ (mean= 6.196). In Muttom, the magnetic susceptibility values range between 5.662 and 83.75 × 10^{-8} m^3kg^{-1} (mean= 34.23) and the SIRM between 0.118 and 6.499 × 10^{-3} $Am^{-1}kg^{-1}$ (mean= 2.949).

In all the samples (excluding THOP) S_{-300} values are below 0.80, which indicates the low quantity of magnetite-like structures. Whereas, in THOP, the value of S_{-300} is of 0.79, so the presence of a small magnetite-like fraction is confirmed. The (small), quantity of magnetite-like structure is corroborated by the values of HIRM%, which are always higher than 10% in KCV, SKM, TPV and MUT samples, with means of 17.58%, 20.91%,12.28% and 15.51% respectively, confirming the significant contribution of canted antiferromagnetic such as hematite structures. In THOP samples, the HIRM% is below 10%.

The SIRM/χ ratio depends on the composition and grain size of the magnetic particles. When the magnetic mineralogy is homogeneous, the ratio indicates the changes in the grain size assemblage of the ferrimagnetic minerals (e.g. Thompson & Oldfield 1986, Moreno et al. 2003). The magnetic mineralogy indicated by the S_{-300} ratio is not homogeneous in KCV, SKM, TPV, and MUT the SIRM/χ ratio only can be considered in the THOP samples. Thompson & Oldfield (1986) considered the mean SIRM/χ value of 10 kAm^{-1} indicates a magnetite grain size of 5 µm. However, Sandgren & Thompson (1990), indicate the value of 6.40 kAm^{-1} is corresponding to a magnetite grain size of 8 µm. Based on those authors, the mean SIRM/χ value of 5.78 kAm^{-1} obtained in our study in THOP indicates an average grain size of the ferrimagnetic particles of ca. 8 µm.

Table 5.16 Various magnetic parameter analysis of each profile

Depth cm	Samples	χ(*10^{-8}m^3/kg)	SIRM(*10^$^{-3}$AM ^2/kg	s-300	s-100	HIRM %	SIRM/χ (KA/m)
10	THOP2-L1	52.49	3.077	0.833	0.481	8.34	5.86
50	THOP6-L1	49.37	2.454	0.844	0.483	7.80	4.97
80	THOP9-L1	55.16	2.902	0.775	0.333	11.27	5.26
150	THOP16-L1	41.49	3.107	0.824	0.401	8.81	7.49
170	THOP18-L1	49.51	3.005	0.805	0.402	9.74	6.07
210	THOP22-L1	48.57	2.763	0.803	0.397	9.84	5.69
220	THOP22-L2	11.67	0.577	0.778	0.313	11.09	4.94
260	THOP5-L2	30.81	2.516	0.823	0.441	8.87	8.17
300	THOP9-L2	36.41	1.975	0.828	0.488	8.62	5.43
330	THOP12-L2	30.91	2.304	0.806	0.362	9.69	7.45
360	THOP3-L3	32.34	2.367	0.780	0.254	11.00	7.32
400	THOP7-L3	34.47	2.882	0.733	0.071	13.36	8.36
440	THOP11-L3	27.89	1.679	0.733	0.219	13.36	6.02
480	THOP15-L3	24.53	1.273	0.566	0.234	21.68	5.19
540	THOP21-L3	21.95	1.044	0.803	0.344	9.87	4.75
570	THOP3-L4	39.75	2.063	0.806	0.490	9.68	5.19
590	THOP5-L4	44.74	1.885	0.837	0.516	8.15	4.21
640	THOP10-L4	35.69	1.545	0.812	0.495	9.40	4.33
670	THOP13-L4	27.90	1.510	0.823	0.467	8.84	5.41
710	THOP17-L4	33.65	1.159	0.819	0.501	9.04	3.44
	Mean	36.47	2.104	0.792	0.385	10.42	5.78
0	KCV-1	62.26	7.067	0.691	0.104	15.47	11.35
40	KCV-5	59.60	8.067	0.681	0.091	15.95	13.54
90	KCV-10	51.58	7.487	0.666	0.046	16.70	14.52
140	KCV-15	49.98	8.228	0.652	0.037	17.40	16.46
190	KCV-20	44.70	7.479	0.662	0.040	16.91	16.73
240	KCV-25	54.88	7.952	0.662	0.021	16.89	14.49
320	KCV-33	21.78	3.452	0.526	0.049	23.70	15.85
	Mean	49.25	7.105	0.648	0.047	17.58	14.71
0	SKM-1	43.92	1.388	0.572	0.092	21.41	3.16
30	SKM-4	73.49	2.424	0.589	0.082	20.53.	3.30
80	SKM-9	100.49	3.211	0.594	0.085	20.28	320
150	SKM-16	88.30	3.210	0.586	0.112	20.69	3.64
230	SKM-24	33.57	0.927	0.587	0.053	20.63	2.76

Table 5.16 (Continued)

260	SKM-27	64.58	1.237	0.590	0.006	20.49	191.57
320	SKM-33	59.33	1.834	0.552	0.095	22.38	3.09
410	SKM-42	76.21	1.888	0.585	0.050	20.76	2.48
480	SKM-49	77.69	1.674	0.579	0.052	21.07	2.16
530	SKM-54	71.44	1.677	0.565	0.083	21.74	2035
610	SKM-62	77.11	1.836	0.547	0.371	22.65	2038
660	SKM-67	75.59	1.690	0.635	0.149	18.26	2.24
	Mean	70.14	1.916	0.582	0.103	20.91	18.53
0	TPV-1	57.41	6.552	0.740	0.214	12.99	114.13
40	TPV-5	56.72	7.668	0.748	0.146	12.58	13.52
90	TPV-10	59.67	6.913	0.771	0.215	11.47	11.59
140	TPV-15	55.85	6.557	0.737	0.207	12.14	11.74
230	TPV-24	61.24	6.360	0.773	0.232	11.35	10.39
290	TPV-30	64.43	6.734	0.764	0.244	11.78	10.45
350	TPV-36	67.40	7.744	0.745	0.272	12.76	11.49
400	TPV-41	11.31	1.042	0.757	0.252	12.15	9.21
	Mean	54.25	6.196	0.754	0.223	12.28	24.06
0	MUT1	47.60	5.531	0.004	0.002	9.758	11.619
40	MUT5	35.17	4.540	0.003	0.001	12.119	12.911
90	MUT10	29.00	3.405	0.002	0.000	13.603	11.743
150	MUT16	52.77	4.752	0.004	0.002	10.103	9.005
170	MUT18	74.05	6.500	0.005	0.003	7.961	8.777
200	MUT21	28.27	3.574	0.003	0.000	14.572	12.645
230	MUT24	47.15	0.118	0.004	0.001	11.267	0.250
280	MUT29	34.56	3.167	0.002	0.000	13.806	9.163
310	MUT32	22.62	2.652	0.002	0.001	17.119	11.726
350	MUT36	78.80	5.852	0.005	0.003	7.187	7.426
370	MUT38	19.85	2.161	0.001	0.000	12.153	10.887
390	MUT40	83.76	5.788	0.005	0.003	6.581	6.911
440	MUT45	17.06	1.518	0.001	0.000	21.488	8.894
550	MUT56	12.79	1.047	0.001	0.000	23.458	8.189
680	MUT69	9.73	0.692	0.000	0.000	23.999	7.110
750	MUT76	8.74	0.612	0.000	0.000	24.563	6.995
840	MUT85	8.56	0.732	0.000	0.000	23.649	8.559
940	MUT95	5.66	0.456	0.000	0.000	25.869	8.046
	Mean	34.23	2.950	0.002	0.001	15.514	8.937

In THOP, the IRM acquisitions curves show saturation in the field between 500 and 600 mT followed by a small increase in intensity in

increasing fields, suggesting that these samples may contain both multidomain magnetite structures and antiferromagnetic minerals such as hematite. In KCV, SKM, TPV and MUT samples, the IRM acquisition curves show saturation level is not obtained at the applied fields, whereas the point towards the presence of a canted antiferromagnetic phase such as hematite (Figure 5.6).

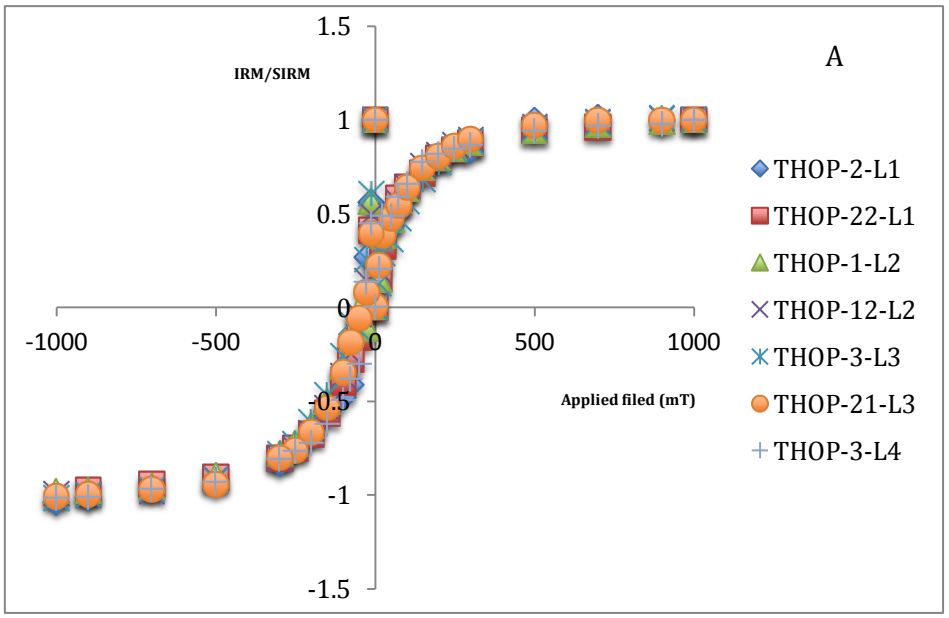

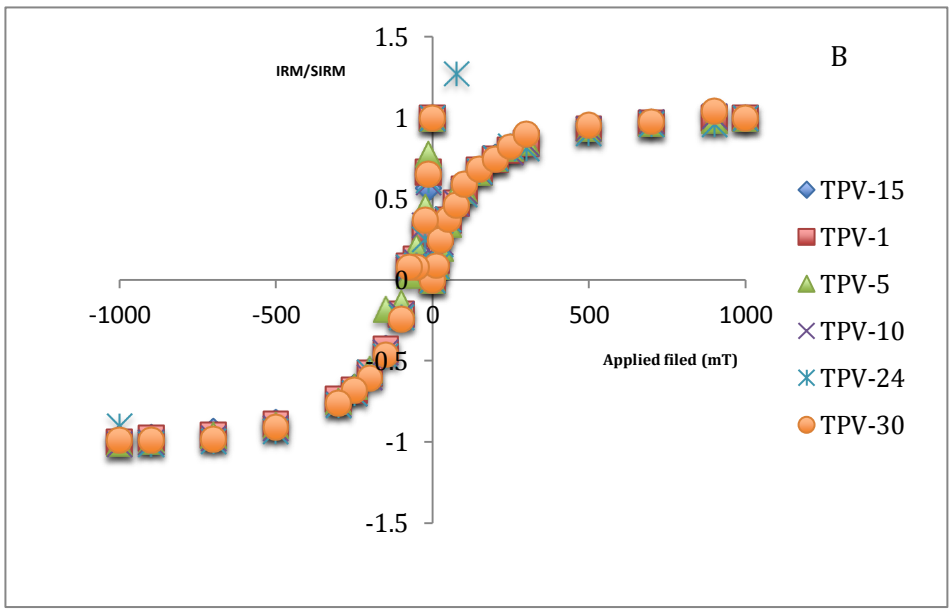

Figure 5.6 (Continued)

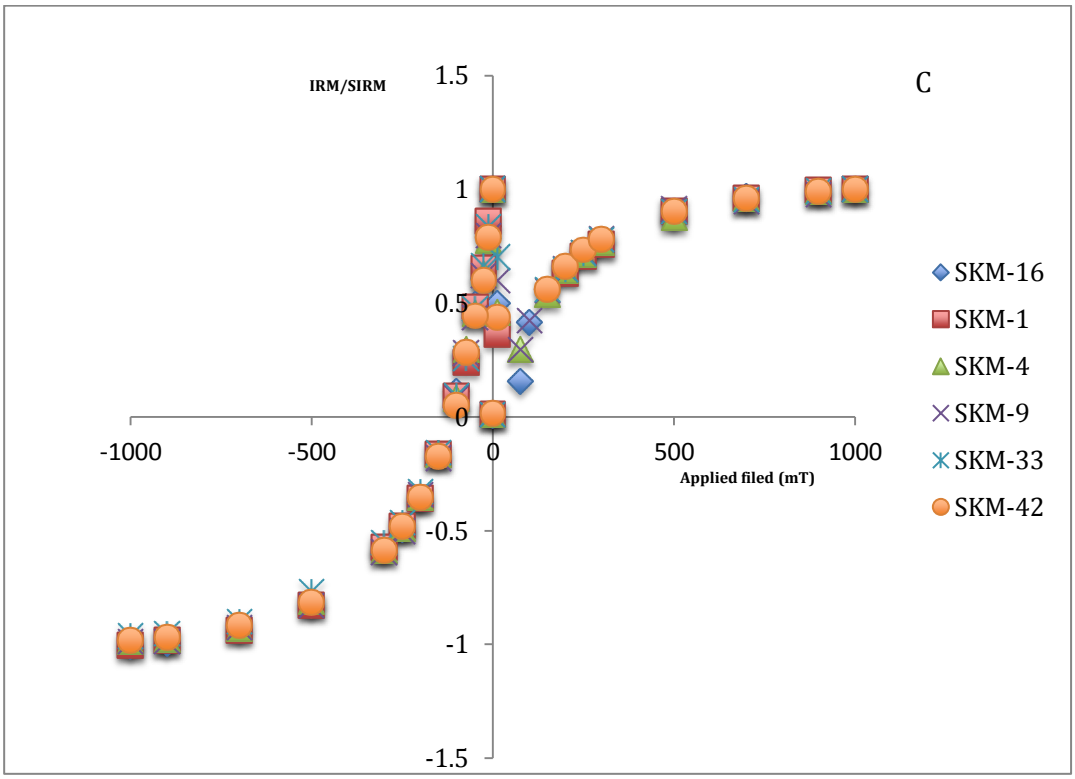

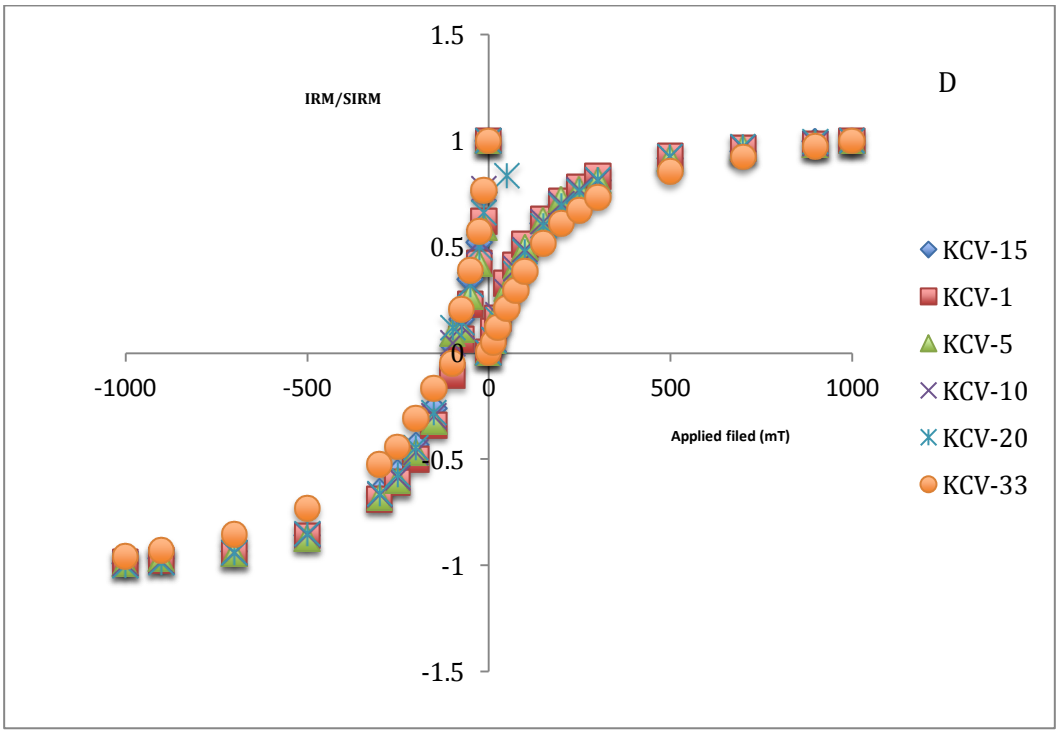

Figure 5.6 (Continued)

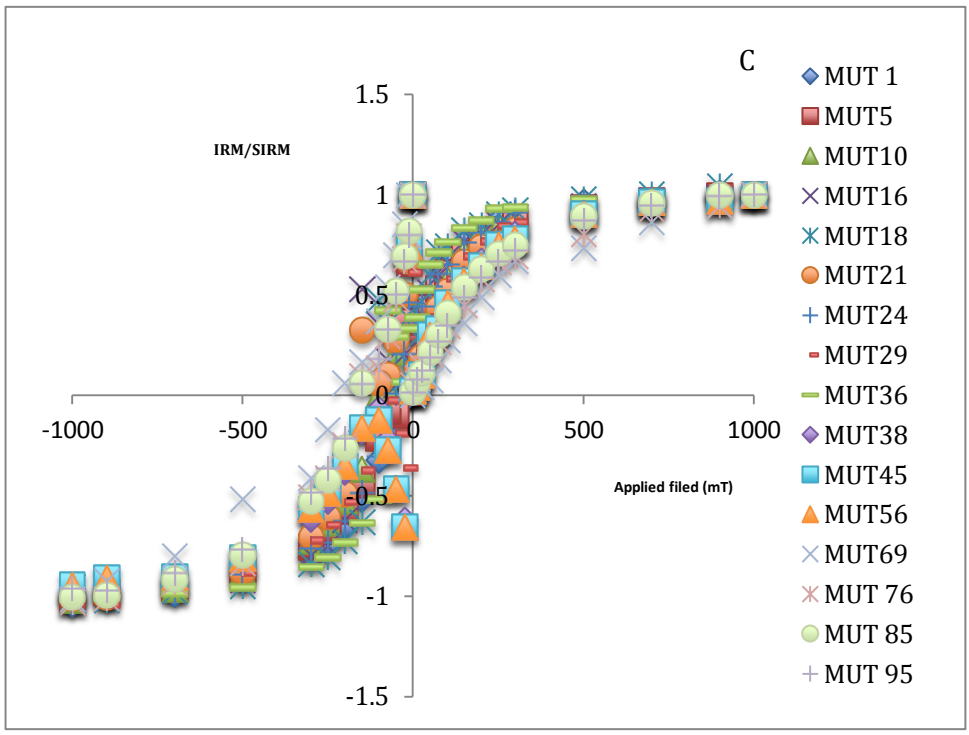

Figure 5.6 IRM curves of A) THOP, B) TPV, C) SKM, D) KCV and MUT

The remanence coercivity parameter, B_{OCR} is obtained from IRM curves (Figure 5.6). SKM samples show B_{OCR} of >100 mT indicates antiferromagnetic minerals presence. KCV samples show B_{OCR} varying between 75-100 mT, which clearly indicates antiferromagnetic minerals presence. In TPV samples, B_{OCR} changing from 50 mT to 75 mT indicates multidomain magnetite or mixed mineral contents of magnetite and antiferromagnetic minerals presence. Finally, some THOP samples show B_{OCR} varies from 50 mT to 75 mT indicates multidomain magnetite or magnetite and antiferromagnetic minerals presence; other THOP samples has B_{OCR} between 25 mT to 50 mT confirms that these samples are magnetite bearing.

Also, MUT area samples show (Figure 5.6) the B_{OCR} variation from 100mT to 150 mT and some varies from 150 mT to 200mT indicating the antiferromagnetic minerals presence. Moreover, MUT area samples show B_{OCR} of <100 mT states that multidomain magnetite or mixed mineral contents of magnetite and antiferromagnetic minerals are present in the samples.

5.7.3 Variation of Magnetic Parameters within Each Profile

Depth changes the magnetic parameters, for the four profiles, are presented in Figure 5.7. In the KCV profile, a steep increase of χ and SIRM occurs at 240 cm, then a sudden decrease. In the SKM profile, an increase of χ and SIRM and a slight decrease of HIRM% can be observed in the depth of 80 cm. An extreme variation occurs at the depth of 230 cm characterized by the decline of χ and SIRM and a slight increase of HIRM%. In THOP samples, at 220 cm, a similar variation occurs: a decrease of χ, SIRM and S_{-300} and a small increase of HIRM%. In TPV profile, χ and SIRM do change with depth.

Finally, in Muttom profile, there was a sudden increase of χSIRM, S_{-300} and S_{-100} in the depths of 170cm, 350cm and 390cm and a steep decrease in the depths of 200cm, 310cm, 370cm, and 410cm respectively. From the profile, we conclude that below the depth of 400cm there is no significant change.

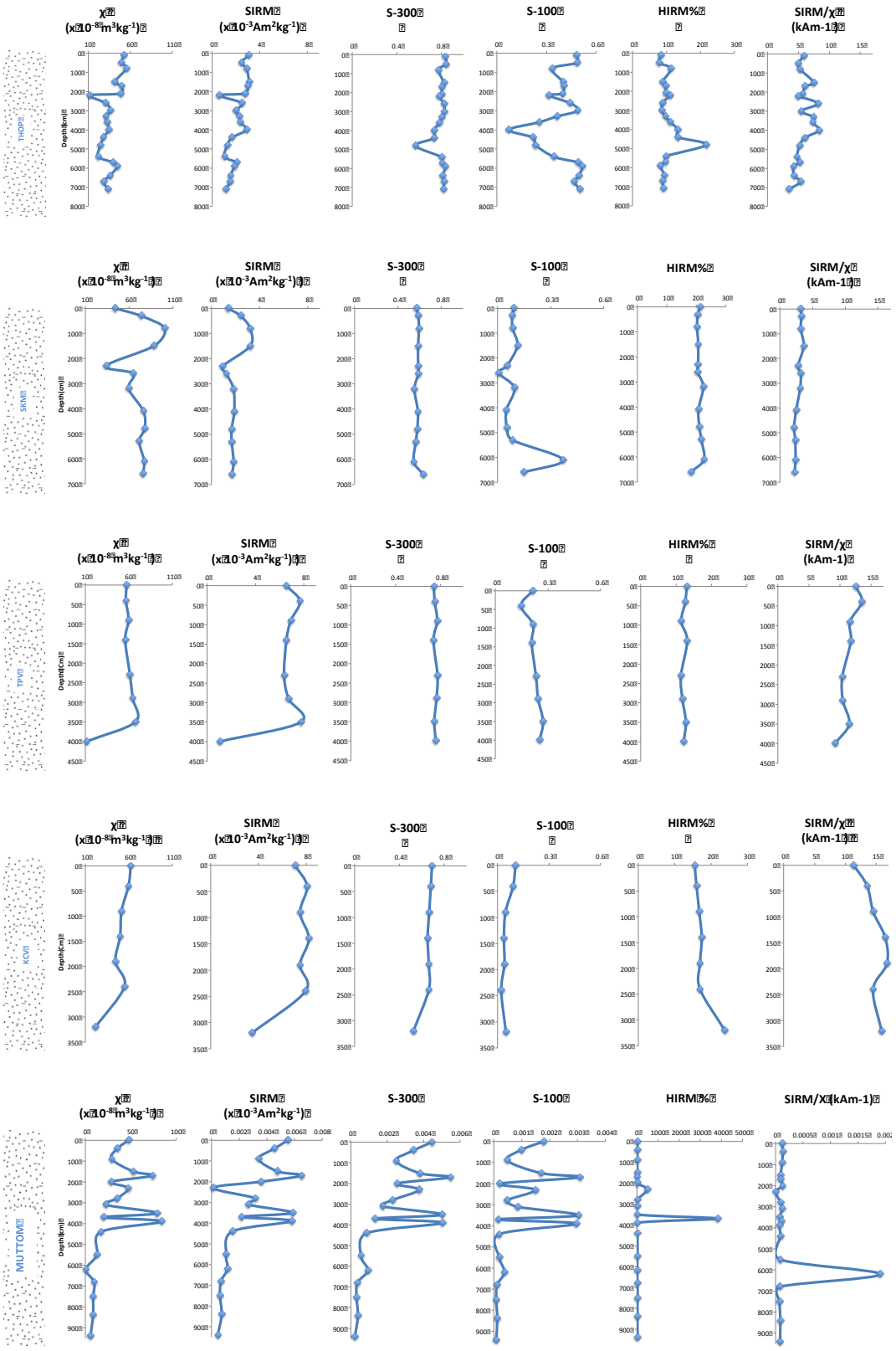

Figure 5.7 Magnetic Parameters of each profile

5.8 MINERAL INFERENCE WITH XRD ANALYSIS

This section deals with the study of X-ray diffraction as a tool to find out the minerals percentage at different depths. From the results, we can roughly determine the type of deposition taken place and its occurrence. In TPV and KCV section (Table 5.17), quartz, rutile, zircon, kaolinite, hematite, magnetite and sillimanite are present. In this section, the presence of quartz is dominant than other minerals. The minerals present in TPV and KCV section are usually found in semi-arid/dry condition. The Aeolian process made a significant role during the TPV deposition.

In THOP, quartz, calcite, rutile, zircon, pyrope and sylvite are present. At 30cm depth, the minerals are supported by Aeolian process, which showed arid deposition with heavy wind flow. Furthermore, at 280cm, calcite mineral depicted the dominance due to shells of dead marine organisms. This proves the presence of paleo minerals (pyrope & sylvite) in abundance in the sea level at a depth of 510 cm. These minerals were formed during dry condition.

Also, in MUT and SKM section (Table 5.17) quartz, almandine, kaolinite, hematite, halloysite and xenotime are present. In these areas, hematite and kaolinite are dominant among other minerals. These minerals are formed during the wet-to-dry period. This is due to ancient paleo sea level or due to primordial lagoon formation.

Table 5.17 Inferred minerals in XRD analysis

Ref.No	Depth/Min	Quartz	calcite	Rutile	Zircon	Pyrope	Almandine	Sylvite	Kaolanite	Hematite	halloysite	Xenotime	Ilmenite	Magnesite	Sillmanite	Magnetite
Thop/L1/4	30cm	✔	✖	✔	✔	✖	✔	✖	✖	✖	✖	✖	✖	✖	✖	✖
Thop/L2/7	280cm	✔	✔	✔	✖	✖	✖	✖	✖	✖	✖	✖	✖	✖	✖	✖
Thop/L3/18	510cm	✔	✔	✔	✖	✔	✖	✖	✖	✖	✖	✖	✖	✖	✖	✖
Thop/L4/20	740cm	✔	✔	✔	✔	✖	✖	✓	✖	✖	✖	✖	✖	✖	✖	✖
Ref.No	Depth/Min	Quartz	calcite	Rutile	Zircon	Pyrope	Almandine	Sylvite	Kaolanite	Hematite	halloysite	Xenotime	Ilmenite	Magnesite	Sillmanite	Magneite
MUT 19	180cm	✔	✖	✖	✖	✖	✔	✖	✔	✔	✔	✔	✖	✖	✖	✖
MUT36	350cm	✔	✖	✖	✖	✖	✖	✖	✔	✔	✖	✖	✖	✖	✖	✖
MUT95	940cm	✔	✖	✖	✖	✖	✔	✖	✖	✔	✔	✖	✖	✖	✖	✖
Ref.No	Depth/Min	Quartz	calcite	Rutile	Zircon	Pyrope	Almandine	Sylvite	Kaolanite	Hematite	halloysite	Xenotime	Ilmenite	Magnesite	Sillmanite	Magnetite
SKM 9	80cm	✔	✖	✔	✔	✖	✖	✖	✔	✔	✖	✖	✔	✖	✖	✖
SKM24	230cm	✔	✖	✖	✖	✖	✖	✖	✖	✖	✖	✖	✖	✖	✖	✖
SKM57	560cm	✔	✖	✖	✖	✖	✖	✖	✔	✔	✖	✖	✖	✖	✖	✖
Ref.No	Depth/Min	Quartz	calcite	Rutile	Zircon	Pyrope	Almandine	Sylvite	Kaolanite	Hematite	halloysite	Xenotime	Ilmenite	Magnesite	Sillmanite	Magnetite
TPV1	0 CM	✔	✖	✔	✔	✖	✖	✖	✔	✔	✖	✖	✖	✔	✖	✖
TPV24	230cm	✔	✖	✖	✔	✖	✖	✖	✔	✔	✖	✖	✖	✖	✔	✖
TPV57	560cm	✔	✔	✔	✖	✖	✖	✖	✖	✔	✖	✖	✖	✖	✖	✖
Ref.No	Depth/Min	Quartz	calcite	Rutile	Zircon	Pyrope	Almandine	Sylvite	Kaolanite	Hematite	halloysite	Xenotime	Ilmenite	Magnesite	Sillmanite	Magnetite
KCV1	0 cm	✔	✔	✖	✖	✖	✖	✖	✔	✔	✖	✖	✔	✖	✖	✔
KCV20	190 cm	✔	✔	✖	✖	✖	✖	✖	✔	✔	✖	✖	✖	✔	✖	✖
KCV 33	320cm	✔	✖	✖	✖	✖	✖	✖	✔	✔	✖	✖	✖	✖	✖	✖

ANNA UNIVERSITY, CHENNAI - 600 025

Figure 5.8 X-ray diffraction analysis THOP 4 at 30 cm depth

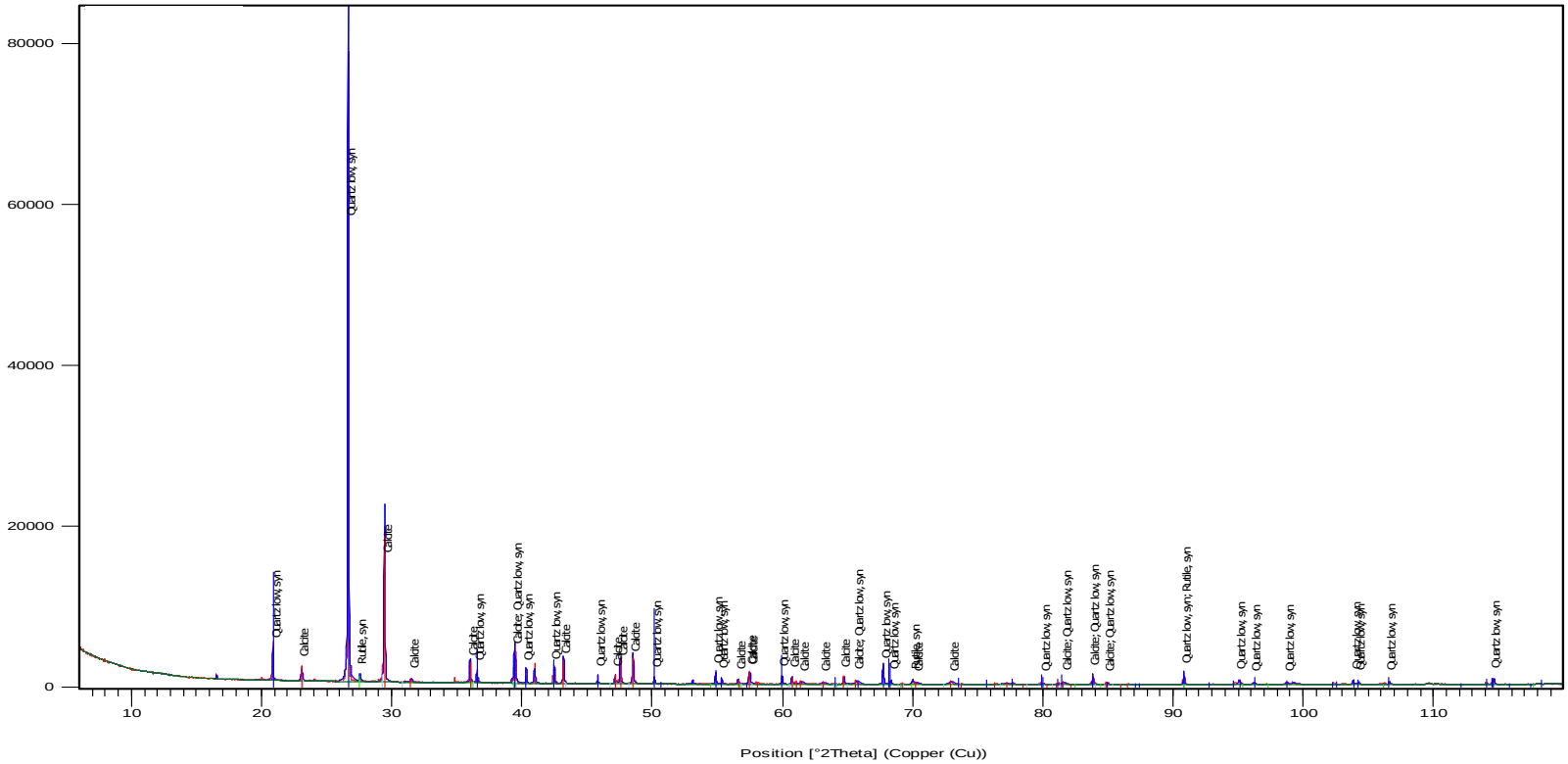

Figure 5.9 X-ray diffraction analysis THOP 7 at 280 cm depth

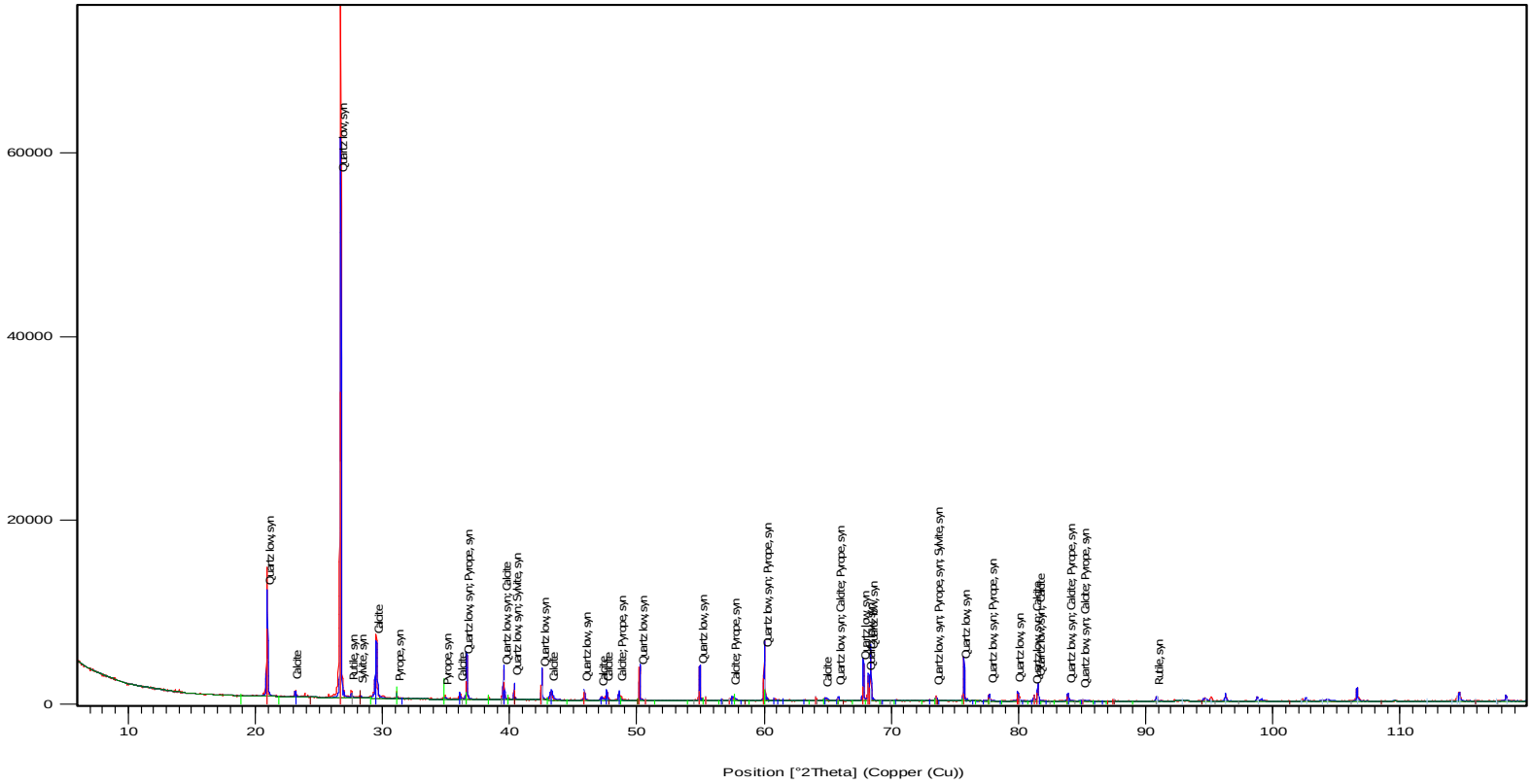

Figure 5.10 X-ray diffraction analysis THOP 18 at 510 cm depth

ANNA UNIVERSITY, CHENNAI - 600 025

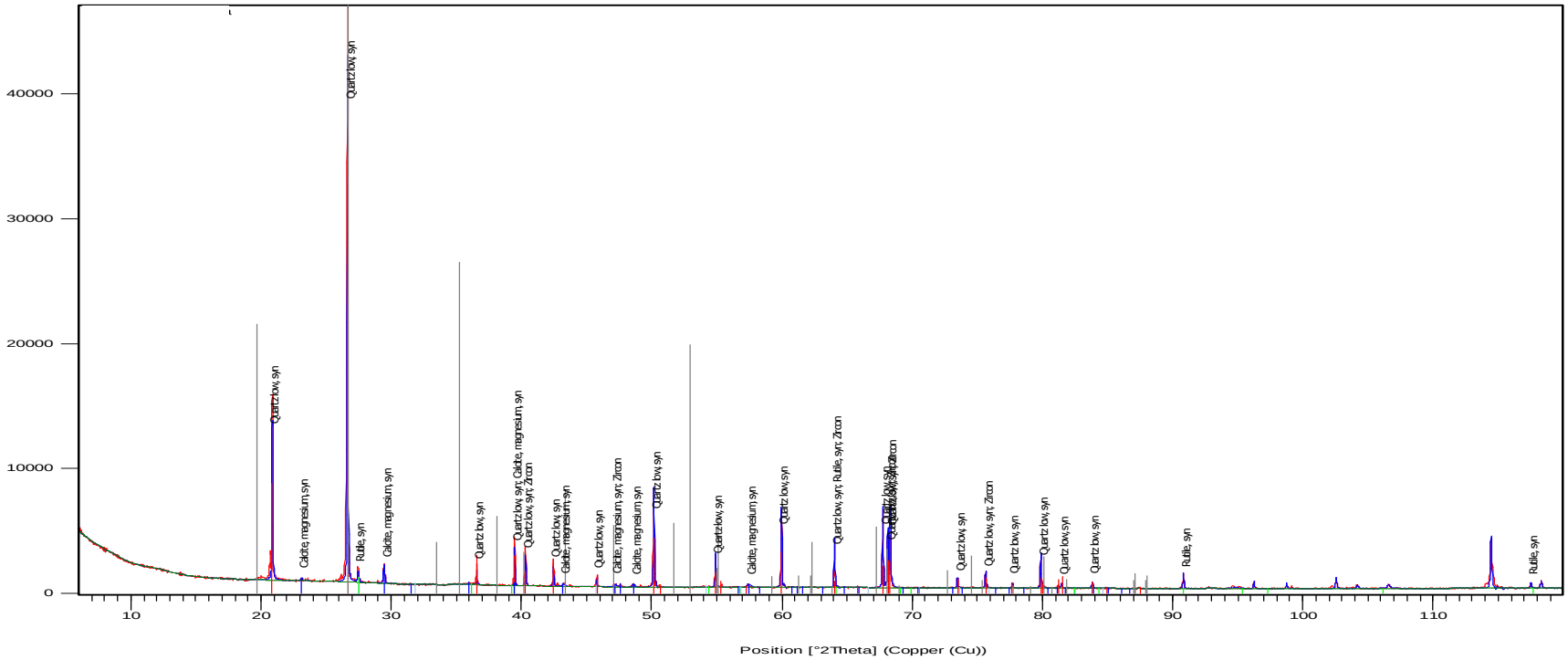

Figure 5.11 X-ray diffraction analysis THOP 20 at 740 cm depth

ANNA UNIVERSITY, CHENNAI - 600 025

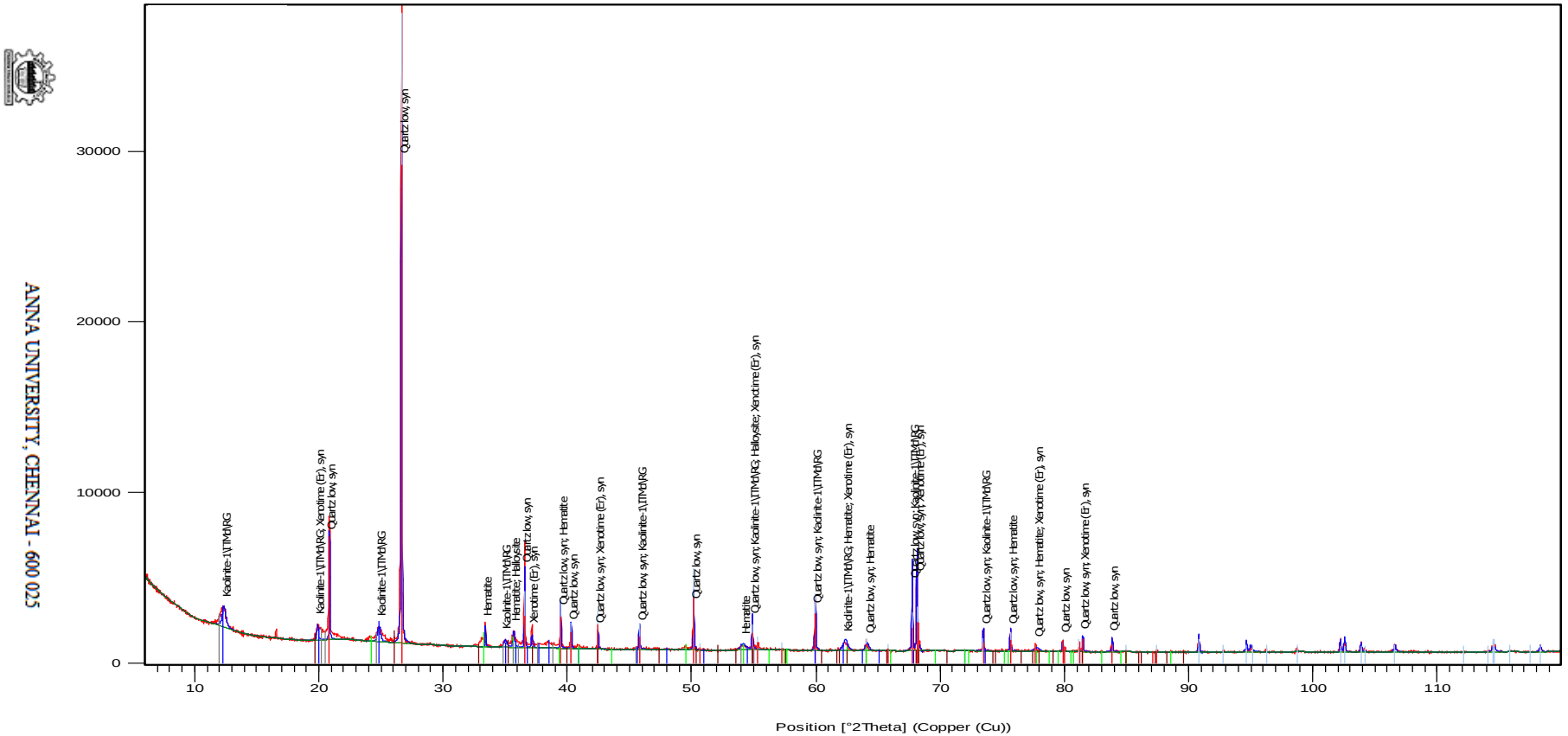

Figure 5.12 X-ray diffraction analysis MUT 19 at 180 cm depth

ANNA UNIVERSITY, CHENNAI - 600 025

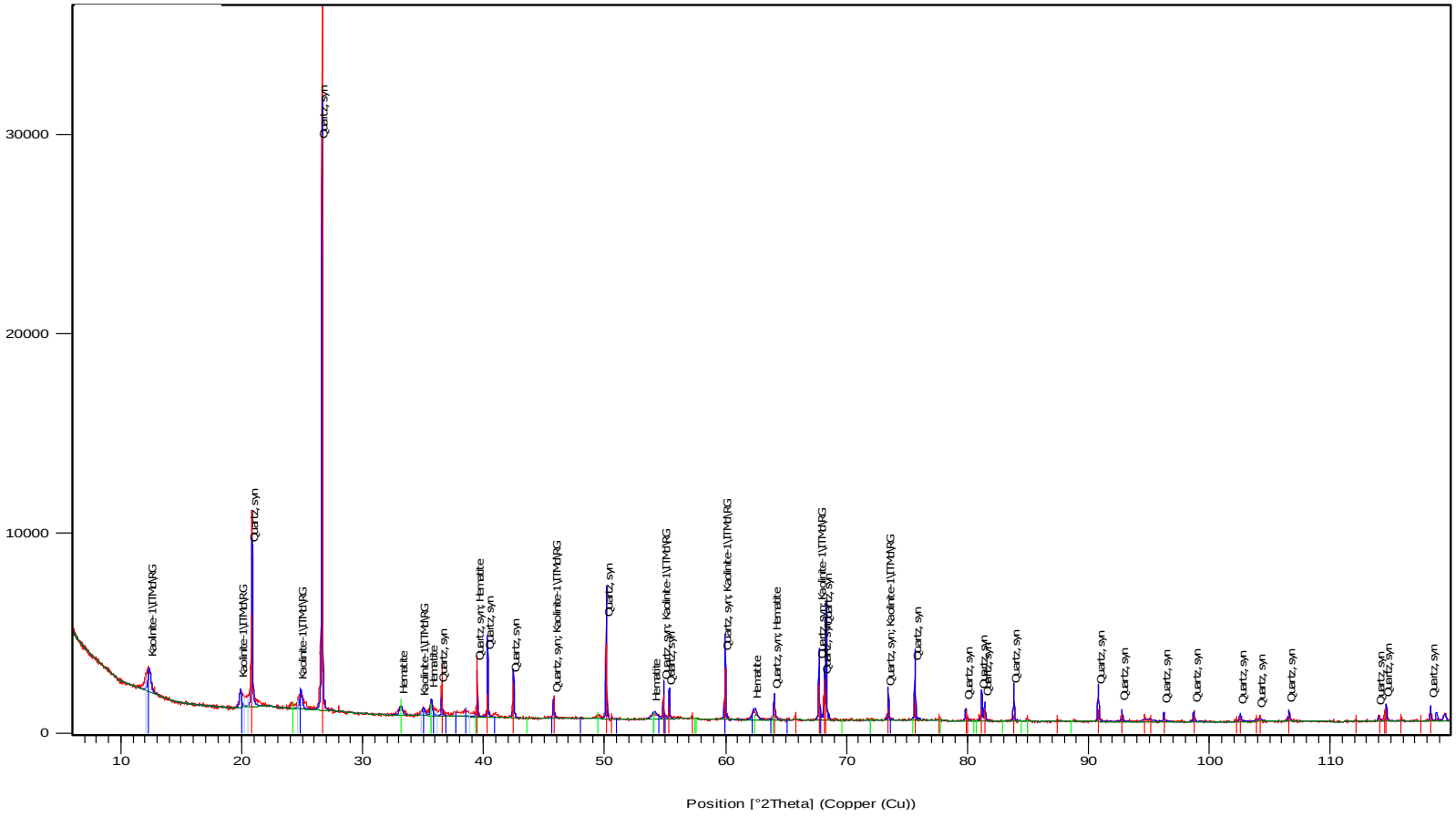

Figure 5.13 X-ray diffraction analysis MUT 36 at 350 cm depth

ANNA UNIVERSITY, CHENNAI - 600 025

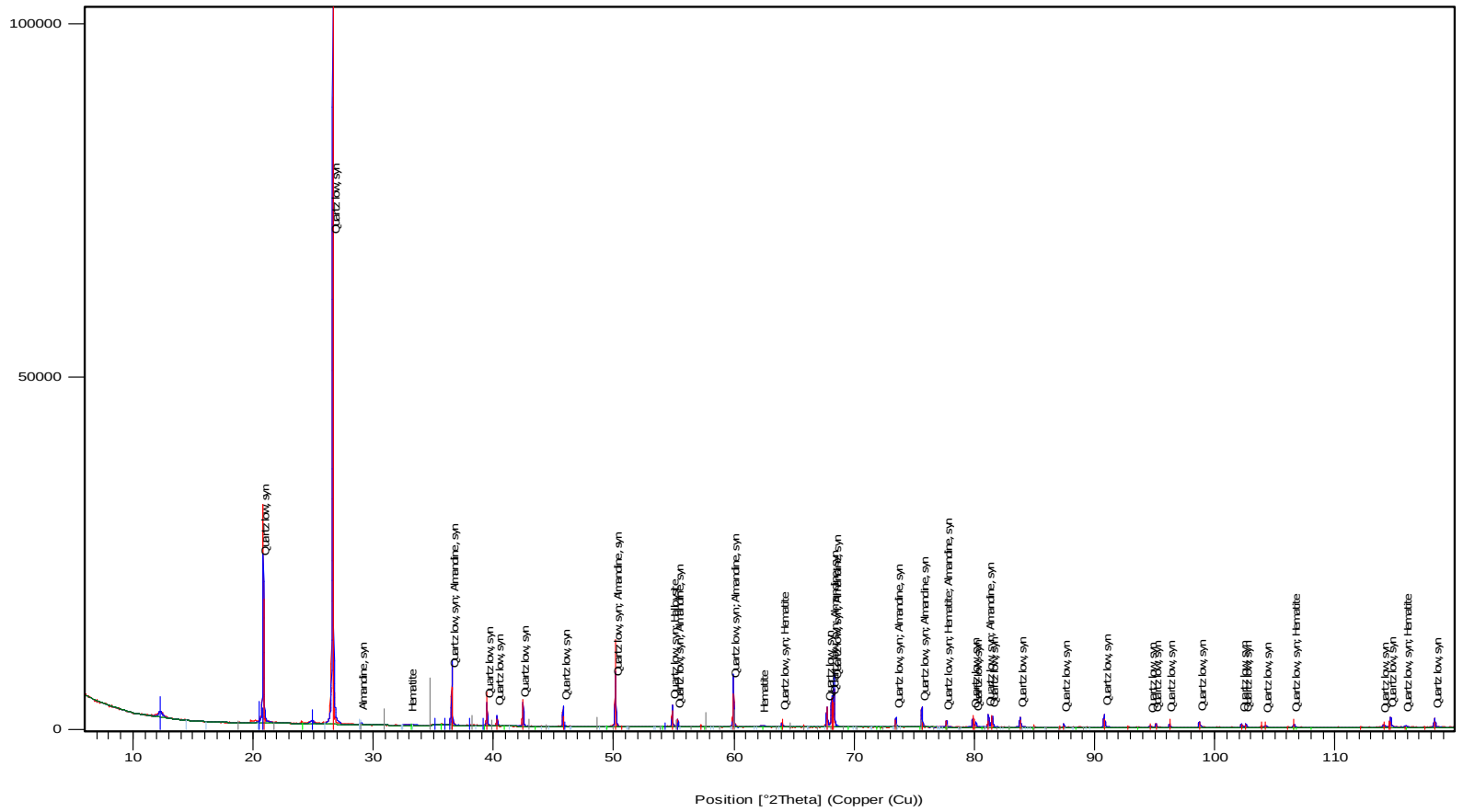

Figure 5.14 X-ray diffraction analysis MUT 95 at 940 cm depth

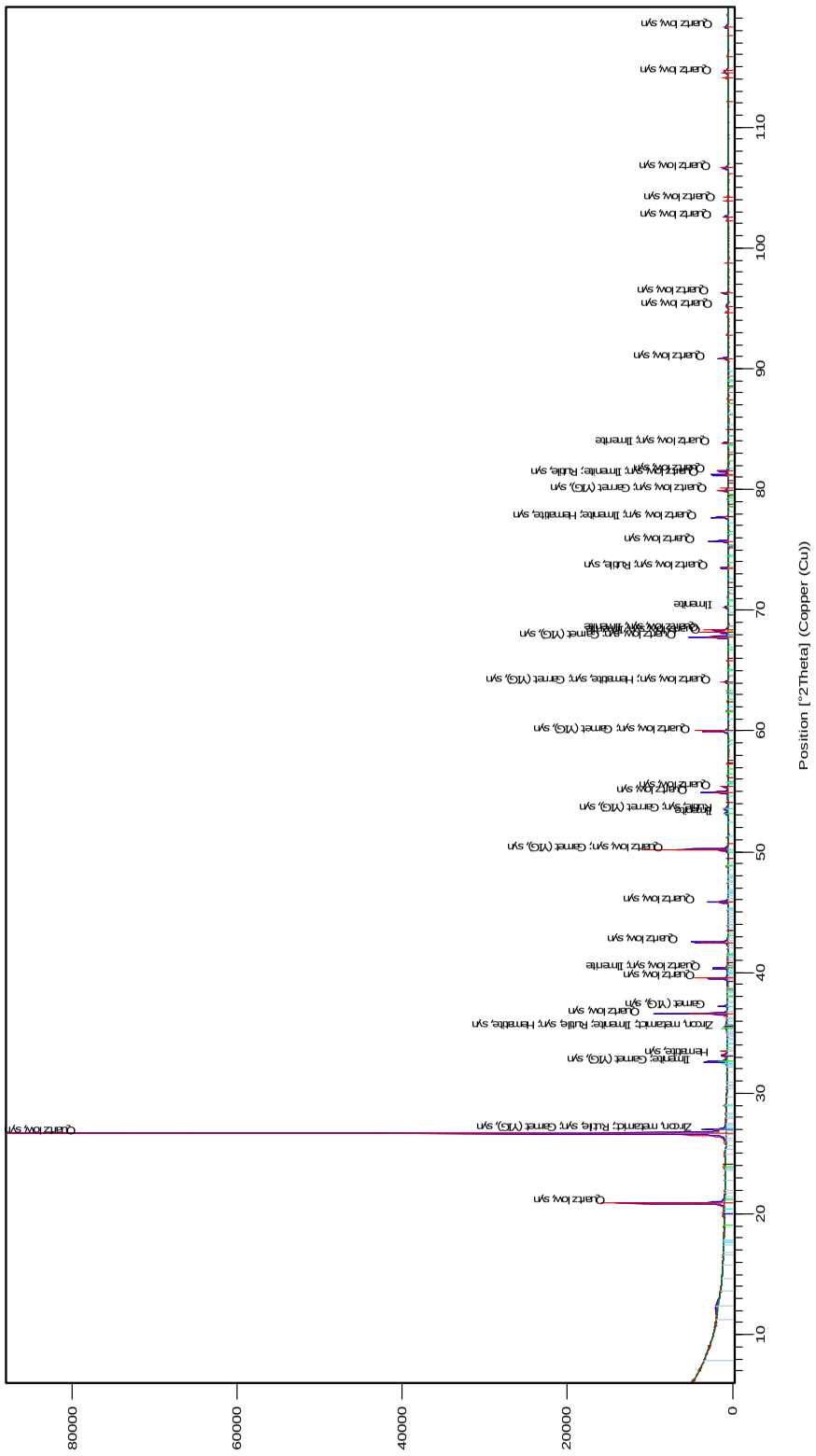

Figure 5.15 X-ray diffraction analysis SKM 9 at 80 cm depth

ANNA UNIVERSITY, CHENNAI - 600 025

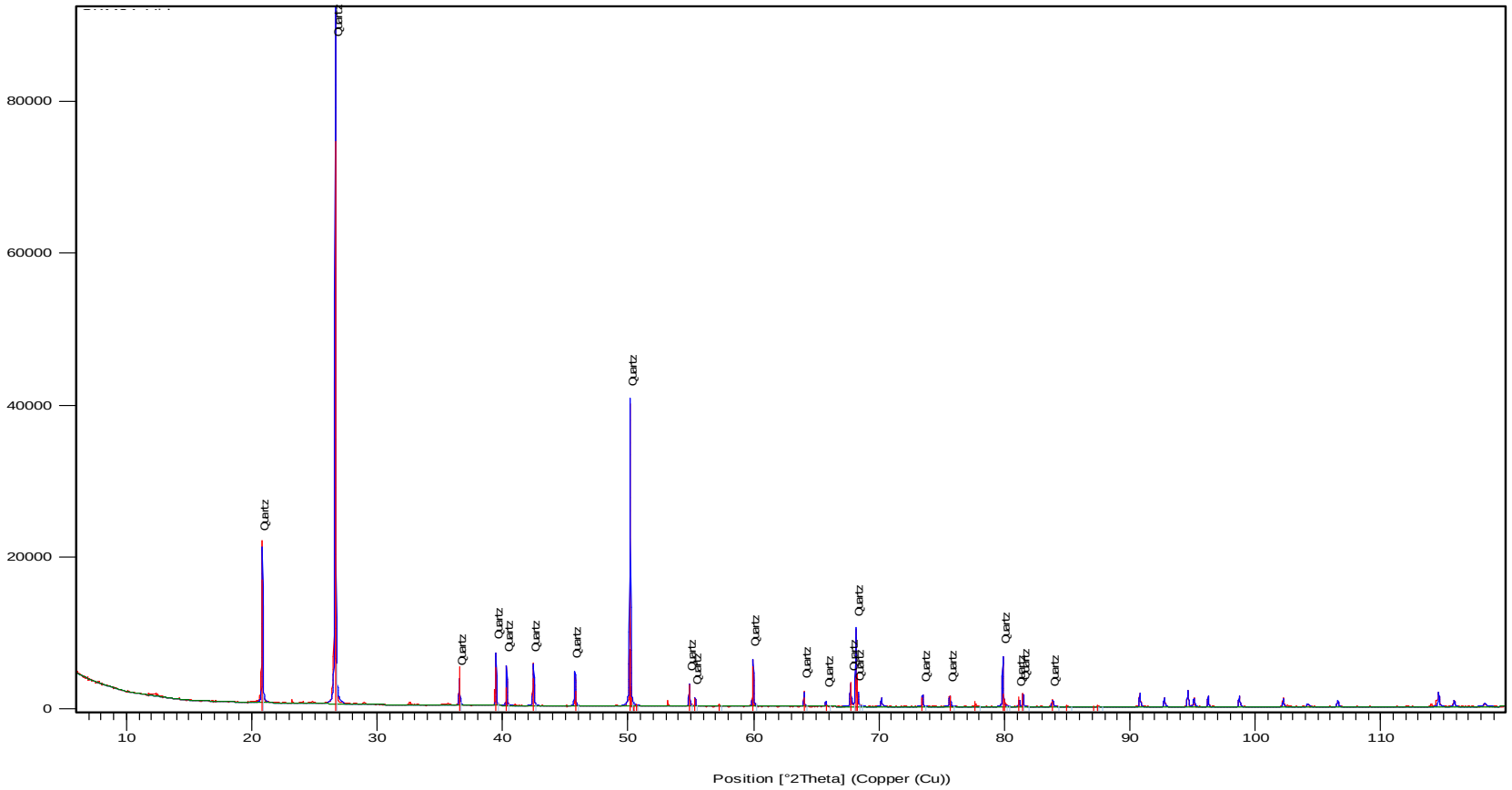

Figure 5.16 X-ray diffraction analysis SKM 24 at 230 cm depth

ANNA UNIVERSITY, CHENNAI - 600 025

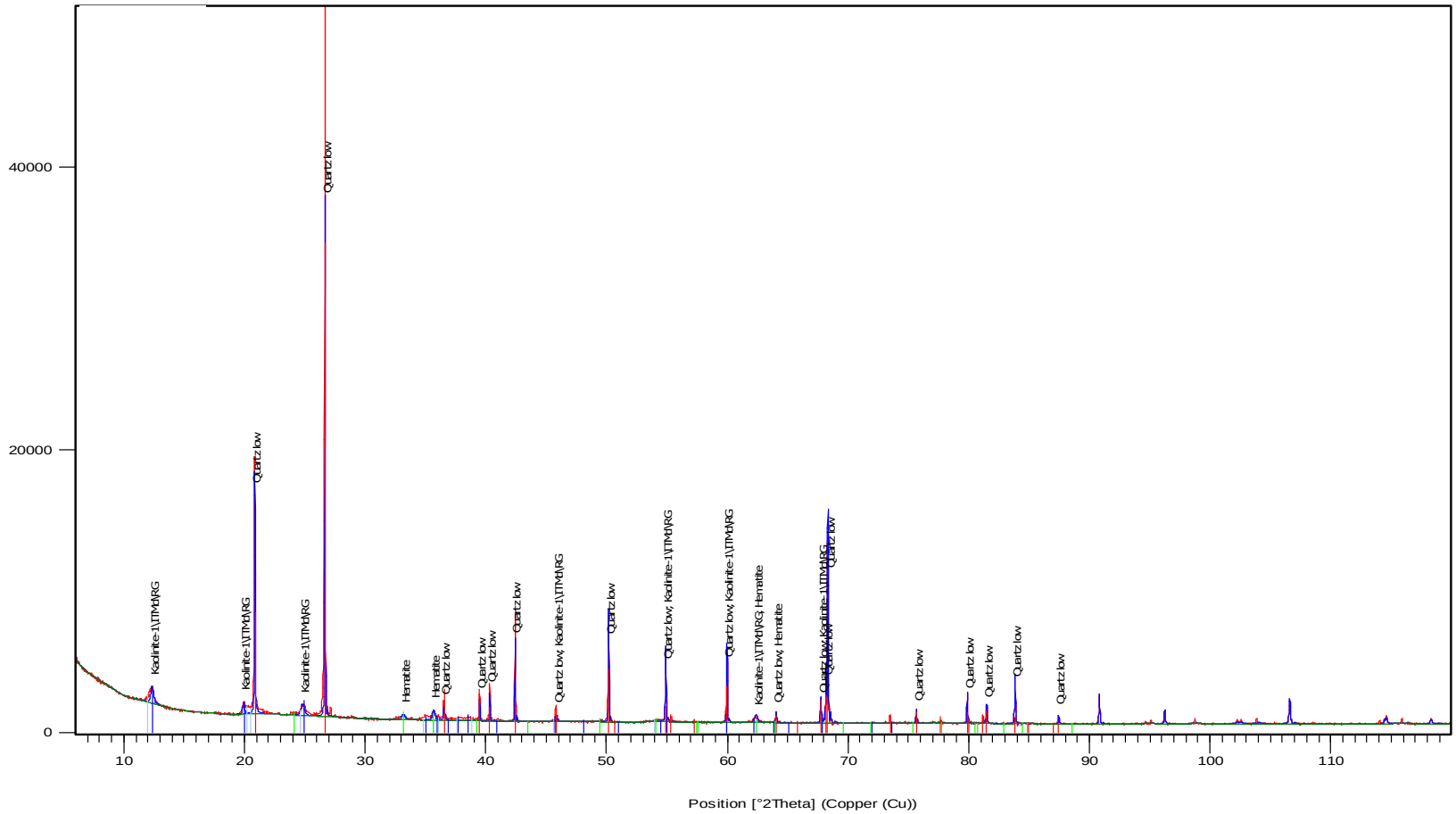

Figure 5.17 X-ray diffraction analysis SKM 57 at 560 cm depth

ANNA UNIVERSITY, CHENNAI - 600 025

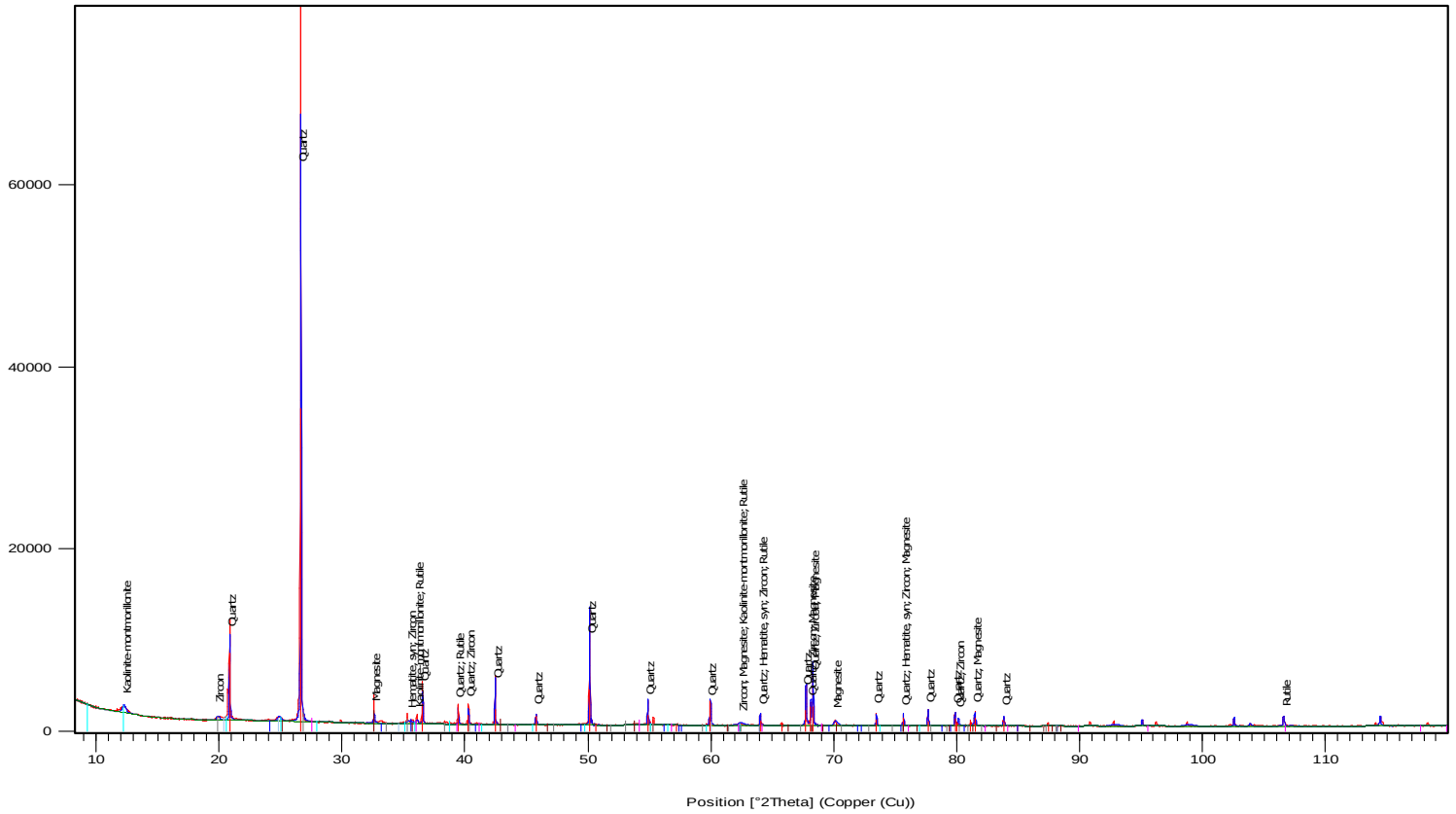

Figure 5.18 X-ray diffraction analysis TPV 1 at 0 cm depth

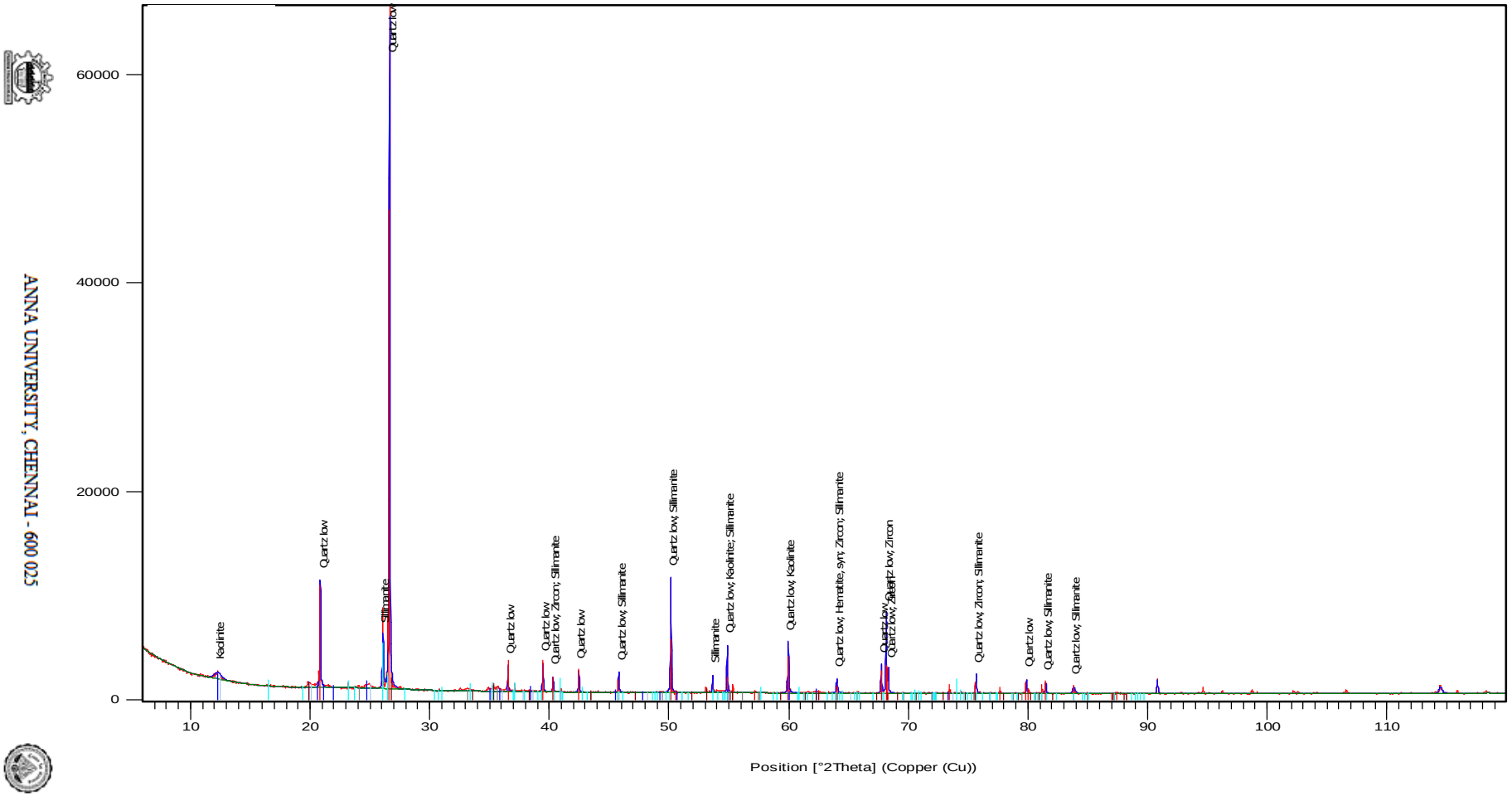

Figure 5.19 X-ray diffraction analysis TPV 41 at 230 cm depth

ANNA UNIVERSITY, CHENNAI - 600 025

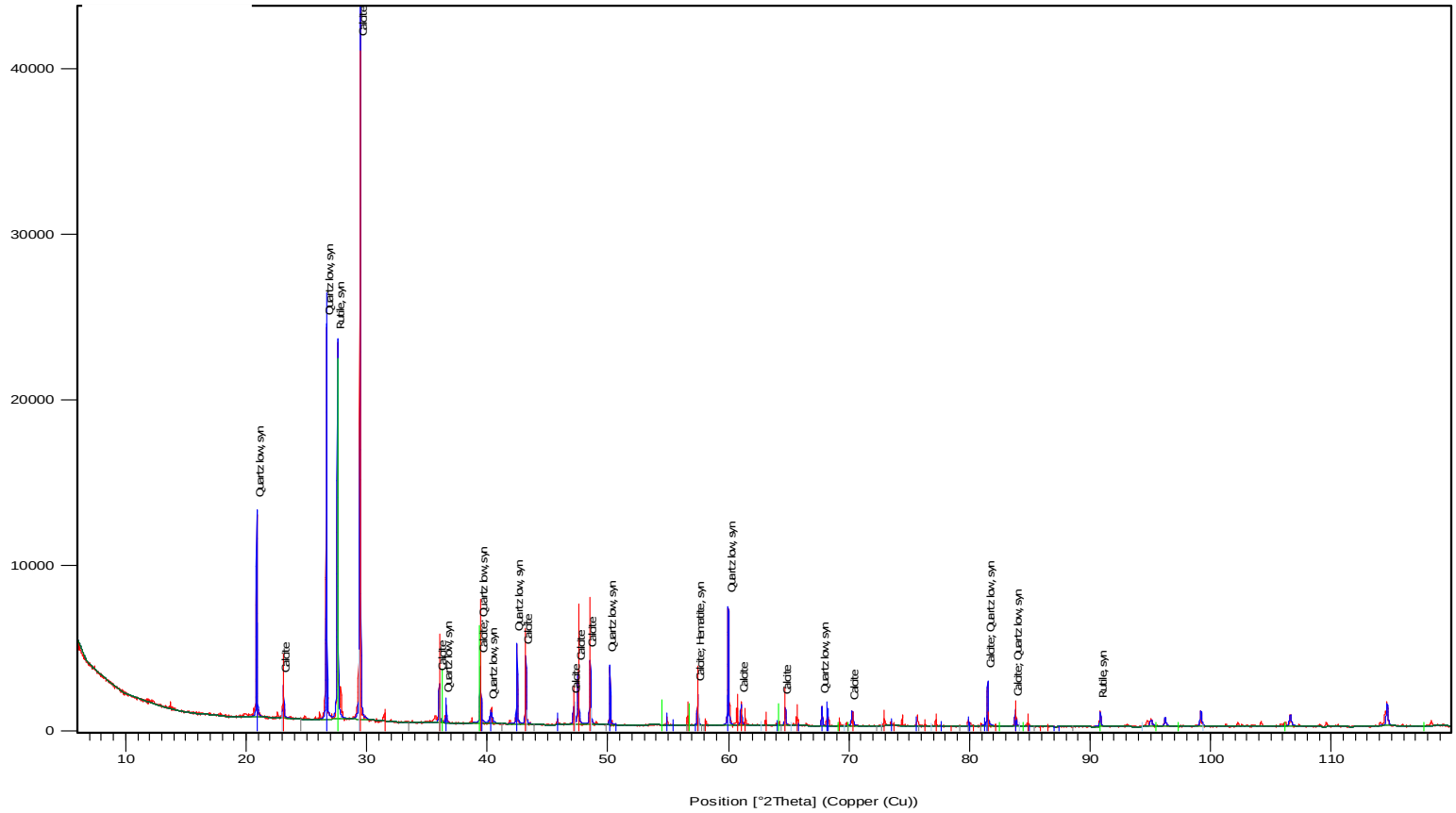

Figure 5.20 X-ray diffraction analysis TPV 41 at 400 cm depth

ANNA UNIVERSITY, CHENNAI - 600 025

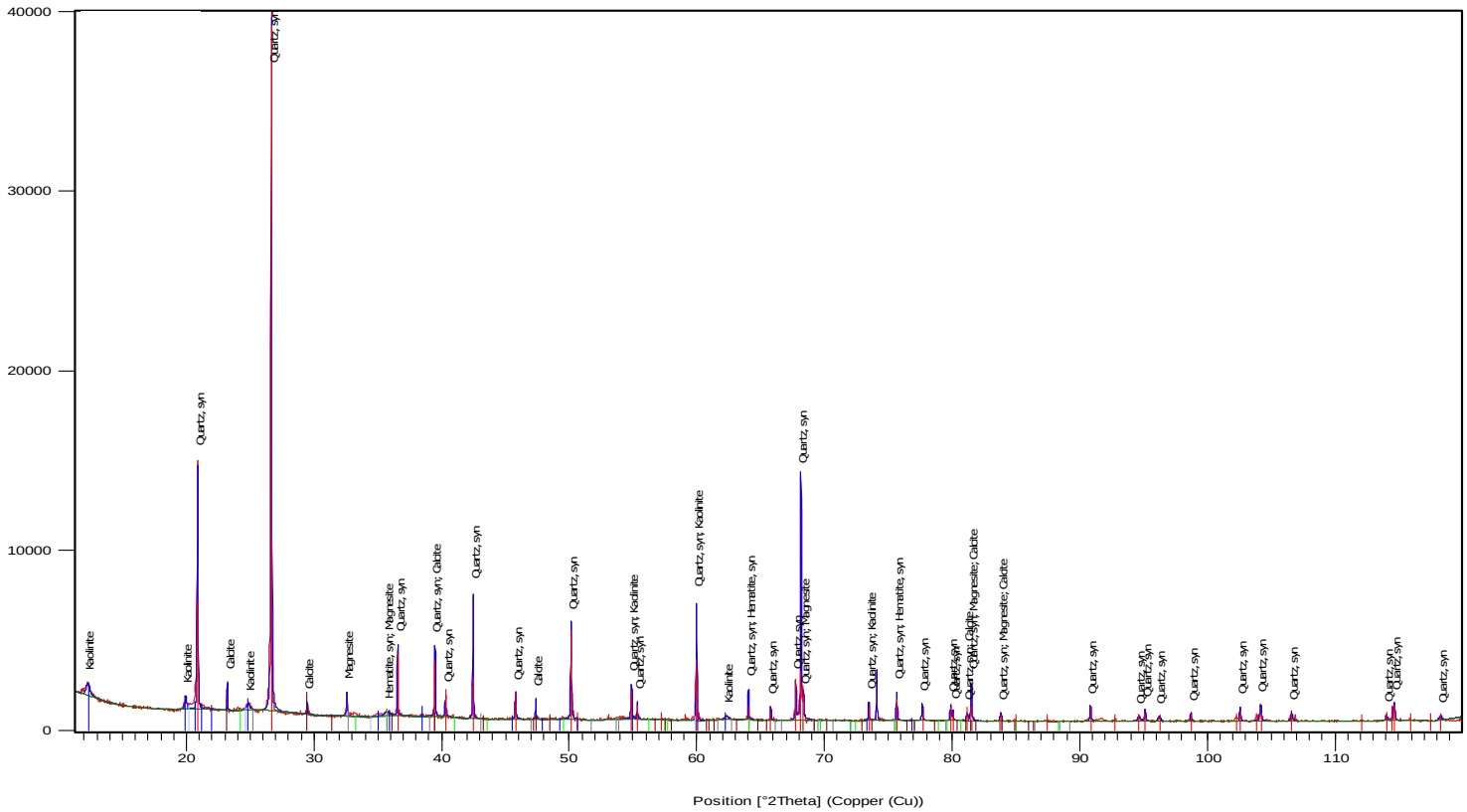

Figure 5.21 X-ray diffraction analysis KCV20 at 190 cm depth

ANNA UNIVERSITY, CHENNAI - 600 025

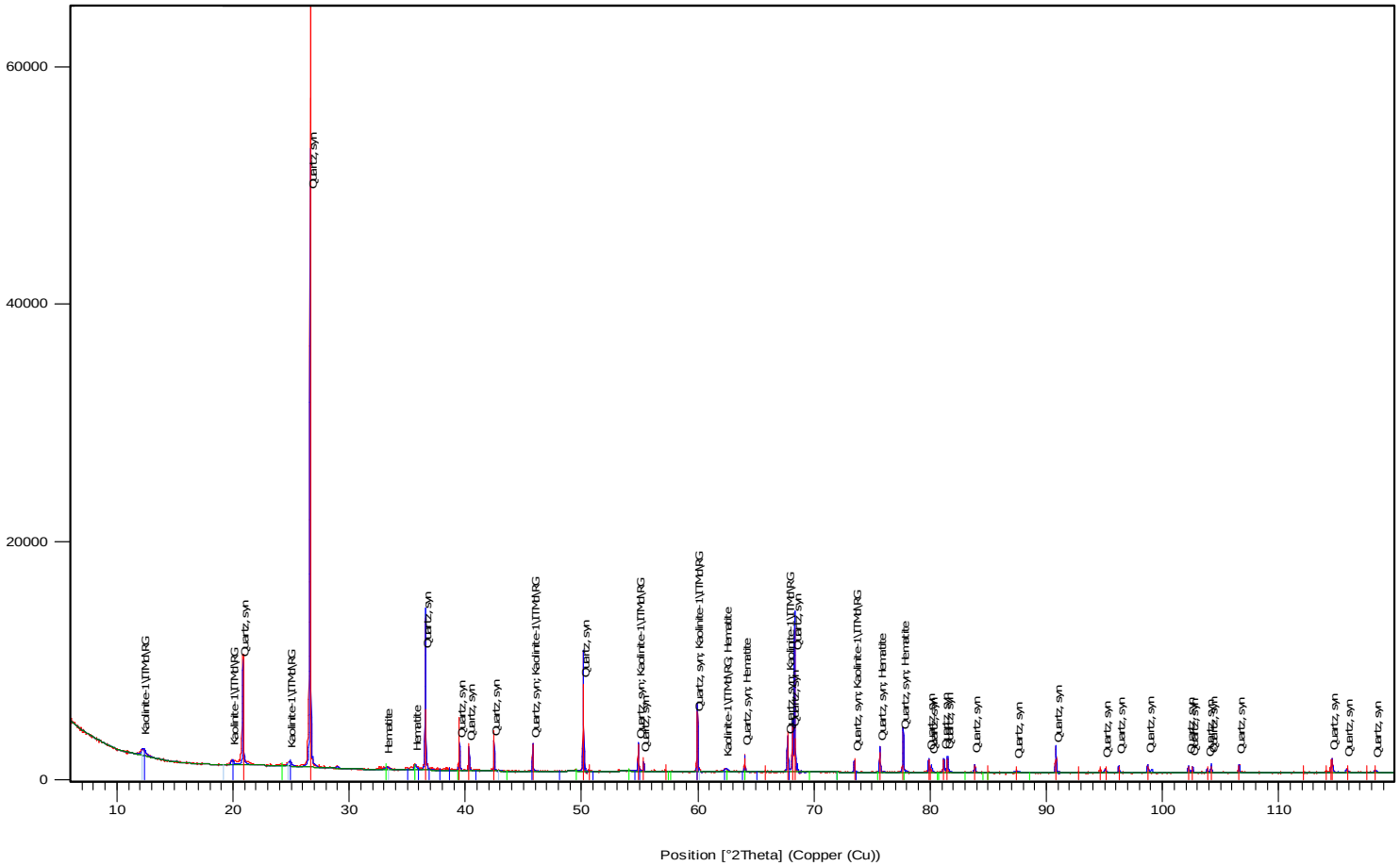

Figure 5.22 X-ray diffraction analysis KCV33 at 320 cm depth

Thus, during Last Glacial Maximum (LGM), continental shelves were wide-open with a vast reservoir of sediments with high landward winds during (NE) winter monsoon and sediments coasted inland until 11.4 ka to form coastal aeolian teri deposits. The Coastal teri reddening happened by in-situ weathering that started at <11.4ka-5.6ka during a humid climate (Jayangondaperumal et al. 2012).

All the results from X-ray diffraction analysis of THOP, SKM, TPV, KCV and MUT are shown below in the Table 5.17.

Thus, during Last Glacial Maximum (LGM), continental shelves were wide-open with a vast reservoir of sediments with high landward winds during (NE) winter monsoon and sediments coasted inland until 11.4 ka to form coastal aeolian teri deposits. The Coastal teri reddening happened by in-situ weathering that started at <11.4ka-5.6ka during a humid climate (Jayangondaperumal et al. 2012).

All the results from X-ray diffraction analysis of THOP, SKM, TPV, KCV and MUT are shown below in the Table 5.17.

5.9 SPEARMAN RANK CORRELATION BETWEEN MAGNETIC PARAMETERS AND GEOCHEMICAL ANALYSIS

The geochemical data is correlated with magnetic parameters and Spearman's rank correlation coefficients were determined to explore possible relationships (Table 5.18). The correlation between SIRM and χ is significant (95% probability/$p < 0.05$) in THOP and SKM sections and strongly positive in TPV section. The correlation between $CaCO_3$ and χ is negative in THOP, SKM and TPV sections. HIRM% and S_{-300} present negative and significant (95% probability/$p < 0.05$) correlation in all the sections.

Table 5.18 Spearman's rank correlation coefficients for geochemical data and magnetic parameters (THOP, N=20; KCV, N=7; SKM, N=12 and TPV, N=8). Values are significant at *p < 0.05.

MUT	χ	SIRM	s-300	s-100	HIRM%	SIRM/χ	Clay	Sand	Silt	OM	Fe	$CaCO_3$
χ	1.0000											
SIRM	0,840*	1.0000										
s-300	0,956*	0,872*	1.0000									
HIRM%	-0.1083	-0.1238	-0.1212	-0.1757	1.0000							
SIRM/χ	-0.3125	-0.1663	-0.1933	-0.1465	-0.0588	1.0000						
CLAY	0,677*	0,723*	0,791*	0,546*	0.0221	-0.2248	1.0000					
SAND	-0,668*	-0,715*	-0,783*	-0,534*	-0.0349	0.2246	-0,999*	1.0000				
SILT	0,519*	0.4359	0.4104	0.3946	0.2190	-0.2840	0.4232	-0.4362	1.0000			
Om	0.1832	0.2552	0.3231	0.0613	-0.0562	-0.0848	0,620*	-0,622*	0.0091	1.0000		
Fe	0.2165	0.3117	0.2067	0.1095	0.3588	-0.3034	0.4806	-0.4853	0.3373	0.1131	1.0000	
$CaCO_3$	0.0788	0.1258	0.2304	0.1232	0.0171	0.0959	0.2152	-0.2301	-0.0607	-0.2185	-0.0603	1.0000

THOP	χ	SIRM	s-300	s-100	HIRM%	SIRM/χ	Clay	Sand	Silt	OM	Fe	$CaCO_3$
χ	1.0000											
SIRM	0.750*	1.0000										
S-300	0.4260	0.1830	1.0000									
s-100	0.4080	-0.0600	0.836*	1.0000								
HIRM%	-0.4260	-0.1830	-1.000*	-0.836*	1.0000							
SIRM/χ	0.0560	0.672*	-0.1800	-0.504*	0.1800	1.0000						
Clay	0.625*	0.729*	0.0570	-0.2540	-0.0570	0.571*	1.0000					
Sand	0.2210	-0.0430	0.4390	0.564*	-0.4390	-0.3250	-0.1890	1.0000				
Silt	-0.2040	-0.4290	0.4390	0.7060	-0.4390	-0.552*	-0.4900	0.3880	1.0000			
Om	-0.0320	-0.1050	-0.0450	0.1340	0.0450	-0.2180	-04430	-0.0430	0.3630	1.0000		
Fe	-0.543*	-0.486*	-0.475*	-0.3210	0.475*	-0.2360	-0.486*	-0.5360	0.0910	0.490*	1.0000	
$CaCO_3$	-0.657*	-0.479*	-0.2860	-0.0790	0.2860	-0.1500	0.725*	-0.4000	0.2910	0.527*	0.654*	1.0000

ANNA UNIVERSITY, CHENNAI - 600 025

Table 5.18 (Continued)

TPV	χ	SIRM	s-300	s-100	HIRM%	SIRM/χ	Clay	Sand	Silt	OM	Fe	$CaCO_3$
χ	1.0000											
SIRM	0.5000	1.000										
S-300	0.3330	0.1830	1.000									
s-100	0.4760	-0.0600	0.3100	1.000								
HIRM%	-0.3330	-0.1830	-1.000*	-0.3100	1.0000							
SIRM/χ	-0.1430	0.672*	-0.6190	-0.762*	0.6190	1.0000						
Clay	0.738*	0.729*	0.0000	0.2620	0.0000	-0.1190	1.0000					
Sand	-0.0950	-0.0430	-0.0480	-0.762*	0.0480	0.762*	-0.3100	1.0000				
Silt	0.0480	-0.4290	-0.3100	0.5710	0.3100	-0.3330	0.1190	-0.741*	1.0000			
Om	0.5480	-0.1050	0.5000	0.833*	-0.5000	-0.786*	0.3810	-0.738*	0.5950	1.0000		
Fe	-0.6670	-0.486*	-0.3570	-0.1900	0.3570	0.1900	-0.741*	-0.0480	0.1900	-0.2380	1.0000	
$CaCO_3$	-0.2620	-0.479*	0.738*	0.2140	-0.738*	-0.738*	-0.3330	-0.3100	-0.1190	0.3810	0.1430	1.0000

SKM	χ	SIRM	s-300	s-100	HIRM%	SIRM/χ	Clay	Sand	Silt	OM	Fe	$CaCO_3$
χ	1.000											
SIRM	0.734*	1.000										
S-300	0.168	0.105	1.000									
s-100	0.203	0.364	-0.238	1.000								
HIRM%	-0.168	-0.105	-1.000*	0.238	1.000							
SIRM/χ	-0.084	0.231	0.315	-0.140	-0.315	1.000						
Clay	0.063	-0.126	-0.399	0.126	0.399	-0.636*	1.000					
Sand	-0.140	0.049	0.378	-0.147	-0.378	0.615*	-0.993*	1.000				
Silt	0.427	0.217	-0.126	0.503	0.126	-0.469	0.685*	-0.706*	1.000			
Om	-0.049	0.364	0.462	0.028	-0.462	0.476	-0.336	0.308	-0.343	1.000		
Fe	0.035	0.469	0.364	0.077	-0.364	0.748*	-0.685*	0.629*	-0.462	0.755*	1.000	
$CaCO_3$	-0.476	-0.014	0.119	-0.126	-0.119	0.483	-0.091	0.112	-0.350	0.783*	0.517	1.000

ANNA UNIVERSITY, CHENNAI - 600 025

Table 5.18 (Continued)

KCV	χ	SIRM	s-300	s-100	HIRM%	SIRM/χ	Clay	Sand	Silt	OM	FE	$CaCO_3$
χ	1.000											
SIRM	0.250	1.000										
S-300	0.929*	0.071	1.000									
s-100	0.393	-0.464	0.536	1.000								
HIRM%	-0.929*	-0.071	-1.000*	-0.536	1.000							
SIRM/χ	-0.893*	0.036	-0.821*	-0.571	0.821*	1.000						
Clay	0.321	0.643	0.429	0.143	-0.429		-0.071	1.000				
Sand	-0.500	-0.500	-0.393	-0.464	0.329	0.464	-0.607	1.000				
Silt	0.000	-0.679	0.143	0.893*	-0.143	-0.321	-0.143	-0.250	1.000			
Om	-0.393	0.429	-0.643	-0.750	0.643	0.536	-0.286	0.214	0.643	1.000		
Fe	0.500	-0.357	0.679	0.964*	-0.679	-0.607	0.321	-0.500	0.786*	-0.857*	1.000	
$CaCO_3$	0.321	0.786*	0.071	-0.607	-0.071	-0.036	0.179	-0.107	-0.821*	0.679	-0.571	1.000

ANNA UNIVERSITY, CHENNAI - 600 025

Fe (%) and S ratios present in good correlations in KCV section. $CaCO_3$ and S ratios shows significant negative correlation (95% probability/$p < 0.05$) in THOP and negative correlation in SKM and TPV sections. Among four sections, no significant correlation was found between OM and χ. In TPV and THOP sections the correlation between χ and clay is significant (95% probability/$p < 0.05$). In KCV, the correlation was not significant but was positive and higher than the correlation with sand or silt. In SKM, no significant correlation between χ with sand, clay or silt. However, the highest positive correlation is obtained with silt.The correlation between SIRM and χ has been found significant (95% probability/$p < 0.05$) in THOP and MUT sections and shows a perfect positive correlation with TPV section. As expected, in MUT section, HIRM% and S_{-300} present significant (95% probability/$p < 0.05$) negative correlation. In MUT section, S ratios and χ shows significant (95% probability) positive correlation.

5.10 PRINCIPAL COMPONENT ANALYSIS (PCA)

In PCA correlation analysis, X-ray diffraction data is used to find out the similar type of mineral deposition in samples. Similar mineral deposition analysis gives an idea about the deposition between The Southeast coast and southwest cost sampling areas. In KCV 33 at 320cm deposition is similar to TPV 24 (230cm) and TPV (0cm) and they 86 % positive correlation. In SKM sample, 57 at 560 cm depth show 81% of positive correlation between TPV1 (0cm), MUT36 (350cm) and MUT 19 (180cm). At MUT 95 (940cm) depth, Muttom sample as shown in Table 5.18 81% correlation between Edayanvillai (TPV) in the depth of 230 - 330cm. Moreover, TPV shows 84% positive correlation between 10cm and 230cm. The PCA correlation confirms that TPV and MUT almost have similar type of mineral deposition.

Table 5.19 PCA correlation between section depositions.

DATA SETS	KCV1	KCV33	KCV 20	TPV41	TPV24	TPV 1	SKM57	SKM24	SKM9	MUT95	MUT36	MUT19	THOP20	THOP18	THOP 7	THO P4
KCV-1	100	60	63	25	58	61	61	44	46	47	56	56	42	33	23	40
KCV33	60	100	82	38	85	87	79	73	73	84	67	68	63	37	35	57
KCV20	63	82	100	36	76	77	75	61	60	73	73	72	61	33	34	50
TPV41	25	38	36	100	34	34	32	37	34	35	29	27	48	44	54	37
TPV24	58	85	76	34	100	84	79	68	67	81	66	69	58	34	34	55
TPV1	61	87	77	34	84	100	80	70	70	79	67	69	56	35	33	53
SKM57	61	79	75	32	79	80	100	60	60	69	83	81	52	33	29	50
SKM24	44	73	61	37	68	70	60	100	74	77	53	53	65	42	42	66
SKM9	46	73	60	34	67	70	60	74	100	70	52	53	59	42	37	66
MUT95	47	84	73	35	81	79	69	77	70	100	65	67	65	37	37	57
MUT36	56	67	73	29	66	67	83	53	52	65	100	88	49	24	26	38
MUT19	56	68	72	27	69	69	81	53	53	67	88	100	46	26	28	41
THOP20	42	63	61	48	58	56	52	65	59	65	49	46	100	47	46	60
THOP18	33	37	33	44	34	35	33	42	42	37	24	26	47	100	54	59
THOP7	23	35	34	54	34	33	29	42	37	37	26	28	46	54	100	43
THOP4	40	57	50	37	55	53	50	66	66	57	38	41	60	59	43	100

ANNA UNIVERSITY, CHENNAI - 600 025

Wherein, THOP does not show any positive correlation with MUT and TPV. Muttom has 88% positive correlation between 180cm and 350cm respectively. Surprisingly, THOP does not show any positive correlation with PCA. In correlation analysis, we identify that THOP may go through a great wash over during the rise in sea level or a seasonal Arroyo/Gulch could have taken place over deposition. We found that THOP is the only sample that is pale yellow compared to TPV and MUT samples, which are a darker red.

5.11 DEPOSITIONAL PERIOD – OSL CHRONOLOGY

Coastal depositions are very sensitive to the environment and have a unique capacity to store the untold story of the period/inference in a deposition. Therefore, with limited resources (Fig. 6) the researchers have compared $CaCO_3$%, OM% and Fe% with each other to draw a distinct line between dry and wet periods. Muttom section (Fig. 26) has three OSL dates, which would give the approximate age of deposition in according to depth. The previous terrestrial record as shown in Table – 19 provides the line drawn between the humid and dry period in this section.

According to Folk (1976), red beds develops from minerals having a source of abundant iron, either heavy minerals or ferruginous clays. They originate from heavy minerals when deposited above the water table for easier access to Oxygen.

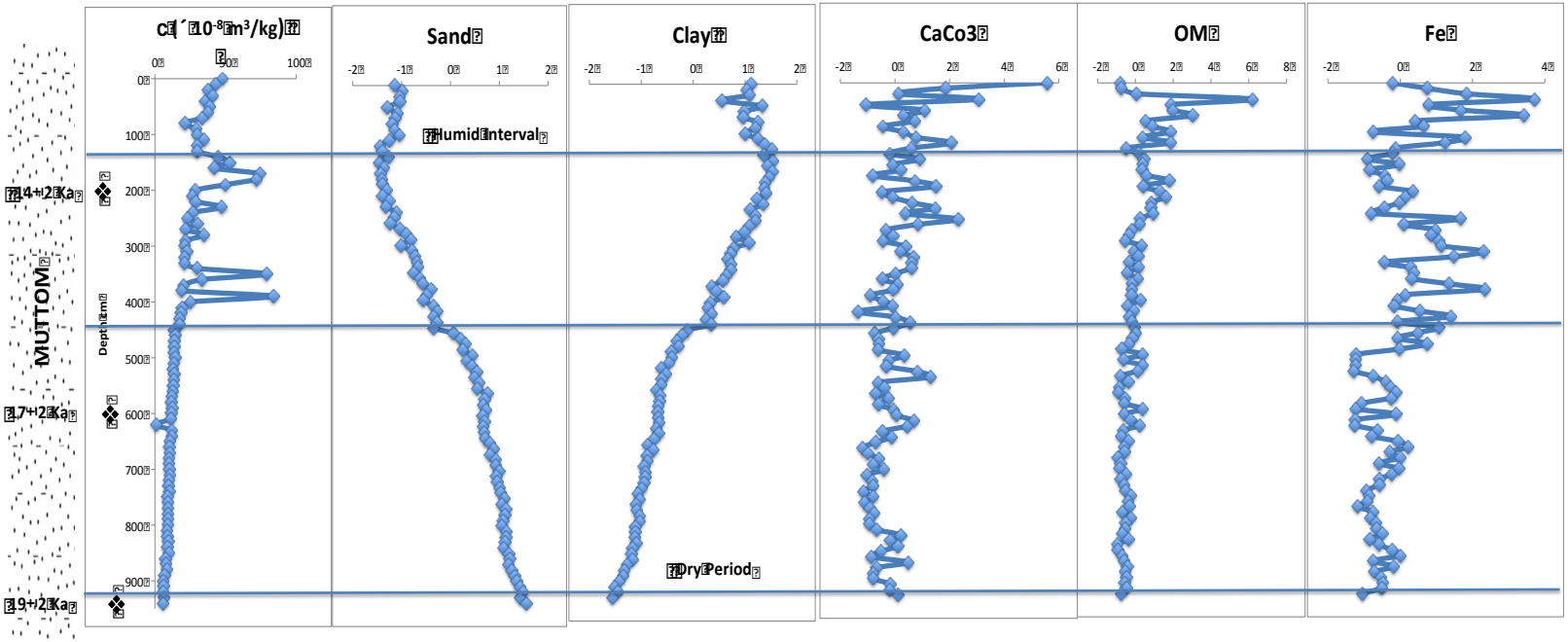

Figure 5.23 OSL dates in Muttom Section with dry and humid interval

ANNA UNIVERSITY, CHENNAI - 600 025

Table 5.20 Previous terrestrial record of South India

EPOCH	Time Interval (Ra)	Climatic Proxy/Method	Location	Inference	Reference
Late Pleistocene – Early Holocene	14.5-7	Pollen	Berijam Lake, Palani hills, S.India	Warm and Humid climate	Bera et al. 1995
	16	$\delta^{13}C$ of peat	Nilgiri Hills, S.India	Arid condition	Raja Gopalan et al.1997
	20-17	Pollen	Berijam Lake, Palani hills, S.India	Cold and dry climatic Condition	Bera et al. 1995
	20-11.0	OSL Dating	S.Margin of THAR desert	Dry climatic condition	Joyal et al.2006

5.12 CONCLUSION

The samples of SKM, KCV, TPV, THOP, MUT are analysed to infer its geochemical characteristics like heavy minerals % sand%, Silt%clay%, $CaCO_3$% and Fe% and other proxies like Environmental magnetism are studied to know its magnetic characteristics like Hematite versus Magnetic presence in the deposition. X-ray Diffraction analysis is used to infer the minerals that are deposited between inland teri sands and Coastal teri sands. Optically stimulated luminescence (OSL) method is used to find out depositional period of the sand dune at its depth. In this Chapter magnetic parameters are correlated with geochemical inference with spearmen Rank correlation. XRD minerals samples are correlated with the help of Principal component analysis.

CHAPTER 6

CONCLUSION

From the characteristics of magnetic parameters and its relationships with geochemistry data analysis we conclude the following results:

- Magnetic parameters show important contribution of canted antiferromagnetic (e.g. hematite) structures to the sands. Gardner (1981) pointed out, in Teri Sands, hematite originated from the chemical alteration of minerals like ilmenite and garnets, which indicates a wet, humid climate and high temperature, and also from the oxidation of magnetite.
- From remanence coercivity parameter, B_{OCR} indicates that SKM and KCV samples have mainly antiferromagnetic minerals. In TPV samples, B_{OCR} indicates the multidomain magnetite or mixed mineral contents of magnetite and antiferromagnetic minerals presence. Finally, In THOP samples, B_{OCR} indicates multidomain magnetite or magnetite and antiferromagnetic minerals; other THOP samples B_{OCR} confirms that these samples are magnetite-bearing. The presence of a high quantity of magnetite in THOP and TPV samples is confirmed with highest values of S_{-300}. In SKM samples, highest quantity of hematite and smallest quantity of

magnetite is present, and thus proved from the highest values of HIRM% and lowest of S_{-300} and SIRM.

- The mean SIRM/χ value of 5.78 kAm^{-1} obtained in our study in THOP indicates a mean grain size for the ferrimagnetic particles of ca. 8 µm.
- As depth varies the in magnetic parameters shows in THOP, SKM and KCV sections around 230 – 240 cm, decrease of χ and SIRM and a slight increase of HIRM%. The changes are related to alterations in the quantity of sand/clay. In TPV profile, χ and SIRM have no change with depth.
- Positive correlations between SIRM and χexists in THOP, SKM, and TPV due essentially to the magnetic signal of ferromagnetic minerals. Negative correlations between $CaCO_3$ and χ in THOP, SKM and TPV sections are justified with diamagnetism of carbonaceous materials. The negative correlation between $CaCO_3$ and S ratios in THOP, SKM and TPV sections are explained. HIRM% and S_{-300} present negative and significant correlation in all the sections, which is explained by the fact that the first parameter is related to the presence of antiferromagnetic minerals and the second is due to the ferromagnetic minerals. No significant correlation is obtained between Fe (%) and χ in TPV, SKM and KCV sections, which is unexpected. However the fact of the whole content of Fe is determined & related, instead of the FeO and Fe_2O_3 contents, which may correlate with magnetite and hematite content. No significant correlation is found between OM and χ, which is unusual. The positive correlation between χ with clay in TPV, THOP, and KCV sections indicates that

the magnetic susceptibility is dominantly controls the variations in the concentration of ferromagnetic minerals and paramagnetic minerals carried in the clay matrix. However, for SKM, the magnetic susceptibility is due to the silt fraction.

- The presence of magnetite in THOP (near coastal) and TPV sections is probably of oceanic origin (biogenic magnetite particles) carried from strong offshore winds and for SKM sections the wind influences and reduced the natural tree barriers and houses.
- In SKM the wet environment is due to the cultivation and which is associated with an arid climate. This contributes the prevalence of the necessary oxidized conditions for the dominant presence of hematite.
- During the Last Glacial Maximum (LGM) continental shelves are exposed with a vast reservoir of sediments with strong landward winds (NE/E) to form aeolian teri and the NE winter monsoon leads to form action of fluvial teri sediments.
- The SW summer monsoon direction also plays a vital role in carrying sediments from one place to another but depends upon the availability of the loose sediments (minerals), in the time of transport.
- The red color of sediments is a robust indicator of climate that is prevailed at the time of diagenetic/pedogenic transformation.
- The three sections of XRD data is correlated with each other and found that MUT and TPV have similar type of deposition. SKM, TPV, and MUT are also consists of similar type of

deposition. Moreover, In THOP a wash during some natural calamities or Arroyo/Gulch may occur in past.

- XRD investigation showed the minerals that exist in TPV section are commonly found to be in semi-arid/slow dry conditions.
- In XRD analysis, THOP section at 280cm depicted calcite mineral is dominant due to shells of dead marine organisms. It also supported the presence of paleo minerals (pyrope & sylvite) in abundance in the sea level at a depth of 510 cm. However, these minerals were formed.
- In XRD analysis, THOP section at 280cm depicted calcite mineral is dominant due to shells of dead marine organisms. It also supported the presence of paleo minerals (pyrope & sylvite) in abundance in the sea level at a depth of 510 cm. However, these minerals were formed during dry conditions.
- PCA correlation of XRD data showed TPV and MUT sections have a similar type of depositions. Also, THOP have has not showed any positive correlation with PCA. The correlation analysis indicated that THOP area would have gone through several wash over during rise in sea level or storm surge being nearer to coastal belt, hence, showed negative correlations.
- In MUT, ~14 ±2ka depositions show the humid interval at ~17±2ka to ~19±2ka, which displays depositions during the dry period.

REFERENCES

1. Abrantes, I & Rocha, F 2007, 'Sedimentary Dynamics of the Aveiro Shelf (Portugal)', Journal of Coastal Research, (SI 50), pp.1005-1009.

2. Adamiec, G & Aitken, M 1998, 'Dose-rate conversion factor: update. Ancient TL'.

3. Alagarsamy, R 2009, 'Environmental magnetism and application in the continental shelf sediments of India', Marine Environmental Research, http://doi.org/ 10.1016/ j.marenvres. 2009.04.003, vol. 68, no. 2, pp. 49-58.

4. Alappat, L, Frechen, M, Ramesh, R, Tsukamoto, S & Srinivasalu, S 2011,'Evolution of late Holocene coastal dunes in the Cauvery delta region of Tamil Nadu, India', Journal of Asian Earth Sciences, http://doi.org/10.1016/j.jseaes.2011.05.019, vol. 42, no. 3, pp. 381-397.

5. Banerjee, PK 2000, 'Holocene and Late Pleistocene relative sea level fluctuations along the east coast of India', Marine Geology, http://doi.org/10.1016/S0025-3227(00)00028-1, vol. 167, no. 3-4, pp. 243-260.

6. Bityukova, L, Scholger, R & Birke, M 1999, 'Magnetic susceptibility as indicator of environmental pollution of soils in Tallinn',Physics and Chemistry of the Earth, Part A: Solid Earth and Geodesy, http://doi.org/10.1016/S1464-1895(99)00122-2, vol. 24, no. 9, pp. 829-835.

7. Blaha, U, Appel, E & Stanjek, H 2008, 'Determination of anthropogenic boundary depth in industrially polluted soil and semi-quantification of heavy metal loads using magnetic susceptibility', Environmental Pollution, http://doi.org/10.1016/j.envpol.2008.02.013, vol. 156, no. 2, pp. 278-289.

8. Bloemendal, J, King, JW, Hall, FR & Doh, S.-J 1992,'Rock magnetism of Late Neogene and Pleistocene deep-sea sediments: Relationship to sediment source, diagenetic processes, and sediment lithology',Journal of Geophysical Research, http://doi.org/10.1029/91JB03068, vol. 97, (B4), pp. 4361.

9. Booth, CA, Walden, J, Neal, A & Smith, JP 2005,'Use of mineral magnetic concentration data as a particle size proxy: A case study using marine, estuarine and fluvial sediments in the Carmarthen Bay area, South Wales, U.K',Science of the Total Environment, http://doi.org/10.1016/j.scitotenv.2004.12.042, vol. 347, no. (1-3), pp, 241–253.

10. Boyko, T, Scholger, R & Stanjek, H 2004,'Topsoil magnetic susceptibility mapping as a tool for pollution monitoring: Repeatability of in situ measurements', Journal of Applied Geophysics,http://doi.org/10.1016/j.jappgeo.2004.01.002,vol.55, no. (3-4), pp. 249-259.

11. Chaparro, MAE, Bidegain, JC, Sinito, AM & Gogorza, CSG 2004, 'Relevant magnetic parameters and heavy metals from relatively polluted steram sediments-vertial and longitudinal distribution a long a cross-city steam in Buenos Aires province', Argenitina. Studia Geophysica et Geodaetica, vol.48, pp.615-636.

12. Chaparro, MAE, Gogorza, CSG, Chaparro, MAE, Irurzun, MA& Sinito, AM 2006, 'Review of magnetism and heavy metal pollution studies of various environments in Argentina',Earth, Planets and Space, vol.58, no.10, pp.1411-1422. http://doi.org/10.1186/BF03352637

13. Chaparro, MAE, Lirio, JM, Nuñez, H, Gogorza, CSG& Sinito, AM2005,'Preliminary magnetic studies of lagoon and stream sediments from Chascomús Area (Argentina) - Magnetic parameters as indicators of heavy metal pollution and some results of using an experimental method to separate magnetic phases',Environmental Geology, vol.49, no.1, pp. 30–43. http://doi.org/10.1007/s00254-005-0049-4

14. Chaparro, MAE, Sinito, AM, Ramasamy, V, Marinelli, C, Chaparro, MAE, Mullainathan, S & Murugesan, S2008,'Magnetic measurements and pollutants of sediments from Cauvery and Palaru River, India',Environmental Geology, vol.56, no.2, pp.425-437. http://doi.org/10.1007/s00254-007-1180-1

15. Dearing, JA, Dann, RJL, Hay, K, Lees, JA, Loveland, PJ, Maher, BA & O'Grady, K1996,'Frequency-dependent susceptibility measurements of environmental materials',Geophysical Journal International, vol.124, no.1, pp.228-240. http://doi.org/10.1111/j.1365-246X.1996.tb06366.x

16. Dearing, JA, Hay, KL, Baban, SMJ, Huddleston, AS, Wellington, EMH & Loveland, PJ1996, 'Magnetic susceptibility of soil: An evaluation of conflicting theories using a national data set',Geophysical Journal International, vol.127, no.3, pp.728-734. http://doi.org/10.1111/j.1365-246X.1996.tb04051.x

17. Duff, MC, Coughlin, JU & Hunter, DB2002, 'Uranium co-precipitation with iron oxide minerals',Geochimica et Cosmochimica Acta, vol.66, no.20, pp.3533-3547. http://doi.org/10.1016/S0016-7037(02)00953-5

18. Ďurža, O1999, 'Heavy metals contamination and magnetic susceptibility in soils around metallurgical plant',Physics and Chemistry of the Earth, Part A: Solid Earth and Geodesy, vol.24, no.6, pp.541-543. http://doi.org/10.1016/S1464-1895(99)00069-1

19. El Baghdadi, M, Barakat, A, Sajieddine, M & Nadem, S2012,'Heavy metal pollution and soil magnetic susceptibility in urban soil of Beni Mellal City (Morocco)', Environmental Earth Sciences, vol.66, no.1, pp.141-155. http://doi.org/10.1007/s12665-011-1215-5

20. Enzel, Y 1999, 'The only evap- orite mineral detected', The clay fraction (<2, 284(April), pp.125-128.

21. Flanders, P 1999, 'Identifying fly ash at a distance from fossil fuel power stations', Environmental Science and Technology, vol.33, no.4, pp.528-532. Retrieved from http://pubs.acs.org/doi/abs/ 10.1021/es980942s

22. Flanders, PJ 1994, 'Collection, measurement, and analysis of airborne magnetic particulates from pollution in the environment (invited)',Journal of Applied Physics, vol.75, no.10, pp.5931-5936. http://doi.org/10.1063/1.355518

23. Gardner, R & Pye, K1981,'Nature, origin and palaeoenvironmental significance of red coastal and desert dune sands',Progress in Physical Geography, vol.5, no.4, pp.514-534. http://doi.org/10.1177/030913338100500402

24. Gautam, P, Blaha, U & Appel, E2005, 'Integration of magnetism and heavy metal chemistry of soils to quantify the environmental pollution in Kathmandu', Nepal. Island Arc, vol.14, no.4, pp.424-435. http://doi.org/10.1111/j.1440-1738.2005.00496.x

25. Goluchowska, BJ 2001, 'Some factors affecting an increase in magnetic susceptibility of cement dusts', Journal of Applied Geophysics, vol.48, no.2, pp.103-112. http://doi.org/10.1016/S0926-9851(01)00083-0

26. Hanesch, M & Scholger, R 2005, 'The influence of soil type on the magnetic susceptibility measured throughout soil profiles', Geophysical Journal International, vol.161, no.1, pp.50-56. http://doi.org/10.1111/j.1365-246X.2005.02577.x

27. Hay, KL, Dearing, JA, Baban, SMJ & Loveland, P1997,'A preliminary attempt to identify atmospherically-derived pollution particles in English topsoils from magnetic susceptibility measurements',Physics and Chemistry of the Earth, vol.22, no.1, pp.207-210. http://doi.org/10.1016/S0079-1946(97)00104-3

28. Hoffmann, V, Knab, M & Appel, E1999, 'Magnetic susceptibility mapping of roadside pollution',Journal of Geochemical Exploration, vol.66, no.1-2, pp.313-326. http://doi.org/10.1016/S0375-6742(99)00014-X

29. Inácio, M, Pereira, V & Pinto, M2008,'The Soil Geochemical Atlas of Portugal: Overview and applications',Journal of Geochemical Exploration, vol.98, no.1-2, pp.22-33. http://doi.org/10.1016/j.gexplo.2007.10.004

30. Jayangondaperumal, R., Murari, M.K., Sivasubramanian, P., Chandrasekar, N., Singhvi, A.K., 2012. Luminescence dating of fluvial and coastal red sediments in the SE coast, India, and implications for paleoenvironmental changes and dune reddening. Quat. Res. 77, 468-461.

31. Jordanova, D, Jordanova, N, Petrov, P & Tsacheva, T2010,'Soil development of three Chernozem-like profiles from North Bulgaria revealed by magnetic studies', Catena, vol.83, no.2-3, pp.158-169. http://doi.org/10.1016/j.catena.2010.08.008

32. Juyal, N, Chamyal, LS, Bhandari, S, Bhushan, R & Singhvi, AK 2006,'Continental record of the southwest monsoon during the last 130

ka: evidence from the southern margin of the Thar Desert, India', Quaternary Science Reviews, vol.25, no.19-20, pp.2632-2650. http://doi.org/10.1016/j.quascirev.2005.07.020

33. Kapika, A, Petrovsk, E, Fialov, H, Podrzsk, V & Dvok, I2008,'High resolution mapping of anthropogenic pollution in the Giant Mountains National Park using soil magnetometry', Studia Geophysica et Geodaetica, vol.52, no.2, pp.271-284. http://doi.org/10.1007/s11200-008-0018-y

34. Kapička, A, Jordanova, N, Petrovský, E & Ustjak, S2000,'Magnetic stability of power-plant fly ash in different soil solutions',Physics and Chemistry of the Earth, Part A: Solid Earth and Geodesy, vol.25, no.5, pp.431-436. http://doi.org/10.1016/S1464-1895(00)00067-3

35. Kapička, A, Petrovský, E, Ustjak, S & Macháčková, K1999, 'Proxy mapping of fly-ash pollution of soils around a coal-burning power plant: A case study in the Czech Republic',Journal of Geochemical Exploration, vol.66, no.1-2, pp.291-297. http://doi.org/10.1016/S0375-6742(99)00008-4

36. Karimi, R, Ayoubi, S, Jalalian, A, Sheikh-Hosseini, AR & Afyuni, M2011, 'Relationships between magnetic susceptibility and heavy metals in urban topsoils in the arid region of Isfahan', Central Iran. Journal of Applied Geophysics, vol.74, no.1, pp.1-7. http://doi.org/10.1016/j.jappgeo.2011.02.009

37. Kim, W, Doh, SJ & Yu, Y 2009, 'Anthropogenic contribution of magnetic particulates in urban roadside dust', Atmospheric Environment, vol.43, no.19, pp.3137-3144. http://doi.org/10.1016/j.atmosenv.2009.02.056

38. Kumaran, KPN, Nair, KM, Shindikar, M, Limaye, RB & Padmalal, D2005,'Stratigraphical and palynological appraisal of the Late Quaternary mangrove deposits of the west coast of India',Quaternary Research, vol.64, no.3, pp.418-431. http://doi.org/10.1016/j.yqres.2005.08.015

39. Kunz, A, Frechen, M, Ramesh, R& Urban, B2010,'Luminescence dating of late holocene dunes showing remnants of early settlement in Cuddalore and evidence of monsoon activity in south east India',Quaternary International, vol.222, no.1-2, pp.194-208. http://doi.org/10.1016/j.quaint.2009.10.042

40. Lang, AKS & A. (n.d.). 66.pdf.

41. Lecoanet, H, Lévêque, F & Ambrosi, JP2001, 'Magnetic properties of salt-marsh soils contaminated by iron industry emissions (Southeast France)',Journal of Applied Geophysics, vol.48, no.2, pp.67-81. http://doi.org/10.1016/S0926-9851(01)00080-5

42. Lecoanet, H, Lévêque, F & Segura, S 1999, 'Magnetic susceptibility in environmental applications: Comparison of field probes',Physics of the Earth and Planetary Interiors, vol.115, no.3-4, pp.191-204. http://doi.org/10.1016/S0031-9201(99)00066-7

43. Limaye, RB, Kumaran, KPN, Nair, KM & Padmalal, D 2010,' Cyanobacteria as potential biomarkers of hydrological changes in the Late Quaternary sediments of South Kerala Sedimentary Basin, India',Quaternary International, vol.213, no.1-2, pp.79-90. http://doi.org/10.1016/j.quaint.2009.09.016

44. Liu, Q, Roberts, AP, Torrent, J, Horng, CS & Larrasoaña, JC 2007, 'What do the HIRM and S-ratio really measure in environmental magnetism Geochemistry, Geophysics', Geosystems, vol.8, no.9, http://doi.org/10.1029/2007GC001717

45. Lu, SG & Bai, SQ 2006, 'Study on the correlation of magnetic properties and heavy metals content in urban soils of Hangzhou City', China. Journal of Applied Geophysics, vol.60, no.1, pp.1-12. http://doi.org/10.1016/j.jappgeo.2005.11.002

46. Lu, S, Wang, H & Bai, S2009, 'Heavy metal contents and magnetic susceptibility of soils along an urban - Rural gradient in rapidly growing city of eastern China',Environmental Monitoring and Assessment, vol.155, no.1-4, pp.91-101. http://doi.org/10.1007/s10661-008-0420-5

47. Maher, BA 1986, 'Characterisation of soils by mineral magnetic measurements',Physics of the Earth and Planetary Interiors, vol.42, no.1-2, pp.76-92. http://doi.org/10.1016/S0031-9201(86)80010-3

48. Maher, BA, Moore, C & Matzka, J 2008, 'Spatial variation in vehicle-derived metal pollution identified by magnetic and elemental analysis of roadside tree leaves',Atmospheric Environment, vol.42, no.2, pp.364-373. http://doi.org/10.1016/j.atmosenv.2007.09.013

49. Marié, DC, Chaparro, MAE, Gogorza, CSG, Navas, A & Sinito, AM 2010, 'Vehicle-derived emissions and pollution on the road autovia 2 investigated by rock-magnetic parameters: A case study from Argentina',Studia Geophysica et Geodaetica, vol.54, no.1, pp.135-152. http://doi.org/10.1007/s11200-010-0007-9

50. Martins, V, Dubert, J, Jouanneau, JM, Weber, O, da Silva, EF, Patinha, C & Rocha, F 2007, 'A multiproxy approach of the Holocene evolution of shelf-slope circulation on the NW Iberian Continental Shelf',Marine Geology, vol.239, no.1-2, pp.1-18. http://doi.org/10.1016/j.margeo.2006.11.001

51. Matysek, D, Raclavska, H & Raclavsky, K 2008, 'Correlation Between Magnetic Susceptibility and Heavy Metal Concentrations in Forest Soils of the Eastern Czech Republic', Journal of Environmental and Engineering Geophysics, vol.13, no.1, pp.13-26. http://doi.org/10.2113/JEEG13.1.13

52. Mayya, YS, Morthekai, P, Murari, MK & Singhvi, AK 2006, 'Towards quantifying beta microdosimetric effects in single-grain quartz dose distribution', Radiation Measurements, vol.41, no.7-8, pp.1032-1039. http://doi.org/10.1016/j.radmeas.2006.08.004

53. Meena, NK, Maiti, S & Shrivastava, A2011, 'Discrimination between anthropogenic (pollution) and lithogenic magnetic fraction in urban soils (Delhi, India) using environmental magnetism',Journal of Applied Geophysics, vol.73, no.2, pp.121-129. http://doi.org/10.1016/j.jappgeo.2010.12.003

54. Mejdahl, V 1979, 'Thermoluminescence dating: Beta - dose attenuation in quartz grains', Archaeometry, vol.21, no.1, pp.61-72. http://doi.org/10.1111/j.1475-4754.1979.tb00241.x

55. Moreno, E, Sagnotti, L, Dinarès-Turell, J, Winkler, A & Cascella, A 2003, 'Biomonitoring of traffic air pollution in Rome using magnetic properties of tree leaves',Atmospheric Environment, vol.37, no.21, pp.2967-2977. http://doi.org/10.1016/S1352-2310(03)00244-9

56. Murti, A, Sarma K & Krishna, GSR 1970, 'Plumbogummite Minerals in Indian Soils', vol.3, pp. 321-327.

57. Nair, KM, Padmalal, D, Kumaran, KPN, Sreeja, R, Limaye, RB& Srinivas, R 2010, 'Late quaternary evolution of Ashtamudi-Sasthamkotta lake systems of Kerala, South West India',Journal of Asian Earth Sciences', vol.37, no.4, pp.361-372. http://doi.org/10.1016/j.jseaes.2009.09.004

58. Nriagu, JO 1974, 'Lead orthophosphates-IV Formation and stability in the environment', Geochimica et Cosmochimica Acta, vol.38, no.6, pp.887-898. http://doi.org/10.1016/0016-7037(74)90062-3

59. Oliveira, A, Rocha, F, Rodrigues, A, Jouanneau, J, Dias, A, Weber, O & Gomes, C2002, 'Clay minerals from the sedimentary cover from the northwest Iberian shelf', Progress in Oceanography, vol.52, no.2-4, pp.233-247. http://doi.org/10.1016/S0079-6611(02)00008-3

60. Padmalal, D, Kumaran, KPN, Nair, KM, Baijulal, B, Limaye, RB & Mohan, SV 2011, 'Evolution of the coastal wetland systems of SW India during the Holocene: Evidence from marine and terrestrial archives of Kollam coast, Kerala', Quaternary International, vol.237, no.1-2, pp.123-139. http://doi.org/10.1016/j.quaint.2010.12.021

61. Petrovský, E, Kapička, A& Jordanova, N2000,'Low-field magnetic susceptibility: a proxy method of estimating increased pollution of different environmental systems',Environmental Geology, vol.39, pp. 1-7. http://doi.org/10.1007/s002540050010

62. Porat N 2006, 'Use of magnetic separation for purifying quartz for luminescence dating', Ancient TL, vol.24, no.2, pp.33-36.

63. Premathilake, R & Risberg, J 2003, 'Late Quaternary climate history of the Horton Plains, central Sri Lanka', Quaternary Science Reviews, vol.22, no.14, pp.1525-1541. http://doi.org/10.1016/S0277-3791(03)00128-8

64. Rajagopalan, G, Sukumar, R, Ramesh, R, Pant, RK & Rajagopalan, G 1997, 'Late Quaternary vegetational and climatic changes from tropical peats in southern India', - An extended record up to 40,000 years BP. Current Science.

65. Romic, M & Romic, D 2003, 'Heavy metals distribution in agricultural topsoils in urban area', Environmental Geology, vol.43, no.7, pp.795-805. http://doi.org/10.1007/s00254-002-0694-9

66. Rosowiecka, O & Nawrocki, J 2010, 'Assessment of soils pollution extent in surroundings of ironworks based on magnetic analysis', Studia Geophysica et Geodaetica, vol.54, no.1, pp.185-194. http://doi.org/10.1007/s11200-010-0009-7

67. Schibler, L, Boyko, T, Ferdyn, M, Gajda, B, Holl, S & Jordanova, N 2002, 'Topsoil magnetic susceptibility mapping: Data reproducibility and compatibility, measurement strategy',Studies in Geophysics and Geodesy, vol.46, pp.43-57.

68. Sheik, M & Chandrasekar 2011, 'A shoreline change analysis along the coast between Kanyakumari and Tuticorin, India, using digital shoreline analysis system', Geo-Spatial Information Science, vol.14, no.4, pp.282-293. http://doi.org/10.1007/s11806-011-0551-7

69. Singhvi, AK, Deraniyagala, SU & Sengupta, D 1986, 'Thermoluminescence dating of Quaternary red-sand beds: a case study of coastal dunes in Sri Lanka', Earth and Planetary Science Letters, vol.80, no.1-2, pp.139-144. http://doi.org/10.1016/0012-821X(86)90027-0

70. Singhvi, AK & Porat, N 2008, 'Impact of luminescence dating on geomorphological and palaeoclimate research in drylands', Boreas, vol.37, no.4, pp.536-558. http://doi.org/10.1111/j.1502-3885.2008.00058.x

71. Spaargaren, CO & Deckers, J 1995, 'The world Reference Base For Soil Resources; An Introduction with Special Reference to Soils of Tropical Forest Ecosystems'.

72. Strzyszcz, Z, Magiera, T & Heller, F 1996, 'The influence of industrial immissions on the magnetic susceptibility of soils in upper Silesia',Studia Geophysica et Geodaetica, vol.40, pp.276-286.

73. Veneva, L, Hoffmann, V, Jordanova, D, Jordanova, N & Fehr, T 2004, 'Rock magnetic, mineralogical and microstructural characterization of fly ashes from Bulgarian power plants and the nearby anthropogenic soils',Physics and Chemistry of the Earth, (13-14 SPEC. ISS.), vol.29,pp.1011-1023. http://doi.org/10.1016/j.pce.2004.03.011

74. Walden, J & Ballantyne, CK 2002, 'Use of environmental magnetic measurements to validate the vertical extent of ice masses at the Last Glacial Maximum', Journal of Quaternary Science, vol.17, no.3, pp.193-200. http://doi.org/10.1002/jqs.666

75. Wu, Z & Wang, W 1998, 'Formation of "old red sands" and paleogeographic environment on South China coasts. Science in China', Series D: Earth Sciences, vol.41, no.3, pp.306-313. Retrieved from http://www.scopus.com/inward/record.url eid=2-s2.0-1542570570&partnerID=40&md5=d602110a9ccf6871f9e44fe0ea7c9ecf

76. Yang, T, Liu, Q, Zeng, Q & Chan, L 2012, 'Relationship between magnetic properties and heavy metals of urban soils with different soil types and environmental settings: Implications for magnetic mapping',Environmental Earth Sciences, vol.66, no.2, pp.409-420. http://doi.org/10.1007/s12665-011-1248-9

77. Zhang, J, Yuan, B & Zhou, L2008, 'Luminescence chronology of Old Red Sandin Jinjiang and its implications for optical dating of sediments in South China',Chinese Science Bulletin, vol.53, no.4, pp.591-601. http://doi.org/10.1007/s11434-008-0001-6

LIST OF PUBLICATIONS

1. Vidyasakar Anburaj, Sant'Ovaia,H., Gomes, C., Lourenço A , Srinivasalu , Seshachalam, 'A magnetic and geochemical characterization of red dune sands (teri sands) of Tamil Nadu coast', Indian Journal of Geo- Marine Science,Vol.44(9) Sep2015,pp.1382-1392 .

2. **Vidyasakar Anburaj**, Sant'Ovaia, H, Linto Allapat, Morthekai, P, Srinivasalu Seshachalam, Singhvi, AK, Ferreira, J & Gomes, C 2016, 'Paleoclimatic registers from semi-arid costal sediments of southeastern India: a multi proxy approach' (accepted for International Water conference entitled "Water Resources in arid areas: the way forward" Accepted for Springer book Special Issue 2016).

3. Linto Alappat, Morthekai, P, **Vidyasakar**, **A,** Srinivasalu, S, Reddy, DV & Singhvi AK, 'Chronology of formation and evolution of red dune sands (teri sands) of south India and its palaeo-environmental implications'(accepted for Geochronometria in special issue 2016/17).